Developing a steady state neutronic model for the PBR-250 HTR using Serpent 2.1.31

OTG Lunga

orcid.org/ 0000-0003-0500-0432

Mini-dissertation accepted in partial fulfilment of the requirements for the degree *Master of Engineering in Nuclear Engineering* at the

North-West University

Supervisor: Prof VV Naicker

Graduation: October 2023

Student number: 27136183

Abstract

The PBR-250 reactor is a Generation-IV pebble bed high-temperature reactor with a rating of 250MWth and has the ability to produce electricity and process heat of up to 1000 °C. The most desirable feature of this reactor is the safety features associated with Gen IV-specific technology. The PBR-250 fuel is said to be unable to melt under design base accident scenarios. This characteristic, together with the large negative temperature coefficient, contribute significantly to the inherent safety characteristics of the reactor type (the other factors being its low power density, large heat capacity and capacity to transfer heat to its immediate surroundings without significant release of radioactivity). The main philosophy underpinning this dissertation is methodology development and the modelling of different reactor states of the PBR-250, as described in the International Atomic Energy Agency (IAEA) Coordinated Research Project (CRP), by using the Monte Carlo code Serpent 2.1.31. The development of this reactor technology brings us closer to realising the full benefits associated with Gen IV reactors while also increasing the knowledge base in research areas such as sensitivity and uncertainty analysis.

Serpent input files of the PBR-250 with different pebble configurations were constructed and different reactor states were analysed. The fresh core (4% enrichment) was found to be supercritical for all pebble configurations i.e., simple cubic (SC), body-centred cubic (BCC), face-centred cubic (FCC), and thus methods to reduce the reactivity were assessed. In view of this, a reactor state in which fuel pebbles (4% enrichment) and dummy pebbles mixed at a ratio of 50:50 was developed, furthermore, the 50:50 setup was optimised to show the effect of incorporating ^{10}B burnable poison into the dummy pebbles (burnable poison pebbles) on the multiplication factor. Finally, the incorporation of control rods would then the reactor to a critical or subcritical state.

The temperature coefficients were calculated to assess the stability and temperature effect associated with the setups. It was determined that the reactor has a very strong Doppler coefficient that renders a negative temperature coefficient for the given reactor states. The reactivity of the PBR-250 is controlled by twelve control rods and a reactor shutdown system composed of twelve shutdown elements. Control rod worth and SCRAM reactivity were assessed for the BCC and FCC setup with the integral and differential rod worth of the BCC and FCC setup plotted for the modelled control rods. The neutron flux profiles for this specific reactor were assessed for different reactor states. Overall, the results give insight into some of the important

aspects of this type of reactor while also developing other key research areas such as uncertainty and sensitivity analysis and model development.

Keywords

High-temperature reactor, pebble bed reactor, criticality, integral rod worth, differential rod worth, temperature coefficient, Serpent, Monte Carlo, NWURCS

Declaration

I, the undersigned hereby declare that the work contained in this project is my own original work,

Olvidio T.G Lunga

Date:15 November 2022

Acknowledgements

Many thanks to the Lord In heaven for His kindness and love. Without you, this would have not been possible.

I would also want to thank my supervisor Prof V Naicker for her time, her extensive knowledge on the subject, and all the advice and input which she has provided tirelessly. Without her patience with me, this would not have been possible.

This masters work was partly funded by the DST Chair in Nuclear Engineering and the Faculty of Engineering, and their contribution has been of utmost importance to the dissertation. Thank you.

I would also like to thank all the lecturers who gave me insight into the world of Nuclear Engineering and for all the support I got from them.

I would also like to thank my family (Wilfred ,Ntando, Olidia and Olivia Lunga), for their support throughout this entire process of writing this dissertation.

List of Abbreviations

ACE	A compact ENDF
A.U	Arbitrary units
AGR	Advanced gas-cooled reactor
BEMUSE	Best estimate methods uncertainty and sensitivity evaluation
BCC	Body-centred cubic
BISO	Bi-structural isotropic particle fuel
BWR	Boiling water reactor
CSG	Constructive solid geometry
CANDU	Canadian heavy water reactor
CPU	Central processing unit
CRP	Coordinated research project
CUD	Core unloading device
DST	Department of Science and Technology
ENDF	Evaluated nuclear data file
FCC	Face-centred cubic
GD	Graphics draw
HCP	Hexagonal close packed
HTGR	High-temperature gas-cooled reactor
HTR	High-temperature reactor
HTR-10	High-temperature reactor-10MW
HTTR	High-temperature test reactor

IAEA	International atomic energy agency
LMFR	Liquid metal cooled fast reactor
LWR	Light water reactor
MEDUL	Mehrfach DurchLauf
MS	Microsoft
NEA	Nuclear energy agency
NWURCS	North-West university reactor code suite
OECD	Organisation for economic co-operation and development
OTTO	One through then out
PBMR	Pebble bed modular reactor
PBR-250	Pebble bed reactor-250MWth
PMR	Prismatic modular reactor
PNG	Portable network graphics
PWR	Pressurised water reactor
RBMK	Russian boiling water reactor with graphite structures
RSS	Reserve shutdown system
SC	Simple cubic
SiC	Silicon carbide
SCRAM	Safety control rod axe man
TRISO	Tri-structural isotropic particle fuel
UAM	Uncertainty analysis in modelling
USA	United States of America

USSR	Union of Soviet Socialist Republics
UHTREX	Ultra-high temperature reactor experiment
VTT	Valtion teknillinen tutkimuskeskus
VVER	Voda voda energo reactor
W/O	Percentage by weight

Contents

List of Figures

List of Tables

Chapter 1: Introduction

1.1 Background

Energy is foundational in growth and advancement since it is a very important component of society that powers businesses, manufacturing, and the transportation of goods. The main drivers for the increase in energy demand is population growth and the development of economies and these elements will continue to be important in the future. Accordingly, countries such as those in Africa, will continue in their positive development trajectory in pursuit of improved standards of living and greater prosperity. According to IAEA (2010:1), worldwide principal energy consumption is anticipated to rise 1.5 to 3 times the current values, and by a factor of 2 to 5 times by the end of the century. It is therefore imperative, that energy demand should be addressed through the development of affordable, dependable, and secure energy supplies that are environmentally sustainable.

The worldwide climate change issue has placed the energy supply in an environmentally sustainable way, as a key concern of worldwide significance. With this in mind, the worldwide political environment objective of the Paris Agreement is to maintain the increase in global temperatures under 2°C, contrasted with pre-industrial levels, and to propose attempts to keep it below 1.5°C (Kameyama, 2021:67). Currently, the agreed-upon commitments by nations are inconsistent with the 2°C set objective and therefore, an even greater reduction of emissions is being encouraged to meet these envisaged targets. The 2°C objective was chosen for practical reasons, a difficult but attainable objective, which restricts the repercussions of climate change to a tolerable limit (Muellner *et al.*, 2021:1). Many energy generating methods have been developed that have a low carbon footprint, such as solar and wind energy, etc,. which all have their associated pros and cons.

Considering the above, this thesis focuses on nuclear energy as an energy source that possesses the potential to address most of the highlighted issues above, thus the development and wide use of nuclear energy could help address the energy deficit in country grids while also promoting economic growth. Despite the controversial risks associated with nuclear energy as highlighted by the catastrophic accidents in Fukushima and Chernobyl, and high initial capital costs, it has relatively low operating and energy production costs. The production of nuclear energy is very competitive with respect to coal and gas in many countries, moreover this type of energy production is very reliable compared to other low-carbon footprint energy sources, such as wind

energy, tidal energy, etc., as the issue of energy storage posed by these weather-dependent energy sources is non-existent with nuclear energy.

Looking back at the climate change and environmental sustainability issues highlighted, nuclear energy production (via the nuclear fission reaction) has a high energy density and does not release any greenhouse gases. While the production of energy using nuclear fission does produce radioactive waste material, significant strides have been made to minimise the release of radioactive material from nuclear power generating facilities over the past decades, which is desirable in terms of environmental sustainability. According to Kugeler and Zhang (2019:3), in Germany, a typical nuclear reactor emits just under 0.5% of the population's radiation load, with substantial quantities coming from medications and natural sources. Despite this, the disasters at Chernobyl, Fukushima, and Three Mile Island (USA, 1979) hindered the progress of nuclear energy as an energy source.

The significant demonstration of neutron fission in 1938 and the successful setup of the first nuclear reactor in 1942 set the trend for the harnessing of atomic energy. From that, many reactor designs have been put forward, built, and operated. Nuclear energy has been a leading contender in many countries' endeavours towards an envisaged clean, low carbon, safe, and efficient base load energy. Table 1-1 provides a summary of the features of reactor types that have already been implemented in the energy industry.

Table 1-1 – Overview of characteristics of reactor types

Aspect	**Reactor type**							
	Unit	**PWR**	**BWR**	**RBMK**	**CANDU**	**AGR**	**HTR**	**LMFR**
Generation		II/III	II/III	II	II/III	II	IV	IV
Characteristic component								
Moderator		H_2O	H_2O	H_2O	H_2O/C	D_2O	C	C
Neutron spectrum		Thermal	Thermal	Thermal	Thermal	Thermal	Thermal	Fast
Fuel		UO_2 PuO_2	UO_2 PuO_2	UO_2 PuO_2	UO_2 PuO_2	UO_2	UO_2 PuO_2	UO2 PuO_2
Type of fuel		Rods	Rods	Rods	Rods	Rods	Pebbles or blocks	Rods
Coolant		H_2O	H_2O	H_2O	D_2O	CO_2	He	Na
Status of coolant		Liquid	Liquid/steam	Liquid/steam	Liquid	Gas	Gas	Liquid
Parameter of design								
Enrichment	Wt %	3–4	3–4	2	>1.5	2	8	10

Fuel burn-up (average)	MWd/kg	45	40	30	10	20	80	100
Core power density	MW/m^3	100	50	4	15	2	3	400
Coolant temperature	°C	290–325	200–285	200–285	200–305	250–650	250–750/950	380–540
Coolant pressure	MPa	16	7	7	4.3	18	18	17
Steam pressure	MPa	6.5	7.0	7.0	9.5	4.0	6.0	1.0
Steam temperature	°C	280	285	285	250	530	530/600	500
Efficiency	%	33	33	32	30	40	40/45	40
Thermal power	MW	3800	3800	3000	1500	1500	200–600	750
Special aspects					Natural uranium		Gas turbine process	Breeding

Adopted from (Kugeler & Zhang, 2019:2)

With respect to Table 1-1, the most widely used reactors are light-water reactors in terms of number of reactors built. In fact, they have proved to be very economical in some Asian countries like South Korea, Taiwan and China, and some European countries like France. The light-water reactor types mainly fall under Generation-II and Generation-III as shown in Table 1-1. Generation-II reactors are large commercial plants with limited safety features while the Generation-III reactors improve the safety measures of these Generation-II reactors. The development of Generation-IV reactors has been taken up worldwide, with interests in progressing the HTGR with its inherent safety measures being renewed worldwide. Several theoretical and experimental studies are being performed to increase the knowledge base about the fuel performance behaviour and fission product release from the reactor's fuel.

1.1.1 High-temperature gas-cooled reactors

This section will introduce the HTGRs, which, according to Kugeler and Zhang (2019:20), were first proposed in mid-1942. By the mid-1950s, several had been developed namely, in the United Kingdom the DRAGON reactor; the USA with the Peach Bottom and UHTREX reactor; and the Federal Republic of Germany with the AVR reactor. These reactors had been effectively evolved and operated exhibiting the possibility and benefits of the HTGRs. The principal motive for the development of these reactors was to produce steam with temperatures exceeding 500°C from the realised high coolant temperatures. As the development of the reactors continued, emphasis on aspects such as nuclear process heat and beneficial safety aspects became more important.

There are mainly two types of HTGR design concepts, namely the pebble bed and the prismatic block type concept. The latter uses helium as a coolant, graphite as moderator, and is a low uranium enriched reactor with a core that is made up of hexagonal fuel-block structures consisting only of graphite. Its basic fuel structure is coated enriched fuel particles, which are contained within the fuel compacts. However, since this study focuses on the pebble bed concept, the prismatic block type reactor will not be discussed further, and the pebble bed concept is introduced in the next section.

1.1.2 The pebble bed reactor concept

This reactor type is mainly composed of graphite, used to construct the structures of the reflector and the fuel pebbles. Consequently, low parasitic absorption of neutrons by graphite attributes to the reactor's good neutron economy. The graphite reflector structures cover the top, bottom, and side structures of the reactor core. For steam turbine systems, high-pressure helium coolant is heated up as it moves down the reactor core, from the top at approximately 250°C to the bottom of the reactor at about 750°C, whereas with gas turbines systems , coolant temperatures leaving the core rise to values ranging from 900°C to 1000°C.

The fuel elements in the reactor comprise of tiny coated fuel particles (TRISO/BISO), embedded in a graphite matrix of the pebbles that make up the core. High burn-up values allow enrichment of between 5% to 8% in which small uranium dioxide fuel kernels with a radius of about 250µm make up the fuel. Small uranium dioxide fuel kernels with a radius of about 250µm make up the fuel.The fuel kernel particle is made up of a uranium which is covered by three layers of carbons (namely two pyro-carbon layers and buffer layer) and ceramic-based materials that ensure that radioactive fission products are not released. The first buffer porous layer is about 50µm to 90µm in thickness, preventing any fission products to escape. The other three layers (C/SiC/C) of a thickness of approximately (40µm /35µm /40µm), respectively, function as reliable containment vessels that almost contain all radioactive products when operating normally and in abnormal conditions, to a limit of 1600°C (Kugeler & Zhang, 2019:5). The TRISO particles serve as the foundation for all HTR concepts with 10,000 to 20,000 of the particles pressed in a graphite matrix, which is then covered by a 5mm thick fuel-free zone (shell) making up the fuel pebble. The graphite shell, and fuel matrix are attached rigidly and made of the same material (Kugeler & Zhang, 2019:5).

The fuel element design is thermodynamically desirable because the heat produced by these fuel elements is almost wholly uniform and the material used to construct these reactor components

(graphite) has very good heat conduction properties. This consequently allows operation at high coolant temperature with relatively lower fuel temperatures. The spherical nature of the fuel pebbles allows flexibility during fuel cycles; more specifically the addition of new fuel pebbles and subsequent removal of spent fuel elements, in and out of the core during full reactor operation. This accordingly removes the necessity for excess reactivity, lending another important safety feature to this reactor type as power density values of between 2MW/m^3 and 4MW/m^3 are realised during operation which are comparatively low to other reactor types.

The 6cm diameter pebbles are placed in the core formed by the inner surfaces of the graphite reflectors and move slowly from the reactor top, parallel to the flow of the helium coolant, to the cone-shaped bottom of the reactor where they exit the reactor. Absorber elements placed inside reflector borings in parallel with the motion of the pebbles, control and shut down the reactor. The strong negative temperature coefficient of pebble bed concept is one of the significant contributors of the inherent safety of the reactor type. To elaborate, during operation or an accident, an increase in the temperature always tends to make the reactor shutdown.

There are two main fuel burnup cycles associated with this reactor type, which are: the MEDUL cycle (Mehrfach DurchLauf = several passes through the core); and the OTTO cycle (once-through-then-out) with only one pass through the core. Spent fuel elements from both cycles are kept in the passive intermediate storage vessels. According to Kugeler and Zhang (2019:6), there are no identifiable accidents from internal/external causes that might result in significant fission products release from this storage system, prolonging the life of intermediate storage. In case active decay heat removal is not available, decay heat passively moves out of the reactor through conduction, convection, and radiation to its surroundings. Limiting power to 250MW in the modular HTRs ensures that temperatures greater than 1600°C will not be achieved in any postulated design base accident; thus, the release of fission products from the TRISO particles is limited to less than 10-5 of inventory. In light of this, it becomes feasible to acknowledge reactors in which meltdown events cannot occur and will not overheat to unallowable levels in the absence of decay heat removal systems..

1.2 Motivation

The key drivers for the advancement of HTR's are factors such as the demand for safe, dependable, affordable, and environmentally sustainable sources of energy fuelled by population growth and country states' demands for improved general livelihood. Nonetheless, the methods and tools for neutronic, transient and thermal hydraulic analysis that are currently present for the

design of the HTR's have always trailed behind other reactor technologies (Reitsma et al., 2006:1). Consequently, this has prompted researchers to not simply test current available methods for HTGRs but to also provide more precise and robust methods for investigating neutronic and thermal fluid behaviour for HTGR safety and design evaluations. The advancement of HTGRs demands several design and safety verification procedures with accurate physics models and high-fidelity codes that are fast and efficient. A typically accepted method of assessing uncertainties in the high-temperature gas reactor's analysis tools is through the use of sensitivity analysis, which is also now accepted in safety studies, and, in some cases, preferred over traditional conservative analysis methods (Reitsma et al., 2012). For example, in neutronics studies, this has given rise to the demand for nuclear data uncertainties that can be applied in uncertainty methods and have been deemed essential in data and simulation improvement.

To tackle the HTGR community's uncertainty analysis and methods, the IAEA undertook a CRP on the HTGR uncertainty and sensitivity analysis in modelling. This was built from predecessor experience of light-water reactors, and VVER domains such as the OECD/NEA BEMUSE program from which the OECD/NEA LWR Uncertainty Analysis in Modelling (UAM) benchmark effort was derived (Reitsma et al., 2012). As a result, two benchmark problems were identified namely the MHTGR-350 (prismatic type) and the modular pebble design, a 250MW design, derived from the InterAtom HTR-module (late Germany 1980s). The main purpose for the benchmark is to get an indication of the uncertainty in the calculation and the relative contributions of the various parameters i.e., related to nuclear and material data, engineering uncertainties, the multi-physics etc.

At the North-West University, previous work on uncertainty analysis has focused on the prismatic reactor type and light-water reactors. However, since both the pebble reactor and prismatic reactors are being developed for power production and other needs, it is important that uncertainty analysis (as applicable to pebble bed reactors) also be developed as an expertise at the university. Nevertheless, before such uncertainty analysis work can be done, robust models must first be built and verified. Overall, this dissertation thus aims to commence the modelling process of the modular pebble design described, by using Serpent to increase the knowledge base of modelling of the HTGRs. Future work on Serpent full core calculations coupled with thermal-hydraulic calculations, safety evaluations burnup calculations etc. on the PBR can then be built from this study.

1.3 Research aims and objectives.

Research aim:

To build and test a computational criticality model of the modular pebble design benchmark, the PBR-250, using Serpent 2.1.31.

Research objectives:

- To construct an input model of the PBR-250 using Serpent 2.1.31;
- To develop different pebble configurations for the PBR-250;
- To construct an input model using NWURCS for Serpent 2.1.31 and compare it with the manually developed input model listed as the first objective;
- To check the convergence of Serpent 2.1.31 for input models, and; lastly
- To perform reactivity and criticality analysis calculations with the PBR-250 model.

1.4 Research benefits

The Unit for Energy and Technology Systems at the North-West University (NWU) began using the Serpent 2.1.31 code quite recently (2021) and this research project will be the first at the university that uses this package to analyse the PBR-250. It will also provide a detailed guide to pebble reactor modelling using the code. PBR-250 input models developed with the NWURCS code will be tested for the first time and a good foundation for further research on design uncertainty will be set by this study with the different pebble configurations analysed in this dissertation.

1.5 Dissertation outline

• Chapter 2 – Literature survey

This chapter contains a literature survey of the methods and tools used to address the above-mentioned problem beginning with neutron transport simulation. The special capabilities that make Serpent 2.1.31 a well-suited program for full core reactor simulations are discussed in the chapter. It also contains various other nuclear characteristics and references relevant to other chapters of this dissertation, such as Doppler broadening and cross-section.

• Chapter 3 – Reactor details and methodology

This chapter outlines the PBR-250 reactor design and how Serpent 2.1.31 was used to model the reactor.

• Chapter 4 – Results and discussion

This chapter contains all the data on the modelling outcome and simulation results of the PBR-250 in which different pebble configurations were studied. The models developed are subjected to different test parameters (different reactor states) and the outcomes conveyed graphically or in tables. The simulations are also discussed and evaluated for the developed reactor states.

• Chapter 5 – Conclusion and recommendations.

This chapter contains the study's conclusions, and its recommendations regarding work that could further stem from this study.

Chapter 2: Literature survey

This chapter focuses on the physics of Monte Carlo simulations that pertain to the modelling of the PBR-250 with Serpent. Background on methods and tools used to optimize Serpent in comparison to traditional Monte Carlo methods, and those used analyze this dissertation's results are examined.

2.1 Introduction

Serpent is a continuous-energy Monte Carlo reactor burnup calculation physics code that was initiated and developed at the VTT Technical Research Centre of Finland and released in 2009. The goal was to create a new Monte Carlo transport code specific for lattice physics applications and especially group constant generation (Leppänen *et al.*, 2015:1). With traditional Monte Carlo codes, reaction rate tallies for every computation needed to be specified individually, and the outcomes, along with their errors, incorporated once the computation was complete. As a result, the numerous tallies increased the extensively restrictive running time. Serpent uses a combination of the surface to surface-tracking method as discussed in Section 2.7.1, and the Woodcock delta-tracking method as discussed in Section 2.7.2 (˘Zohar *et al.*, 2021:2), to reduce to an extent, the time limitations previously highlighted. Another aspect is the employment of a single unionised energy grid (Appendix B-7) over all reaction cross-sections, which reduces the amount of grid search iterations (Leppänen, 2009:880).

It is important to highlight that the ability of the continuous-energy Monte Carlo method to deal with complex geometry and physics interactions without significant approximations, is a much-desired feature for reactor analysis. Accordingly, Monte Carlo programs, when used for spatial homogenisation, can generate complex three-dimensional full-scale heterogeneous solutions, which constitute the most ideal reference answer for full-scale reactor physics computations. The size of the task limits the scope of applications since modelling of large-scale reactors requires numerous reaction rate tallies and excessive amounts of CPU time.

2.2 Neutron transport simulation

A desirable outcome of neutron transport simulation is to have detailed time-dependent, three-dimensional particle transport simulations performed competently and precisely. Neutron transport simulation was initially successfully done by using deterministic approaches (numerically solving the Boltzmann neutron transport equation) but, as computer performance

improved, stochastic (Monte Carlo) simulation programs gained importance in both geometry and physics modelling (Vaz, 2009:835). In recent years, hybrid approaches that aim to tackle defined problems using both deterministic and Monte Carlo methods have also been created.

2.2.1 Deterministic methods

The underlying principle of deterministic methods is to disregard the random details of single particle histories, then compute the neutron transport equation by discretising it with regard to each of its variables and solving the subsequent algebraic set of equations. One limitation of deterministic methods is the number of unknown variables that can be held during a calculation. This dissertation will only examine Monte Carlo simulations and will not focus on the deterministic approaches. See Appendix B-1 for the equation used to calculate the multiplication constant deterministically.

2.2.2 Stochastic methods (Monte Carlo simulations)

In contrast to deterministic methods discussed above, stochastic methods disregard all the mathematical descriptions associated with the problem at hand and simulate the numerous particle histories, with the objective to simulate and average an adequate populace of neutrons to such an extent that it creates a decent enough estimate of the flux. The fission source starting conditions, (namely spatial distribution, isotropic directional distribution, energy distribution, etc.) are randomly sampled from prescribed probability distributions (cumulative distribution functions and probability distribution functions) utilising random number generators. Following this, the interactions that occur during neutron transport are sampled and recorded (neutron history) in accordance with cross-sections until the neutron departs the set system or is absorbed, at which point the next independent neutron history begins. This method has stochastic uncertainties rather than truncation errors. Moreover, Monte Carlo can be used to compute fixed source calculations and criticality calculations. With fixed source or shielding calculations, a given set number of neutron histories is simulated and all neutrons at the start have a specific energy, angular, and spatial distribution. The outcome is averaged over the histories with their variances.

2.3 Transport algorithm in Monte Carlo simulations

The Monte Carlo method computes mathematical problems using statistical sampling. While the problems usually have some probabilistic structure within, the method is not limited to these types of problems. According to Serpent.vtt.fi (2021), a Monte Carlo simulation is comprised of

numerous particle histories in which a random walk of a single particle is tracked from birth to its eventual demise, through either by being absorbed or leaving the defined geometry which consists of homogenous material cells. This is to say that the transport simulation follows a random walk from one interaction to the next; sampling the length of travel between interactions; transporting the particle to the interaction site; and then sampling the interaction that occurs at the interaction point. For a scattering interaction, the procedure is restarted by sampling the distance from one interaction to the next. Lastly it is important to note that the particle energy and direction are changed in every scattering interaction.

2.4 Criticality problems

For the most part, Monte Carlo is used to calculate sample means and variances, and if a problem is defined it can be applied to compute the multiplication constant and its related eigen solution for the flux distribution. When it comes to criticality problems, the initial computational cycle uses an arbitrary constant spatial fission source distribution or a previously computed spatial fission source condition (Wolters, 2011:9). From this, the neutron histories are all followed in parallel for each generation of neutrons until they are absorbed or leak out of the system. As a result, the next generation has a different fission source distribution but is based on the fission neutrons from the preceding succession, and the operation is repeated until the ratio of all the fission neutrons generation after generation is a close statistical estimate of the multiplication constant. The procedure for calculating the statistical mean and its accompanying variances is illustrated in the section below.

2.5 Statistical estimation

This section assumes the reader has a basic understanding of probability theory. A useful definition of the probability distribution function $f(x)$ is shown in Appendix B-4 for the reader. For the outcome of a Monte Carlo run, the parameter at hand is commonly reported as the sample mean of individual estimates generated by the repetition of simulation runs. According to Stacey (2018:383), if we assume that x is a random variable showing a particular property of a neutron history; the function h(x) has a mean value set in terms of the probability distribution function for the variable x such that [a ≤ x ≤ b] and is given by:

$$\langle h \rangle = \int_a^b dx h(x) f(x) \qquad 2\text{-}1$$

with standard deviation, σ, given by

$$\sigma(\mathrm{h}) = \{\int_a^b dx[h(x) - \langle h\rangle]^2 f(x)\}^{\frac{1}{2}} = [\langle h^2\rangle - \langle h\rangle^2] \quad \text{2-2}$$

During the calculations of k-eigen values in Serpent, scores recorded in running cycles are collected into batches to form batch-wise estimates. If the batch scores are derived from a single cycle, we can say that the batch-wise estimate is the same as the cycle-wise estimate. According to Kaltiaisenaho, (2014:9), if N batches are generated with x_n being the batch-wise estimate, the final estimate in Serpent is given by:

$$\bar{x} = \frac{1}{N}\sum_{n=1}^{N} x_n \quad \text{2-3}$$

and the result's accuracy conveyed as the standard deviation of $\bar{x}$ given by:

$$\sigma_{\bar{x}} = \sqrt{\frac{1}{N(N-1)}\sum_{n=1}^{N}(x_n - \bar{x})^2} \quad \text{2-4}$$

2.6 Mean free path.

According to Lamarsh & Baratta, (2001:58), when a neutron beam of intensity (I_0) comes in contact with a material, the strength of the beam exponentially decreases with the path length (x) of the beam in the material. If the intensity of the neutrons that have not collided in penetrating I_x the distance x the ratio $\frac{I_x}{I_0} = e^{-\Sigma_t x}$ is equal to the probability that a neutron can move through this distance colliding. If we let $p(x)dx$ be the chance that a neutron will collide in dx in the vicinity of x. This is equivalent to the probability that the neutron will endure up to x without colliding and the probability that it will do so at a distance of dx. Since Σ_t is the probability of interaction per path length, $p(x)dx$ is given by $\Sigma_t e^{-\Sigma_t x} dx$. The average path that a neutron travels between successive interactions is called the mean-free path (λ) and is the mean value of x. This is obtained from the probability function $p(x)$ by determining the average distance travelled (Lamarsh & Baratta, 2001:59), that is:

$$\boldsymbol{\lambda} = \int_0^\infty x p(x) dx$$

$$\lambda = \Sigma_t \int_0^\infty x e^{\Sigma_t x}\, dx \quad \text{2-5}$$

$$\lambda = 1/\Sigma_t$$

2.7 Geometry and particle tracking in Serpent.

According to Serpent.vtt.fi (2022), the webpage specific to this section; like MCNP, the geometry in Serpent depends on a universe based CSG model thus enabling any 2D/3D structures to be described. This model's geometry is made up of homogenous material cells that are defined by basic and derived surface types, linked via intersections and complements.

As neutrons move through the specified problem geometry, they must be tracked. Therefore, after the birth of a neutron, the distance travelled in a straight line should then be sampled before interaction. The distance following this distribution can be sampled by generating a pseudo-random number and using inverse transform sampling (discussed in Appendix B-6). The particle transport in Serpent is based on the combinations of surface-tracking and the Woodcock delta-tracking method. The Woodcock tracking process has shown to be effective and ideal for geometry with long neutron mean-free paths (Section 2.6) compared to their dimensions, which is dominant with fuel assemblies and particles in the HTGR. The processes of the tracking methods highlighted will be looked at in the following sections.

2.7.1 Surface-tracking

According to Serpent.vtt.fi (2022), since the interaction probability per covered path length is independent of particle event history, the start of a path can be considered at any point in a material region. If the path being sampled crosses a boundary between two material regions, the track is stopped at one of the material region boundaries and a new path is resampled in the new material region by using the new area's cross-sections. Most Monte Carlo computation programs use surface-tracking. However, if the cell has many surfaces, this method can become quite computationally expensive. Secondly, when the mean-free path is longer than the dimensions of the geometry, stopping the particle track at each boundary causes a computational hold-up.

2.7.2 Woodcock delta-tracking

Having looked at surface-tracking, we will now consider delta-tracking. In the 1960s, Woodcock developed the delta-tracking technique (which relies on particle path length rejection sampling) as an alternative to surface-tracking. In that regard, the basic idea behind this technique is to successfully homogenise the total cross-sections of the material with the result that the path lengths that are sampled are true over the whole geometry (Leppänen 2010:716). This idea is

based on virtual collisions, which are fictive interactions that retain particle direction and energy. Because virtual collisions are not collisions at all, they do not affect the random walk statistics. According to Serpent.vtt.fi, (2021), the material's cross-sections Σ, can be adjusted with an arbitrary virtual collision cross-section Σ_0 such that:

$$\Sigma'(r,E) = \Sigma(r,E) + \Sigma_0(r,E) \qquad 2\text{-}6$$

without altering the simulation result. The material cross-section for different regions can therefore be adjusted freely: i.e., $\boldsymbol{\Sigma'_1(E) = \Sigma'_2(E) = \Sigma'_3(E) = \cdots = \Sigma_m(E)}$ where $\Sigma_m(E)$ is the majorant cross-section. If the value $\Sigma_m(E)$ given by equation 2-7 are defined as the maximal material Σ sum at each energy point, defining the virtual cross-section becomes absolute. The majorant cross-sections are independent of the spatial coordinates.

$$\Sigma_m(E) = \max[\Sigma(\mathrm{r},\mathrm{E})] \qquad 2\text{-}7$$

with ξ being a uniformly distributed random variable on the unit interval and the same value of Σ across the entire geometry, being used for sampling path lengths (l),where:

$$l = -\frac{1}{\Sigma_m} log\xi \qquad 2\text{-}8$$

The statistical validity of values is maintained regardless of the number of material boundaries crossed. Consequently, the requirement to halt the random walk between two material regions is removed, thus removing the necessity to compute surface distances. This is replaced by a tracking routine that handles virtual collisions, where for each collision and, at the end of the sample path, rejection sampling is performed. The probability to accept a collision is given by the physical cross-section to majorant cross-section ratio:

$$P = \frac{\Sigma(\mathrm{r},\mathrm{E})}{\Sigma_m(E)} \qquad 2\text{-}9$$

If the interaction is rejected, a new path length is sampled using Σ_m and the neutron is transported to the next interaction point.

2.8 Serpent validation and verification

Verification is carried out to firstly, to ascertain whether the equations provided with the set initial and boundary conditions are programmed correctly, and secondly to establish whether the code works properly. Validation confirms using comparisons/benchmarks that the code provides sufficiently accurate results.

The extensive utilisation of computational tools to predict the nuclear system conditions is important in demonstrating nuclear safety in nuclear operations. In terms of validation and verification of Serpent, versions are checked and compared to MCNP by carrying out a set of assembly calculations. According to Leppänen *et al.* (2015:2), if the same ACE library is employed in the computation, all the multiplication factors and homogenised few-group reaction cross-sections fall within the statistical accuracy of the reference standards. Furthermore, the differences in the effective multiplication factors with other Monte Carlo codes, i.e., KENO, have been found to be marginal, while in deterministic codes, the differences are relatively larger in nature due to fundamental reasons.

The webpage (https://serpent.vtt.fi/mediawiki/index.php/Validation_and_verification) presents all validation and verification documents for the Serpent code. Validation documents for criticality safety, fuel burn-up, research reactors, the photon transport capabilities of Serpent, and full core (2D or 3D) models can be found there, additionally documentation related to validation and verification of Serpent can be added to the webpage list.

2.9 Cross-sections

The extent to which a neutron and nuclei interact is given in cross-sections and represented by the symbol σ. The quantity σ (in barns) is expressed as the probable reaction rate for n neutrons travelling with speed (v) a distance (dx) in a material with N nuclides per unit volume (Stacey, 2018:6). Another term to consider is the flux, which is the product of the neutron number per unit volume (cm^3) in a neutron beam and the speed of the neutrons.

The microscopic cross-section (σ), in which the subscripts *e,i,f...* indicate definable nuclear interaction, is used to quantify the chance of a nuclear interaction between a neutron and a nucleus. The total microscopic cross-section (σ_t) is given by:

$$\sigma_t = \sigma_e + \sigma_i + \sigma_f + \sigma_\gamma + \cdots \qquad 2\text{-}10$$

The value quantifies the probability that any nuclear interaction happens when neutrons hit nuclei. The sum that absorption interactions occur is known as the absorption cross-section (σ_a) and is given by:

$$\sigma_a = \sigma_\alpha + \sigma_f + \sigma_\gamma + \cdots \qquad 2\text{-}11$$

The total microscopic scattering cross-sections give the total probability that when scattering interactions occur between nuclei and neutrons, it can be inelastic or elastic scattering and is given by:

$$\sigma_s = \sigma_e + \sigma_i \qquad 2\text{-}12$$

The macroscopic cross-section is then:

$$\Sigma = \sigma . N \qquad 2\text{-}13$$

where

N – atomic number density (nuclei/cm^3), and

σ – microscopic cross-section (cm^2)

2.10 Reactivity feedbacks and coefficients

The combined feedback of nuclear reactor properties (temperature, neutron population, densities etc.) determines the stability of nuclear reactors. This feedback is described mathematically using reactivity coefficients. For this study, we will consider the temperature coefficient of reactivity, which describes the degree to which reactivity is influenced by temperature variation (Lamarsh & Baratta, 2001:365).

During reactor operation, variation of power levels results in temperature changes. For instance, when increasing the reactor power, the neutron population increases due to more fission reactions, hence the heat produced from the fission reactions and fuel temperatures increase. The resultant changes in temperatures affect the neutron population in different ways and this is a very important aspect to consider for the design and operation of reactors. The temperature changes also affect the shapes and properties of reactor components (moderator, fuel material, etc.) in the reactor which also produces changes in reactivity.

2.10.1 Temperature coefficients of reactivity

Lamarsh and Baratta, (2001:365-366) define the temperature coefficient as

$$\alpha_T = \frac{\partial \rho}{\partial T} = \frac{\partial}{\partial T}\left(\frac{k-1}{k}\right) = \frac{1}{k^2}\frac{dk}{dT} \cong \frac{1}{k}\frac{dk}{dT} \qquad 2\text{-}14$$

The value of k in this approximation is close to unity, so $k^2 \cong k$. The temperature coefficient can be said to be the rate of change of reactivity per unit of temperature change.

- A positive α_T results in an unstable reactor and any flux disturbances tend to amplify themselves (Massimi, 1976:147). A positive temperature coefficient implies that the reactor must be controlled under strict conditions.
- A negative α_T results in a self-stabilising reactor system.

Different components in a reactor are subject to different temperatures at different times; thus, these different components have different temperature coefficients.

2.11 The nuclear Doppler effect.

Having considered the importance of the temperature coefficient in the previous section, it is now necessary to describe the nuclear Doppler effect. With most of the available designed reactors, the prompt temperature coefficient is negative due to the nuclear Doppler effect. To begin with, nuclei in atoms are always in continual vibrational motion due to their thermal energies. Therefore, a beam of single-energy neutrons impinging a target seems to have a continuous spread of energy, which influences the shape of an observed resonance (Lamarsh & Baratta, 2001:367). Compared to nuclei at rest, the resonances observed for nuclei in motion is shorter and wider, and the effects become more pronounced as their temperature increases. This effect is shown for the scattering cross-sections of ^{238}U in Figure 2-1 below as adopted from Becker, (2010:25).

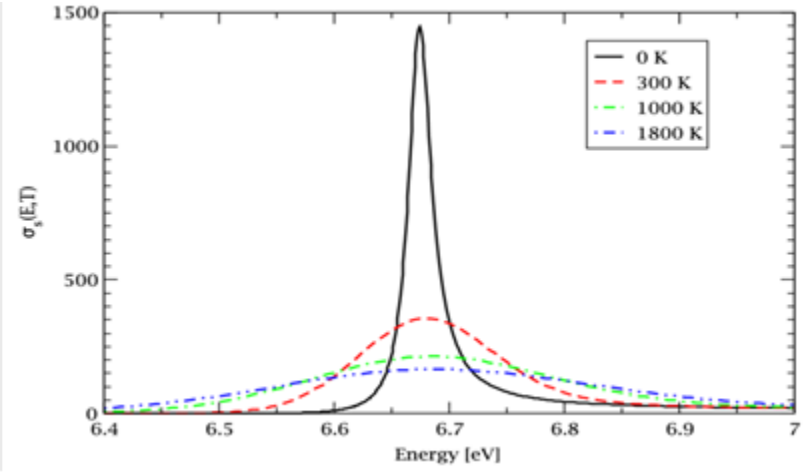

Figure 2-1: Doppler broadening of ^{238}U scattering cross-section

2.12 Source convergence and Shannon entropy

By default, Serpent determines the k-eigenvalue by performing cycle-wise runs, with the source distribution in each cycle defined by the preceding cycle's fission distribution. With that in mind,

before collecting results from criticality calculations, inactive cycles are undertaken to let the initial fission source distribution to be statistically constant. The cycles are user-defined, and it is imperative that the correct number of cycles is skipped so that the fission source at the beginning has the appropriate distribution.

Having considered the importance of source convergence, we will now consider its link with the Shannon entropy. Shannon entropy data, which can be obtained in Serpent is useful in addressing the issue of knowing whether the fission source distribution has converged. According to (Mokhtari & Mazrou, 1994:2), Claude Shannon defined the Shannon entropy as:

$$H_{src} = \sum_{i=1}^{N} P_i log_2 P_i \qquad 2\text{-}15$$

where

N is the region count, and;

P_i is the ratio of the source sites count in the *i*th region to the total fission source sites.

They also state that the Shannon entropy tends to converge to a single value whenever the neutron distribution manages to achieve its stationary form. This will be applied to determine the number of inactive cycles.

2.13 NWURCS

Computer codes that have been utilised to produce suitable input files for one code, and extract data from the output files for use in other codes have been developed and are called code wrappers. NWURCS is one such code, a FORTRAN developed suite of codes that began in 2012 at the School of Mechanical and Nuclear Engineering of the North-West University, South Africa (Du Toit *et al.*, 2018:2). The NWURCS suite is a code capable of generating input files utilised for neutronic codes (Nyalunga *et al.*, 2016:67). For instance, it can produce steady-state RELAP5 input files for different core states, with the ability to couple flux and temperature computations, i.e., MCNP6 and RELAP5. Furthermore, NWURCS can also retrieve information from an MCNP6 or RELAP5 output file. These capabilities enhance efficiency during the evaluation process. Having considered some of the capabilities of NWURCS, in this study, it was developed further to produce an input file for the Serpent code for verification purposes.

2.14 Uncertainty analysis and propagation

Uncertainty analysis is a very important component in neutronic calculations as it quantifies the reliability of best estimate calculations. For accurate results, all aspects that affect the reliability of a result should be looked at and quantified; for instance, a measured quantity has an inherent uncertainty which originates from the measuring process. Additionally, in computer simulations, the combination of assumptions, simplifications, methodology, modelling, etc also influence the output result's reliability. The concepts used for calculating uncertainty in this dissertation are covered in Appendix E and the derivation of the equation:

$$\delta\alpha_\rho = \frac{1}{T_2 - T_1}\sqrt{\frac{\delta {k_1}^2}{{k_1}^4} + \frac{\delta {k_2}^2}{{k_2}^4}} \qquad 2\text{-}16$$

used in calculating the uncertainty in the values of the temperature coefficients is also covered in the section.

Chapter 3: Reactor details and methodology

3.1 Reactor details

This section will focus on a specific type of pebble bed reactor; namely the PBR-250 reactor, a 250MWth variant of the Interatom HTR-module. The pebble bed reactor concept is outlined in Section 1.1.2 and the reader is referred to that section for a basic understanding of the reactor. This section covers the relevant details regarding the reactor, such as its features and characteristics, and is based on the main references: Lohnert (1990); Kugeler and Zhang (2019) and Reitsma *et al*. (2012).

3.1.1 The PBR-250

The PBR-250 is based on the 200MW rated Interatom Company's HTR-module core design. It has the same design and dimensions as the HTR-module but with an increased axial height to allow for power increase. The geometrical representation of the PBR-250 adopted from Reitsma *et al.* (2012) is shown in Figure 3-1 below.

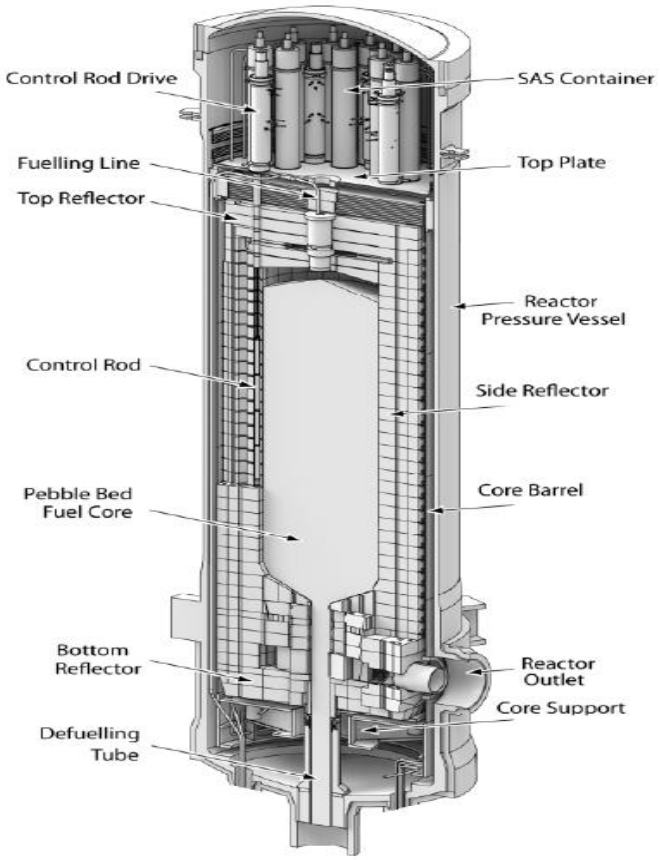

Figure 3-1: Core geometrical illustration of the PBR-250

The studies carried out in this dissertation focused on the IAEA CRP proposed reactor design parameters shown in Table 3-1. Furthermore, this study also adapted design parameters from other similar pebble bed reactor types like the HTR-module, HTR-PM, PBMR, HTR10, etc for design parameters not given in the table below e.g., control rod specifications.

Table 3-1: Major CRP specified design parameters.

Reactor design specifications	
Parameter	**Value**
Thermal power	200MW
Fuel core diameter	3m
Core height	11m
Side reflector thickness	100cm

Inlet temperature	250°C
Outlet temperature	750°C
Pressure	7MPa
Mass flow	96kg/s
Fuel: Pebble type	
Pebble radius	3cm
Thickness of fuel-free zone	0.5cm
Density of graphite in matrix/fuel-free zone	1.74g/cm^3
U-235 enrichment of uranium	8.9wt.%
HM mass	7.0g
Coated particles:	
Kernel diameter	500µm
Kernel density	10.4g/cm^3
Number of coated particles within the graphite matrix	11 600
Coating material	C/C/SiC/C
Layer thicknesses	95/40/35/40µm
Layer densities	1.05/1.90/3.18/1.90g/cm^3
Dummy balls	
Pebble radius	3cm
Graphite density	1.74g/cm^3

Adopted from Reitsma *et al*. (2012)

3.1.2 Safety design

In general, to ensure the safety of nuclear systems, several fundamental safety requirements must be met. This is to say that the safe removal of decay heat; the protection of fission-product retention barriers; radiation protection, and control of reactivity should be satisfied to guarantee

safety in nuclear systems (Kugeler *et al.*, 2021). These safety aspects are covered in the sections below.

3.1.3 Decay heat

It is imperative that nuclear safety systems have a provision to effectively remove the decay heat. This is because the decay heat produced by the decay of fission products in most reactors is estimated to be around 6% of their nominal power immediately after shutdown, dropping to 1% of their nominal power after one hour (Kugeler *et al.*, 2021). Following from this, it is also important that the decay heat be considered for long-term storage of spent fuel.

Having considered the importance of effective removal of decay heat, we will now look at the features of the PBR250 that enable this. Active cooling systems are not employed for the removal of decay heat since the reactor can release the decay heat via passive heat transport modes independent of the reactor coolant, such as conduction, radiation, and natural convection. As a result, the PBR-250 does not have the primary issue of being unable to get rid of decay heat without forced cooling.

3.1.4 Fission products

The PBR-250 incorporates the inherent safety features of modular HTRs. In terms of the fuel elements, the radioactive substances created in fission reactions are contained in the TRISO particles during normal operation and in the event of an accident. The tiny TRISO particle is externally pre-stressed by the graphite matrix of the fuel pebble and this active barrier limits the fission products to the point at which extremely substantial activity releases from the coated particles can be excluded (Kugeler & Zhang, 2019:5). The particle coating's design and the maximum possible temperature (of 1600°C) ensure the safe containment of radioactive materials. The temperature limit in this reactor is due to the combination of the low power density and the temperature resistance of the independent fuel particles. While neutronic studies for severe accident conditions have not been undertaken for the PBR250, peak temperatures of almost 1600°C for the PBMR (reactor based on the same concept with a higher power rating) have been recorded (PBMR-SA, 2012).

Radioactive materials that do escape the particles, either due to design-defective coatings or partial release from non-defective coatings, are partly contained in the fuel matrix. The radioactive material that makes its way out of the matrix enters the primary circuit. In the primary circuit, Lohnert (1989:267) states that the decay of radioactive material, removal using the helium

purification plant, and deposition on the surface in the primary circuit reduces gas-borne activity from the pebbles. This means that the primary circuit acts as a layer that prevents the release of fission products, with its component structures designed to account for all mechanical stresses, i.e., thermal stationary and thermal transient stresses, in terms of maximum allowable loads under normal and accident conditions. Leakages in pipes are avoided because of proper quality assurance measures (Lohnert, 1990:264). In the event of a leak, only very low levels of gas-borne primary circuit activity and deposited activity on the surface of the primary circuit are released into the reactor building. Because of the great retention properties of the TRISO particles, the released activity is low and can be released unfiltered into the surroundings. The reactor building is constructed using reinforced concrete that also functions as a barrier against fission product release into the outer environment and external impact.

3.1.5 Reactivity control

The PBR-250 has two independent shutdown systems, namely, control rods and a RSS (Reitsma *et al.*, 2012). To begin with the control rods, during normal operation, the electrically driven rods change the extent of the criticality of the reactor to lower or raise the power level of the reactor. They also maintain the reactor's criticality by compensating for any reactor system property changes over its lifespan. If the power to these rods is interrupted, they drop under gravity to the lowest position of the reactor borings on the side reflector initiating a reactor scram. Because the reactor can be continuously fuelled, large amounts of excess reactivity is not necessary, and thus a large capability for reactivity control is not required. Turning to the RSS, it compensates for any reactivity increase due to the cold core (50-100 °C fuel temperature) and guarantees subcriticality for long periods to enable even maintenance conditions (Kugeler & Zhang, 2019:39). The RSS is a requirement by nuclear regulators and should be capable of shutting down the reactor.

3.1.6 Chemical stability

The PBR-250 uses helium as its primary coolant since this gas has certain properties that make it a very suitable coolant. Helium is both chemically and radiologically inert; stated otherwise, when it passes through the reactor's primary circuit, it does not react or interact with other chemicals, it is non-combustible, and does not become radioactive (PBMR-SA, 2012). Despite this, there is a small number of other gaseous impurities that can be found in the primary circuit, these include N_2, O_2, H_2O, CO_2, CO, CH_4, and H_2. The graphite at high temperatures poses a risk of oxidation in the presence of some of these impurities, i.e., O_2 and H_2O. Even though the helium

purification system ensures minimal amounts of these impurities during normal operation, two possible scenarios may occur, where there is ingress of reactive substances into the core region.

Firstly, moisture could enter the primary core from steam generator leaks since Rankine cycle water pressures are higher than that of the primary circuit. At temperatures greater than 800°C, the moisture can react with graphite giving the oxidation products of CO and H, which react violently with air. According to PBMR-SA, (2011), the analysis of such events depends on the layout and size of the reactor buildings; however, with the HTR-module design, it was possible to demonstrate that no flammable mixture could result as there was a limited chance of emissions into the reactor building. The oxidation process in turn results in a radioactivity increase from the graphite.

The second scenario would entail the ingress of air through breakages of the reactor pressure boundary. This scenario cannot be assessed without possessing details pertaining to the pipe and vessel connections to the reactor pressure vessel; however, this scenario was analysed for the HTR-module design. The ingress of air into the pressure vessel would result in the introduction of the impurities such as N_2, O_2, H_2O, and CO_2. The studies revealed that the resistance of airflow from the pebble bed decreased the possibilities for air ingress.

3.1.7 Mechanical stability

Fast neutrons from nuclear reactions cause damage to the reactor's graphite structures, and in particular, neutron energy values of 0.1 MeV have been considered the lower limit for neutron energies beyond which significant displacements in the graphite structure (Kugeler & Zhang, 2019:43) are caused. Correspondingly, when the reflector material is exposed to radiation, shrinkage occurs, followed by a phase of expansion.. This affects the mechanical and thermal properties of the graphite. Many studies on the behaviour of graphite during irradiation have been conducted, with the maximum dimensional changes dependent on dose and temperature being identified. These findings have been used to extend the life of the graphite structure by restricting temperatures and irradiation energies in high-temperature reactors. In addition to the above-mentioned considerations, the Wigner effect must be avoided. To elaborate on the Wigner effect, the inner energy of graphite at temperatures under 200°C increases, creating annealing effects, with the release of energy resulting in spontaneous temperature increases. The cold gas temperature is thus maintained at 250°C to reduce this Wigner effect to insignificant levels (Kugeler & Zhang, 2019:44). Lastly graphite also maintains its stability up to a temperature of

3600°C which is beneficial as these temperatures give a good buffer area in terms of the temperature parameter.

3.1.8 Core layout

This section provides the description of the base core model as was simulated in Serpent. To begin with, the assumptions for the core were based on those in the CRP as highlighted by Frederik *et al.* (2012). These assumptions include:

- constant material thermal properties;
- the removal of the bottom cone; and
- the flattening of the reactor bed upper and lower surface.

The PBR-250 core was based on the design parameters given in Table 3-1. The outside structure of the core is made of graphite, which functions as a side reflector, forming a cylindrical vessel that carries the pebbles (Lohnert, 1990:264). The side reflectors contain borings close to the inner walls of the reactor core that provide for the insertion of control rods and the secondary shutdown system. Towards the outer walls of the reactor, more borings are present for the provision of reflector coolant flow. With the flow of helium in the core, it runs up through the latter described reflector coolant flow channels; down through the top reflector; then the void before the pebbles, and through the pebble bed to cool the pebbles. The collected heat flows out from the bottom reactor structures to the generators.

The removal of the top and bottom structures from the developed model affects the effective multiplication factor, therefore it was necessary to evaluate the consequences of removing them. To investigate this, a model with a 30cm reflector material at both the top and bottom of the base model, together with a 30cm void region at the top (between the graphite structure and the pebble bed filled with helium), was developed, as shown in Figure 3-2 below. The density of the added reflector material was varied to approximate a homogeneous mixture of helium and graphite; the flux and effective multiplication factors of the models was investigated.

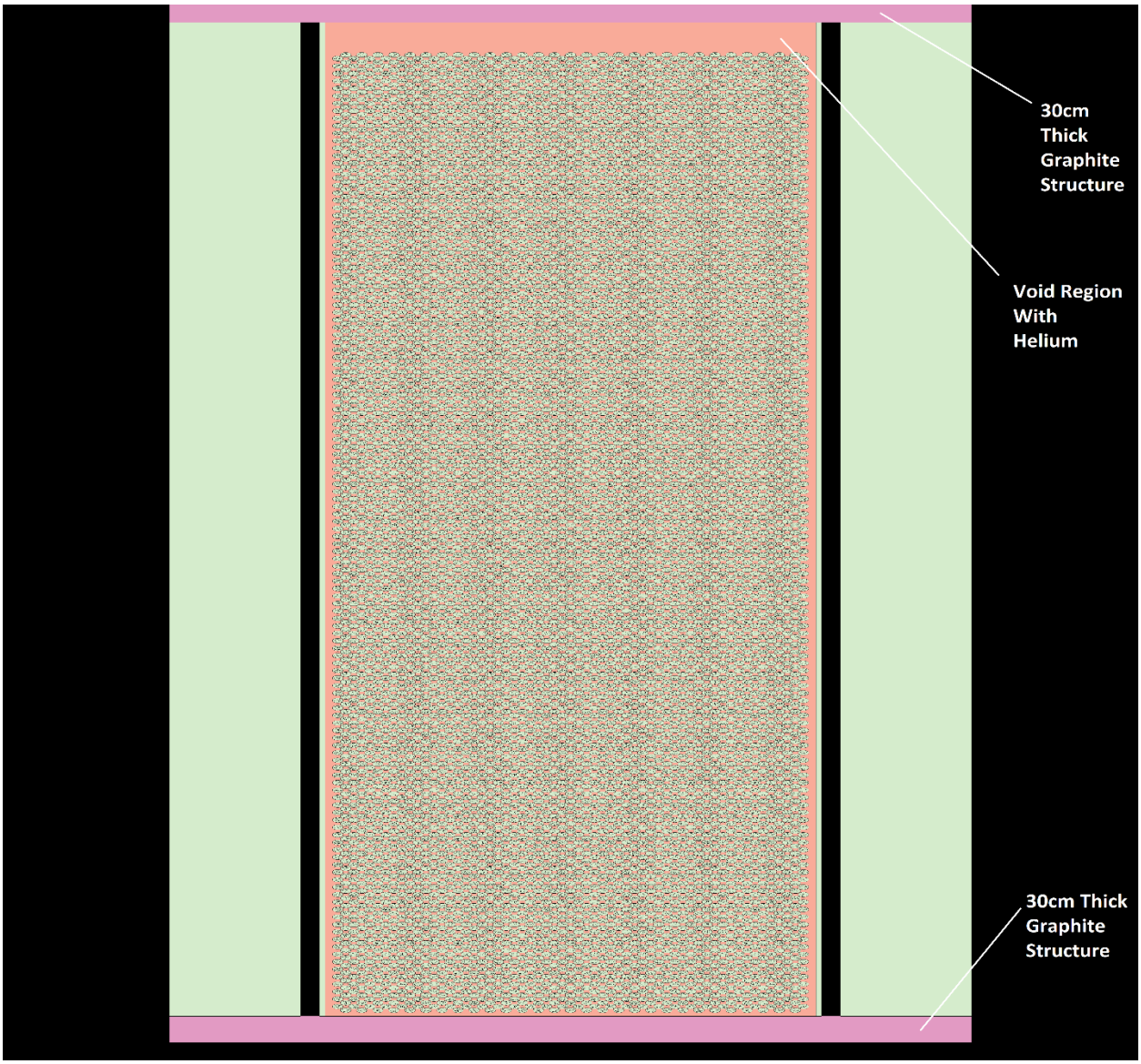

Figure 3-2: The Serpent model used to study the effect of the removal of reactor structures.

3.1.9 Fuel pebble design and arrangement

Having considered the core structures, we will now consider the pebbles in the core. The fuel pebble elements are composed of TRISO particles embedded in a graphite matrix (Kugeler & Zhang, 2019:4). The dimensions and material makeup of these particles are given in Table 3-1 and depicted in Figure 3-3. The fuel particles are pressed into a graphite matrix that make up the fuel zone. The fuel zone is then enclosed by a fuel-free graphite shell as depicted in Figure 3-4. The graphite, which is the moderator, has low parasitic neutron absorption properties, resulting in a good neutron economy.

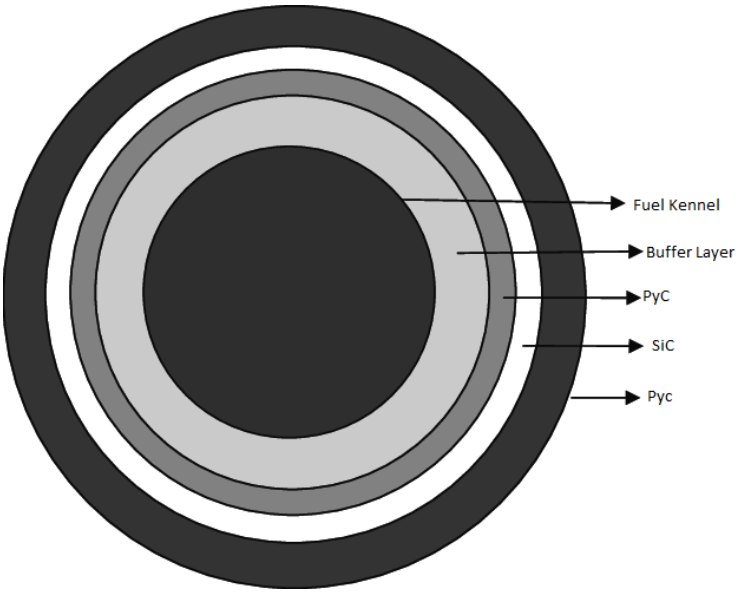

Figure 3-3: Fuel particle

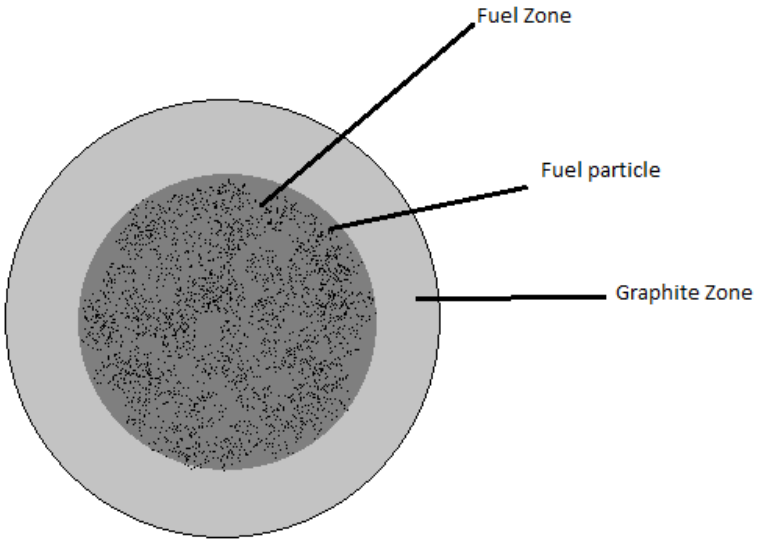

Figure 3-4: Fuel pebble

Moving on to the placement of the pebbles in the core, explicit modelling was used in the placement of pebbles. The reader is referred to Appendix A3-g for the description of Explicit modelling. Since the actual positions of pebbles in a real PBR-250 reactor were not available, various pebble configurations were modelled for comparison namely SC, BCC, and FCC unit cell arrangements. It is noted that, a real pebble bed reactor is composed of a combination of these structured arrangements, resulting in what may be a random packing. While the core with a random configuration is useful for engineering development of reactors and refuelling, it poses a

significant problem for precise thermal-hydraulic predictions (Ferng & Lin; 2013:66). Despite the benefits of using a random configuration, numerous neutronic and thermal-hydraulic calculations have been carried out using BCC and FCC arrangements as suggested by Rosales et al., (2014:3), who modelled the HTR-10 benchmark reactor, (a 10 MWt prototype HTGR also based on the HTR-MODUL) using MCNPX.

The simplest configuration is the SC structure which is made up of pebbles closely packed next to each other to form a layer of pebbles. The layers are then stacked above each other vertically. It is important to note that this is not the best representation of the packing as the spheres are not packed as closely as in reality. The packing only fills approximately 52% of the total volume it occupies, with each layer consisting of a pebble in contact with only six other pebbles (Flowers *et al.*, 2012). For all the pebble configurations, the coordination number describes the number of pebbles that each pebble is in contact with in the configuration. This convention helps visualise the number of pebbles in the vicinity of a given central pebble. Therefore, the coordination number of the SC configuration is six.

The BCC configuration has a cubic unit cell with a pebble at its centre and pebbles at all its corners. The corner pebbles are not in contact with each other but do touch the pebble at the centre, furthermore, any pebble in the structure is in contact with four pebbles above and below the layer; thus, the coordination number for this arrangement is eight.

Lastly we will consider the FCC pebble arrangement, which has the densest packing structure compared to BCC and SC; occupying approximately 74% of the given volume. It is made up of pebbles at each corner and face centre, forming a cubic structure close packing. Each pebble has twelve close neighbouring pebbles, giving it a coordination number of twelve (Flowers *et al.*, 2012). It is important to note that, there is also the hexagonal closed-packed system (HCP) which has the same coordination number and packing fraction as FCC but differ in their actual packing. Given the common packing fraction, it was decided that only the FCC packing would be studied. It is also accepted that the real packing of the pebbles would not be completely FCC or BCC. A random packing might also be considered. However, given the scope required to study packing of a random nature, such studies were left for further work.

Burnable poison pebble design

The parameters of the burnable poison particles that were employed in the core are given in Table 3-2 below. The poison particles were modelled as spherical particles and placed in the pebbles explicitly and in a random arrangement. The random arrangement was developed using the

disperse function available in Serpent (discussed in Appendix A3-h). The modelled burnable poison pebbles that contained B_4C were of one type i.e., pebbles with burnable poison particles only.

The burnable poison pebbles in this study were designed to demonstrate:

i. a method to lower the multiplication factor during reactor start-up
ii. how burnable poison particles described can be loaded to flatten the axial power profile of the core.

Table 3-2: Selected parameters of the burnable poison particle

Parameters	**B_4C**
Number of BP particles	1600
Radius (μm)	70

Adopted from Tran & Hoang (2012)

3.1.10 Control rods and worth

The study's assumptions based on the CRP are as follows:

- the^{10}B concentration should be given for the control rod and RSS (Reitsma *et al.*, 2012); and
- the control rods and the RSS can be modelled as distinct cylindrical channels.

The second assumption above simplifies a modelling problem, that a real control rod is made of short cylindrical-shaped segments (absorber pins) joined end-to-end to form a long control rod, while the RSS is composed of small absorber spheres. The control rods function by absorbing free neutrons within the rod vicinity, resulting in a negative reactivity addition and changes in the neutron flux (Rahgoshay & Noori-Kalkhoran, 2013:323). In that regard, the way the presence of control rods influences the flux is covered in this dissertation with parameters like control rod position in the reactor (Figure 4-29), being studied. Effective rod function and a relatively even flux distribution can be achieved by evenly distributing the rods within the side reflectors. Consequently, the reactivity control system modelled consisted of twelve control rods and twelve RSSs all evenly distributed around the reactor.

The control rods and the RSS contained B_4C with an assumed density of 1.7g/cm^3 as the neutron absorber. The isotopic abundance of ^{10}B in the control rods was assumed to be 90% and 50% in the RSS. These values are possible as the number density of ^{10}B in boron can be enriched from its natural isotopic abundance of 19.9% IAEA (2012:285) to possible enrichment values of 90%

(IAEA, 1996:8). The steel sleeves used in the HTR-10 were employed in the model. Their composition with an assumed density of 7.9g/cm^3, is presented in Table 3-3 below.

Table 3-3: Steel sleeve composition

Material	Composition
Cr	18%
Fe	68.1%
Ni	10%
Si	1%
^{55}Mn	2%
C	0.1%
Ti	0.8%

Adopted from IAEA (2012:236)

3.1.11 Pebble loading and operation phase of the core

Very particular conditions are required to achieve equilibrium conditions in the pebble bed reactor core. At the start with fresh core operation, the absorption of neutrons by the products of fission does not occur. The fresh core at the beginning, should therefore contain less fissile material. With that in mind, dummy pebbles are placed with normal fuel pebbles to limit the amount of fissile particles. According to Kugeler and Zhang (2019:75), a share of 50% of normal fuel pebbles to dummy fuel pebbles is a typical value for a modular HTR. The enrichment of uranium in the fuel can then be a free variable, and an enrichment of around 4% is sufficient for it to reach full power. The fresh core (without fission products) has excess reactivity thus neutron poisons must also be added during this operation phase and the control rods put place i.e., put in the reactor at a position that compensates for the excess reactivity while maintaining criticality.

Reactivity changes due to the combination of the temperature effects and build-up of neutron absorbing material e.g., Xenon-135 that occur during reactor start-up must be compensated for. When the core is brought up from a cold state, the control rods are withdrawn until slight supercriticality is achieved, resulting in a neutron population increase. The consequent increase in neutron population results in fission heat; raising the reactor's internal temperature in turn decreasing the reactivity. With this effect in mind, withdrawal of control rods must therefore always be offset to compensate for this reactivity decrease.

After about a day of reactor operation of the fresh core for xenon-135, and a few days for samarium-149, their equilibrium is reached and the excess reactivity decreases. Similarly, equilibrium is reached for samarium-149 after a few days' operation. To compensate for this decrease, the control rods in position are moved out. Control rods are used to control reactivity rather than manipulating neutron poison pebbles or dummy pebbles, which are difficult to remove. As more fission products are produced during operation, the fissile content in the core is raised by the net removal of graphite dummy pebbles and replacement with fuel pebbles. The dummy pebbles are, therefore, all removed from the fuel cycle in the first months of operation.

From the bottom of the configuration, pebbles are sent to a core unloading device (CUD) where the pebbles are characterised, with defect/faulty pebbles being removed from the line. The pebbles deemed to be non-defective are then made to pass through a Gamma Activity measurement machine which distinguishes between normal fuel pebbles and dummy fuel pebbles (Grimod, 2010:20). Normal fuel pebbles are then pneumatically moved to where they are assayed for burn-up. The fuel pebble is either sent back to the reactor or the spent fuel storage after the burn-up is determined. In this dissertation, only the fresh core state will be modelled and studied. Other aspects that occur in these reactors such as the movement of pebbles, fuel burn-up etc. will be investigated in further studies.

3.2 Methodology

Having described the PBR-250, this section will now consider how its core model was developed in Serpent. The installation and setup instructions for the Serpent computer code are provided on the following webpage: http://serpent.vtt.fi/mediawiki/index.php/Installing_and_running_Serpent. The version used throughout this dissertation is Serpent 2.1.31.

3.2.1 General details regarding Serpent input

Serpent does not have an interactive user interface as edits are made in input files and results are printed to output files. The input file is separated into several data blocks known as cards. These cards are divided by the start of the following card; that is, once a new line begins with a card, the preceding card is no longer read. A description of the syntax of the cards used in the input file is given in Appendix A:3. The interested reader is referred to Leppänen, (2015:15).

3.2.2 Full core Serpent model of the PBR-250

The Serpent model of the PBR-250 has been designed with the specifications described in Section 3.1.1. All the dimensions and structures were designed in accordance with Table 3-1, and the reader is referred to Appendix D:D for the depiction of the developed core with its dimensions.

3.2.2.1 Full core

This section describes the base core model with reference to Figure 3-5. All the core structures were built in universe 0 and consisted of three cylindrical surfaces with a shared axial centre but different radii. The inner cylindrical volume inside cylindrical surface 1 contained the pebbles and the helium coolant. Following from this, the volume between cylindrical surfaces 1 and 2 was composed of graphite with cylindrical borings for control rods and helium coolant channels, while the volume between the cylindrical surfaces 2 and 3 was composed of helium. Lastly, the space outside cylindrical surface 3 was a void, meaning that there was no material contained in that volume region.

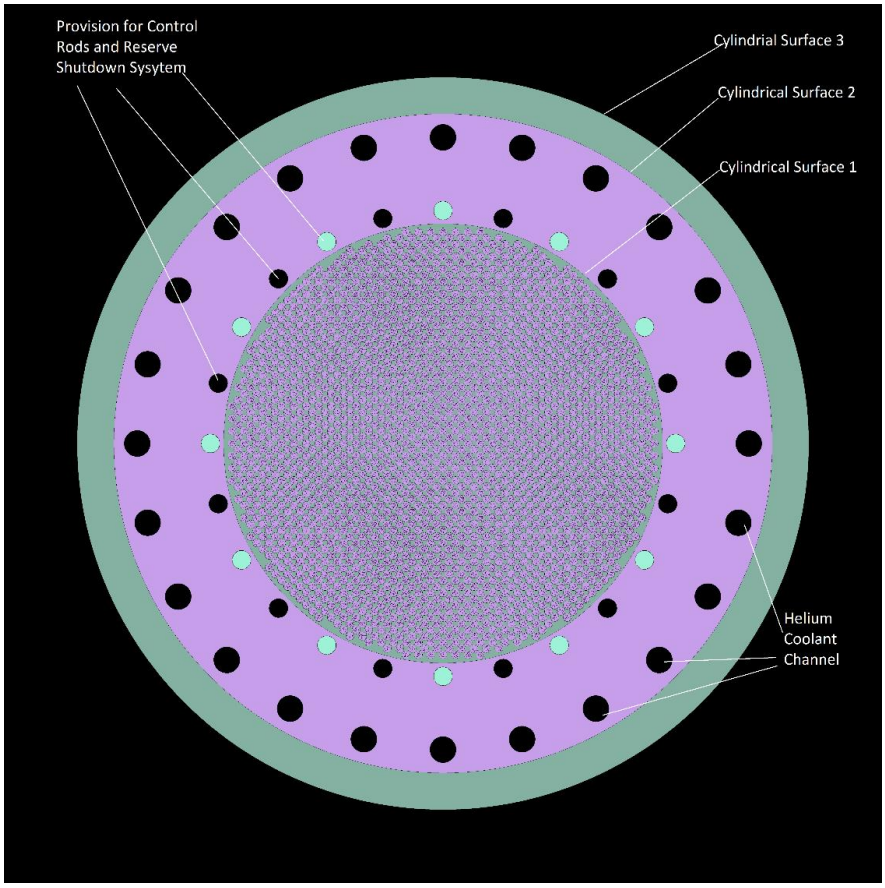

Figure 3-5: Serpent model top view of PBR-250

3.2.2.2 Fuel pebble elements

The pebble elements generated for Serpent input were of three types, namely, normal fuel pebble elements, dummy pebble elements and burnable poison pebbles. All the pebbles were generated such that they have the same structure as that shown in Figure 3-4 i.e., fuel zone and a fuel free graphite shell, just varying the type of particles present in the fuel zone. For example, the normal fuel pebble just contained fuel particles whereas the dummy pebbles did not contain any particles in the fuel zone. Following from this, the burnable poison particles described in Table 3-2 were used as the basis for the modelling of all poison particles in the pebbles. TRISO fuel and burnable poison particles were modelled implicitly. In other words, TRISO particles and burnable poison particles were placed in the graphite matrix with their position in the graphite matrix being defined in another file. The positions of the particles in the pebbles were stochastically developed using the Serpent disperse function.

The spherical pebble elements were also placed in the core explicitly, with their positions in the reactor core (cylindrical surface 1) defined in a separate file with FCC, BCC, and SC lattice structures. The centre coordinate [x;y;z] for the pebbles anywhere in the core from the centre [0;0;0] were calculated manually using adopted formulas shown in Table 3-4 below, where [a] is length of the cubic lattice and r is the radius of the pebble.

Table 3-4: Formulas for lattice structure positions

Lattice structure	Centre coordinate formulae
SC	$[a] = 2r$
BCC	$[a] = \frac{4r}{\sqrt{3}}$
FCC	$[a] = 2r\sqrt{2}$

All pebbles were modelled in such a manner that they were tightly packed and do not clip the edges of the core (cylindrical surface 1 in Figure 3-6). Therefore, all pebbles were contained in the cylindrical volume. The universe structure was such that, the fuel particles were contained in the universe made up of the matrix, and the matrix containing the particles universe made up the inside of the fuel pebble. The fuel pebble universe, surrounded by helium, then made up the inside volume of cylindrical surface 1 in universe 0 as shown by the side view of the core containing FCC arranged pebbles in Figure 3-6. The horizontal zoomed-in view of the FCC-arranged pebbles is shown in Figure 3-7. The pebbles in Figure 3-7 appear to be of different sizes because the plot

does not cut through their centres. The plot cut was intentionally offset from the centre of the cubes' faces to show the pebbles in a different parallel lattice plane.

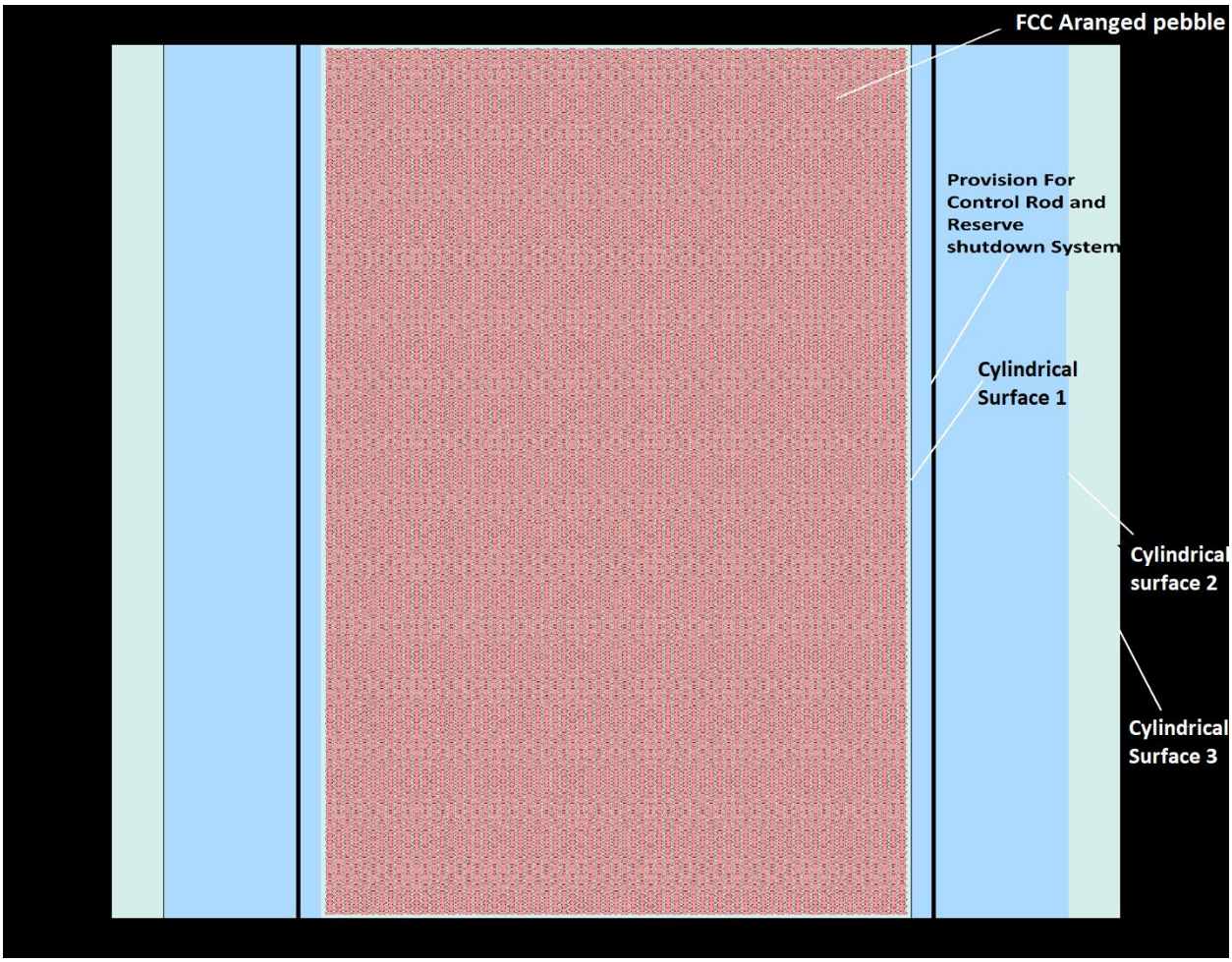

Figure 3-6:Serpent model side view of PBR-250

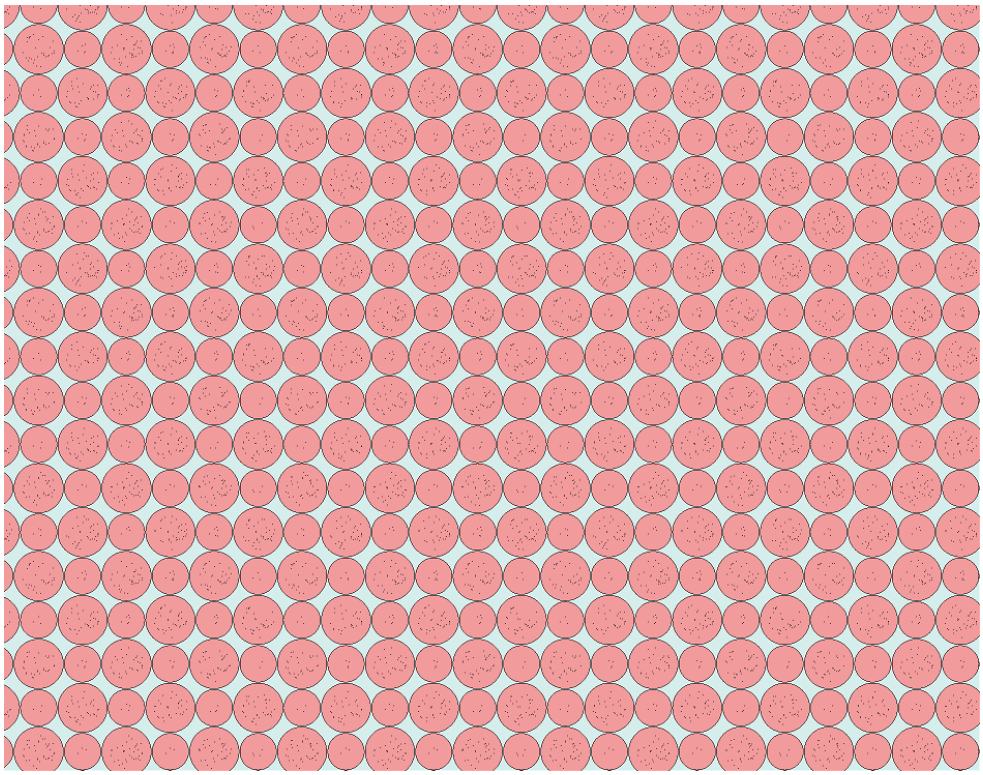

Figure 3-7: FCC Pebble arrangement

3.2.2.3 Control rods

Lastly we will consider the sleeved control rods used in this study. The rods were all modelled in universe 0 but defined in separate files to reduce the length of the main file. Different material regions of the control rods were separated using cylindrical surfaces. The depiction of the control rods developed in Serpent are shown in Figure 3-8. In that view, the volume inside cylindrical surface C_1 contained the neutron absorber material, while the volume between cylindrical surfaces C_1 and C_2 contained the sleeve material. The volume between cylindrical surfaces

C_3 and C_2 was a void region. For the RSS, the volume inside cylinder surface S-1 contained the neutron absorber material.

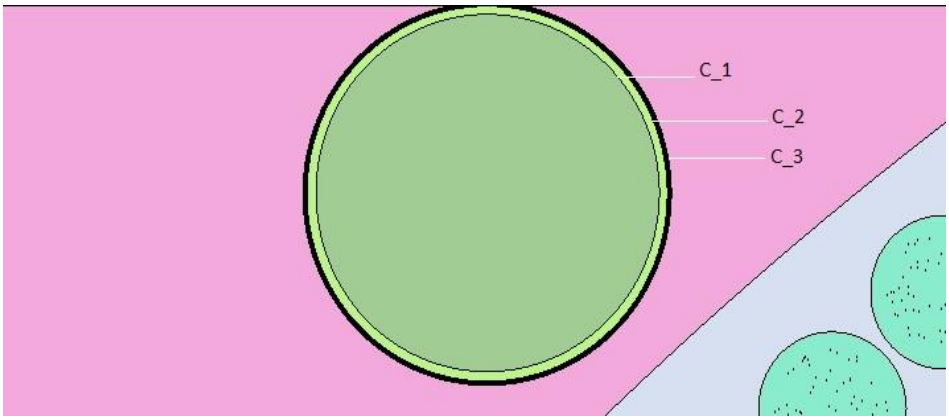

Figure 3-8: Serpent top view of control rod with sleeve

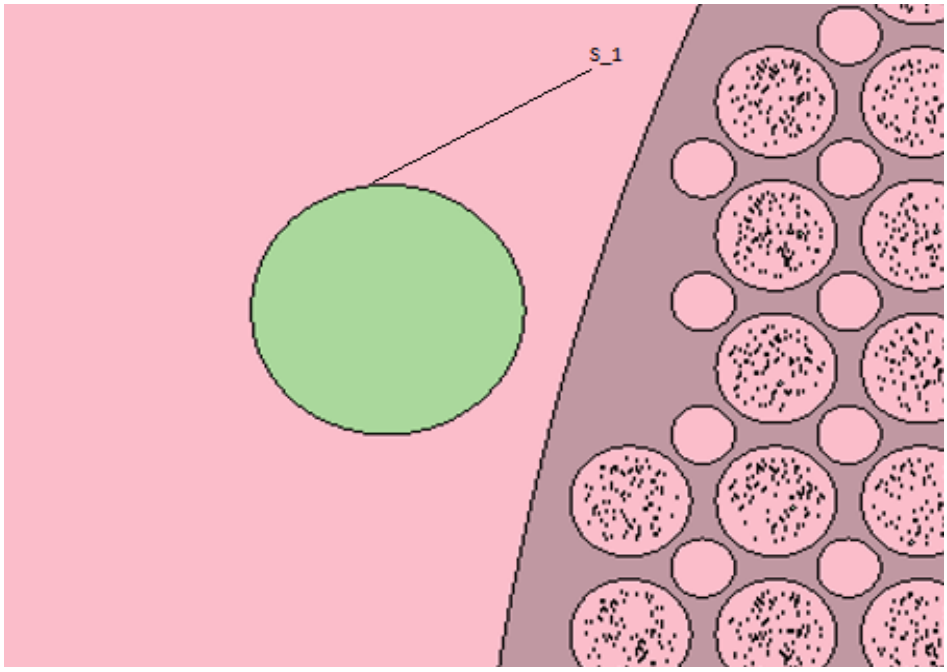

Figure 3-9: Serpent top view of RSS

3.2.2.4 Material composition

The list of the reactor materials shown in Table 3-5 below were employed as the default material data for all calculations as applied in the manually developed Serpent input file given in Appendix A. Either the atomic density or the mass density is provided for the materials as they were sufficient for the full description of the material in Serpent.

Table 3-5: Material data

Material name	Density g/cm^3	Atomic density (10^{24}/cm^3)	Isotopes	% composition
Fuel	10.4	-		
			^{238}U	80.3050
			^{235}U	7.8450
			O_2	11.8490
Helium	-	2.65156E-05		
			He	100
Control rod sleeves	7.8	-		
			Cr	18.0000
			Fe	68.1000
			Ni	10.0000
			Si	1.0000
			^{55}Mn	2.0000
			C	0.1000
			Ti	0.8000
Carbon buffer layer	1.05	-		
			C	100.0000
Pyrolytic carbon layer	1.9	-		
			C	100.0000
Silicon carbide layer	3.18	-		
			Si	70.0000
			C	30.0000
Graphite in matrix/fuel-free zone	1.74	-		
			C	

Neutron absorbing material in control rod (40% by weight of ^{10}B)	1.8	-		
			^{10}B	29.4209
			^{11}B	48.5216
			C	22.0575

3.2.3 Investigating the flux distribution of reactor models

Various core states were run in Serpent to investigate the flux distribution from mesh detectors that consider the cartesian geometry of the reactor $[x;y;z]$. The reader is referred to Appendix A3-n for the relevant option that needed to be set to give the flux results in Serpent. Considering the mesh detector, it makes a super-imposed uniform square mesh over the geometry. To demonstrate how Serpent was used to analyse the flux, let's consider the flux along the z-direction with $[x;y] = [14;14]$ and 20 mesh bins. For this 3-dimesional $20\times20\times20$ mesh, the flux values at mesh bins centres along a line that passes through the point of interest, $[x;y] = [14;14]$ parallel to the z-axis are collected and processed. Table 5-2 in Appendix C-2 provides the spatial coordinates of the mesh bin centres corresponding to the chosen number of 3-dimesional mesh bins in the $[x;y;z]$ direction, namely 20 and 40, for the flux profile analysis of the developed reactor models in this research.

For the flux studies carried out, only the bin centres located in the core were studied along the z direction. Furthermore, it should be noted that the reactor models have their centre at the coordinate $[0;0;0]$. Finally, investigations on the flux profiles of some reactor models in terms of energy were conducted, with the energy groups chosen for this study presented in Table 3-6.

Table 3-6: Neutron energy group

Ref no	Neutron group	Lower bound (MeV)	Upper bound (MeV)
1	Cold neutrons	0	2.50×10^{-8}
2	Thermal neutrons	2.50×10^{-8}	1.00×10^{-6}
3	Slow neutrons	1.00×10^{-6}	1.00×10^{-5}
4	Resonance neutrons	1.00×10^{-5}	3.00×10^{-4}

5	Intermediate neutrons	3.00×10^{-4}	1
6	Fast neutrons	1	20

Adopted from info@nuclear-power.com

Chapter 4: Results and discussion

This chapter covers the results of the models developed for the PBR-250 and if not specified, the description of the base core model discussed in Section 3.2.2.1 was used for the calculation. In summary, firstly the assessment of simulation convergence was carried out on the PBR-250 reactor model with an SC-setup; the results of the convergence studies were applied to all Serpent calculations. Secondly; full core calculations were then carried out to evaluate the multiplication factors, temperature coefficients and the control worths of the developed core. Furthermore; Serpent tally output were used to evaluate the flux profiles of the reactor models at different reactor states; in particular, the reactor states with neutron absorber material at different concentrations and positions in the core. Unless specified, for all the flux profiles the neutron energy is of group 2 (Ref No 2) described in Section 3.2.3. Lastly the SC Serpent model generated was verified with the NWURCS generated model. All in all, a PBR-250 model was created and tested.

4.1 Source convergence

This section focuses on the source convergence assessment of the PBR-250 full core, in which the results would be inaccurate without this exercise. The importance of assessing convergence is further covered in Section 2.12. To assess the convergence, two core models were employed, both with control rods fully withdrawn. Both models had a SC pebble configuration with model 1 having only fuel pebbles while model 2 had fuel and dummy pebbles at a ratio of 50:50. The reason for the adoption of two running models was to assess the effect of fuel concentration on the number of inactive cycles and the Shannon entropy of the system. Following the simulation, two sets of findings were produced, namely the cycle-wise Shannon entropy plot, and the cycle-wise multiplication factor plot. The assumptions for model 1 and model 2 runs are summed up below:

- Fuel enrichment was assumed to be 4%;
- The user-defined neutron population was set to 10 000;
- The user-defined inactive cycles set at 250; and
- Control rods are fully withdrawn.

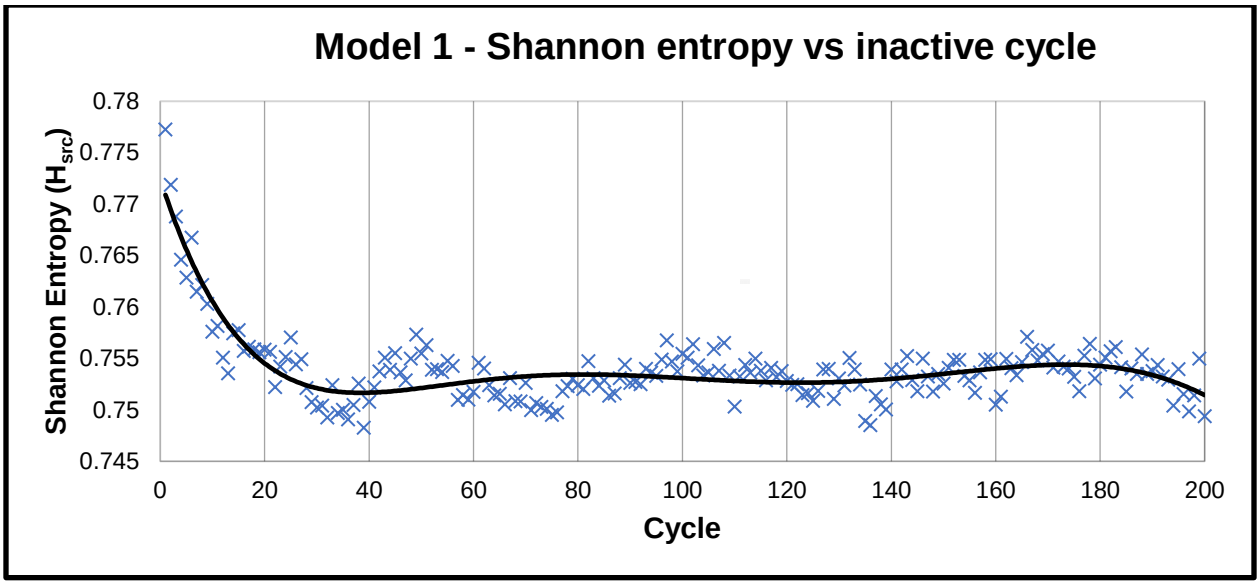

Figure 4-1: Hsrc vs number of cycles for Model 1

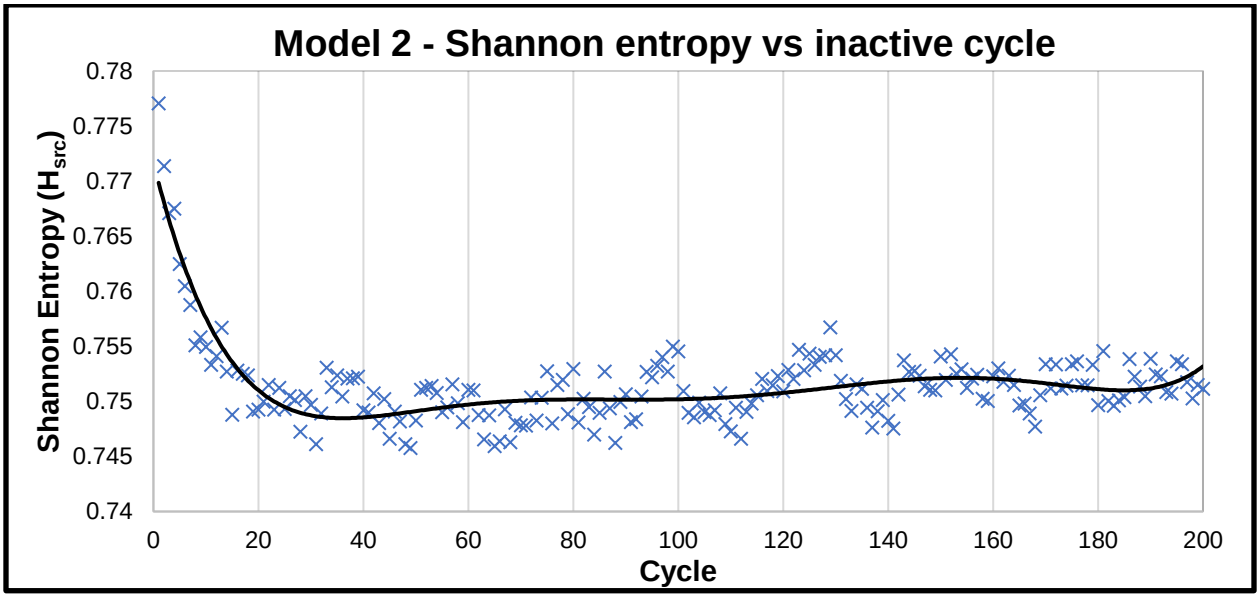

Figure 4-2: H_{src} vs number of cycles for Model 2

We will now consider Figure 4-1 and Figure 4-2 above, which represent the cycle-wise value of the Shannon entropy of source point distribution (H_{src}). As shown in Figure 4-1 and Figure 4-2, the Shannon entropy (H_{src}) of both models initially decreased as the cycle index value increased. Moreover, looking at the average line for both models, the Shannon entropy (H_{src}) attained a constant average value at about 30 skipped cycles. Consequently, convergence could then be assumed as attained after 30 cycles and a value higher than 30 skipped cycles was thus

recommended for transport calculations. The effect of fuel concentration on the cycle-wise H_{src} is marginal as can be seen that when the concentration is halved i.e., model 1 vs 2, the difference in the y-axis values of the plots is not significant.

Now considering the cycle-wise k_{eff} for both the afore-mentioned models, Figure 4-3 and Figure 4-4 show that the k_{eff} value for both models began at a default value of unity, and increased initially with the cycle number. More importantly, the examination of the average lines for both models revealed that the k_{eff} began to attain a constant average value at about 30 skipped cycles. It becomes evident that the cycle-wise Shannon entropy followed a similar behavioural trend as the cycle-wise multiplication factor. From this study, in all, to ensure that all models were conservative, a value of 80 skipped cycles was adopted. The cycle-wise Shannon entropy for the BCC and FCC setup is shown in Appendix C-1, confirming that the chosen number of inactive cycles was sufficient for fission source distribution to be statistically constant.

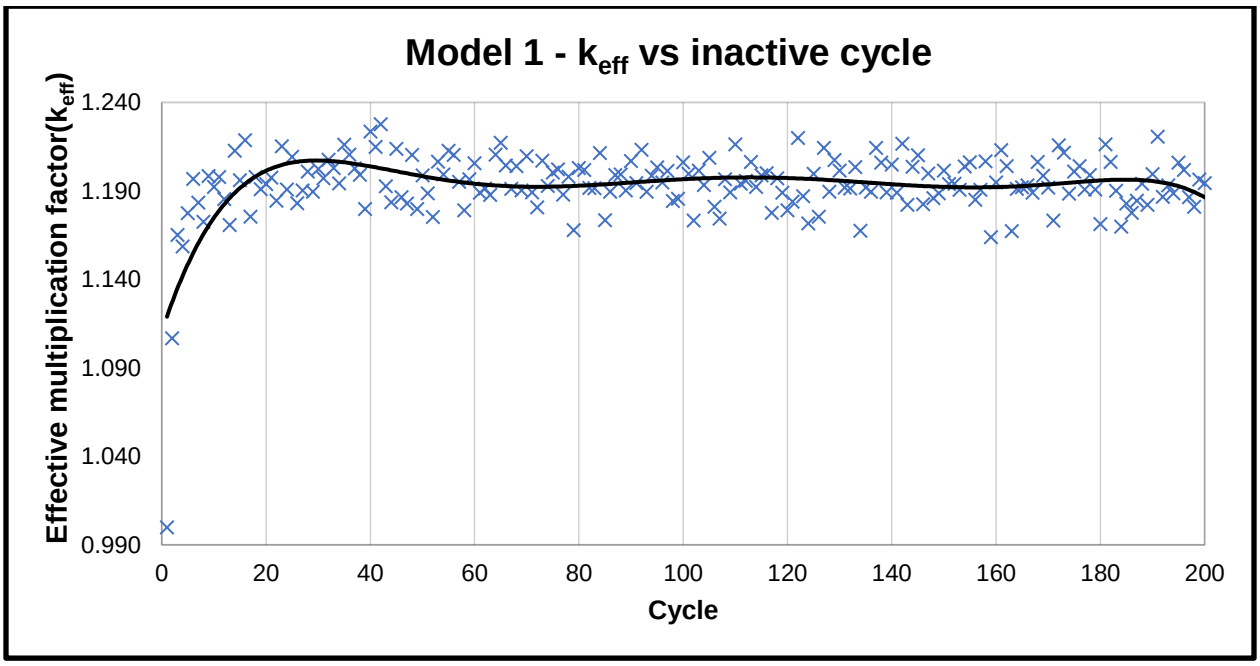

Figure 4-3: k_{eff} vs. number of cycles for Model 1

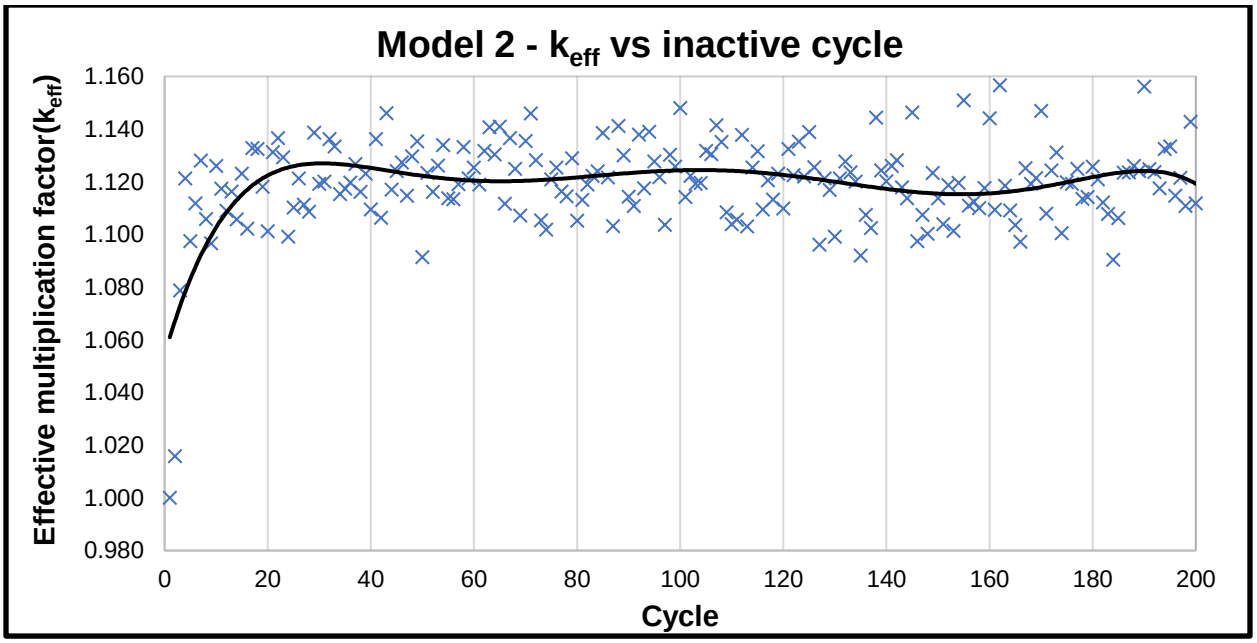

Figure 4-4: k_{eff} vs. number of cycles for Model 2

4.2 Full core model

Overall, this section assesses the effective multiplication factor of different reactor-states from criticality calculations. We begin by looking at the fresh core and establish possible ways in which we can arrange the fresh core such that it is within range of achieving criticality i.e., employing dummy pebbles, burnable poison pebbles etc. Moving on to the sensitivity analysis aspects, the temperature coefficients for the model was examined as inherent safe temperature regulation is an important safety priority for the safety of the PBR-250. The temperature fields (temperatures at all points in a given space at a given time) of a reactor are a major parameter that determines the state of a reactor. This emphasises the point that the reactor does not have a single temperature anytime during operation despite the assumption of relatively constant temperatures for all materials in the calculations. The safe shutdown and the required performance for reactivity balance in reactor systems is a fundamental topic in reactor safety, thus the control rod worth and SCRAM reactivity were therefore assessed for the base core model.

4.2.1 Initial multiplication factor

Four different core configurations with their parameters given were built to assess their multiplication factor. The reader is directed to section 3.2.2.1 for the core description.

Model 1 configuration parameters:

1. the enrichment of fuel was assumed to be 4%;
2. the configuration for the pebbles had a 50% ratio of dummy to normal fuel pebbles; and
3. the influence of control rods and burnable poisons was not included.

Model 2 configuration parameters:

1. the enrichment of fuel was assumed to be 4%;
2. the core contained fuel pebbles only; and
3. the influence of control rods and burnable poisons was not included.

Table 4-1: The multiplication factors obtained from Serpent for the core models 1 & 2.

Model	SC	BCC	FCC
1	1.11562 +/- 0.00009	1.22416 +/- 0.00009	1.25262 +/- 0.00009
2	1.18589 +/- 0.00009	1.26027 +/- 0.00009	1.28035 +/- 0.00009

Table 4-1 above gives the multiplication factors obtained from Serpent for models 1 and 2. All values recorded indicate a supercritical reactor setup with model 2 showing higher multiplication factors in comparison to model 1. From this, the notable difference between the multiplication factors was due to the difference in the amount of fissile material between the models. Furthermore, it is evident from the above table that the multiplication factor is larger for the FCC calculation compared to the BCC calculation. However, this had been expected since the packing fraction of FCC is greater than of BCC, resulting in a higher amount of fissile material in the FCC model.

We will now consider the effect of the packing fraction on the multiplication factor in more detail. We begin by looking at Table 4-3, which shows the number of pebbles in each reactor configuration with the SC configuration having the least number of pebbles and the FCC configuration having the most pebbles due to the reasons highlighted in Section 3.1.9. For pebble-packing in the core region, it is important to note that it was carried out in such a manner that the dimensions of the reactor were kept constant (Height=11m and Radius=1.5m) and the reactor filled with pebbles in a way that ensured that they did not clip the edges of the reactor core. To investigate the effect of the packing fraction on k_{eff}, the number of pebbles in the FCC setup were matched (by removing pebbles) with those in the BCC configuration, in the following manner:

$$Number\ of\ pebbles\ in\ BCC\ setup\ = Number\ of\ pebbles\ in\ FCC\ setup = 444\ 293 \quad (4\text{-}1)$$

This scenario is analogous to a setup in which a BCC configuration is shaken into a FCC configuration. Matching of the number of pebbles between the BCC and the FCC configurations renders the effective height of the FCC (matched pebbles) to be less than that of the BCC as pebbles are more closely packed in the FCC configuration. The multiplication factor of the FCC (matched pebbles) setup was found to be 1.27859 +/- 0.00009, which is greater than the value obtained for the BCC (model 2) setup in Table 4-1. The difference between the FCC models i.e., FCC matched vs FCC unmatched, was 0.00145 or 145pcm, and that between the FCC and BCC i.e., given by equation 4-1, of the same number of pebbles was 0.01832 or 1832pcm. The pcm unit is approximated by multiplying the difference in the multiplication factor by 10^5 since it is a suitable number to utilise in comparisons.

The outcomes of the simulations showed that:

1) the packing fraction has a very significant influence on the multiplication factor;
2) the multiplication factor increases with the packing density; and
3) the effect of changing the packing fraction is more significant than changing the number of pebbles as seen summarised in Table 4-2:

Table 4-2: Summary of on packing fraction findings

Criteria for comparison	**Difference in the value of K_{eff}**
FCC packing with 483 293 pebbles against FCC packing with 444 293 pebbles	145pcm
BCC packing with 444 293 pebbles against FCC packing with 444 293 pebbles	1832pcm

Since this reactor was configured with a constant temperature profile, no control rod insertion, and radial and axial symmetry, the flux profile was predicted to be like that of a cosinusoidal profile in the axial direction; stated otherwise, it was expected that the flux peaks at the axial centre of the core, as was observed in section 4.2.6.1. Consequently, this indicates that the density of pebbles in this region was of importance as the density of pebbles remained the same in both the FCC models. This could, therefore, explain why the multiplication factor did not change a great deal. However, because the number of pebbles had decreased, effectively decreasing the amount of ^{235}U, there was a corresponding decrease by 145pcm.

Table 4-3: Number of pebbles per design

Setup	Number of pebbles
SC	346 842
BCC	444 293
FCC	483 293

Overall, models 1 and 2 each indicated the extent to which the multiplication factor was affected by the type of packing which was utilised. Despite this, it is noted that a random close packing proved to be the structure closest to a real-life scenario. A random packing fraction of 0.61 was used for the PBMR reactor in both neutronic (Ardiansyah *et al*., 2021:2) and safety studies (Van Heerden *et al*., 2006:1). As such, it is recommended that future research include studies of random packing utilising the disperse function described in Appendix A3-h to verify the above since time constraints related to the current project prevented its in-depth exploration. Furthermore, it was noted that a packing fraction of 0.61 lies between the SC and BCC lattice packing.

We will now consider model 3, which was used to assist to find a reactor state in which criticality could be achieved by providing a parameter overview of incorporating ^{10}B to the fresh core on the multiplication factor. This would be very useful for the purpose of the reactor design as it captures the initial conditions of an actual reactor at the beginning of its cycle, in which there was no parasitic absorption by fission products, as described in Section 3.1.11.

Model 3 configuration parameters:

1. the enrichment of fuel was assumed to be 4%;
2. the configuration for the pebbles had a 50% ratio of normal fuel to burnable poison pebbles;
3. the burnable poisons in the pebbles were B_4C particles; and
4. the analogue k_{eff} was calculated for a concentration range of ^{10}B in B_4C particles.

Figure 4-5 below presents a range of concentrations of ^{10}B assessed and records the multiplication factor. It was noted that a target of $k_{eff} = 1.00000$ was not required using the burnable poisons, since effects, such as the temperature defect and xenon and Samarian build-up, reduce the value of k_{eff} during reactor start-up. It is noted that, for the reactor state at t=0, insertion of the control rods will push k_{eff} to be 1.00000 or lower. The calculated values capture the two packing

schemes, namely BCC and FCC, with the multiplication factor decreasing as the enrichment of ^{10}B (the significant neutron absorbing component) is increased. The variation for both setups is almost linear with higher multiplication values recorded for the FCC setup compared to the BCC setup for the same reasons highlighted in model 2 (higher packing fraction in FCC compared to BCC).

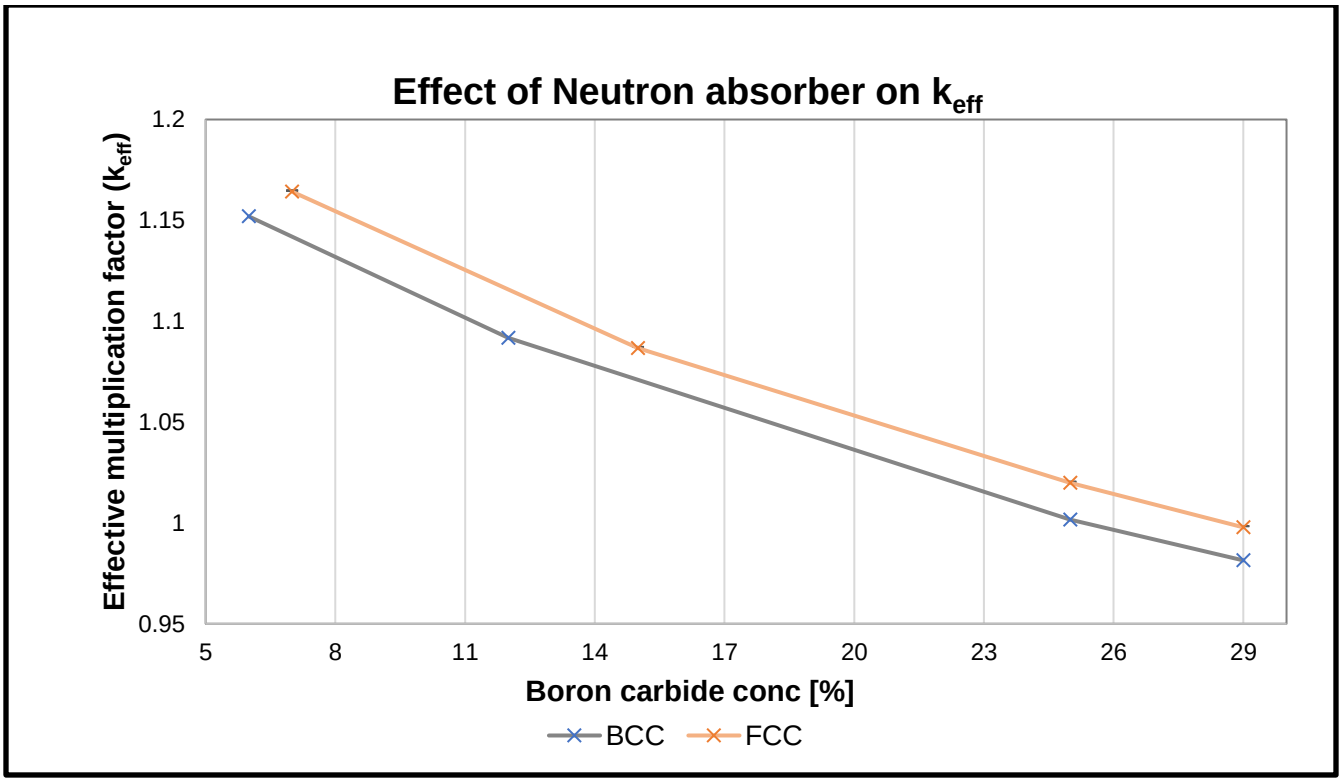

Figure 4-5: The effect of neutron absorbers on the multiplication factor

We will lastly now discuss model 4, which was developed to overcome the problem described in Section 3.1.8 about how the effect of removing the top and bottom structures effects the value of k_{eff}.

Model 4 configuration parameters:

1. the enrichment of fuel was assumed to be 4%;
2. the core contained fuel pebbles only and was of FCC configuration; and
3. the influence of control rods was not included.

The depiction of the model is shown in Figure 3-2. The chosen densities for the top and bottom reflector material used for the calculations with their subsequent multiplication factor, are shown in Figure 4-6 below.

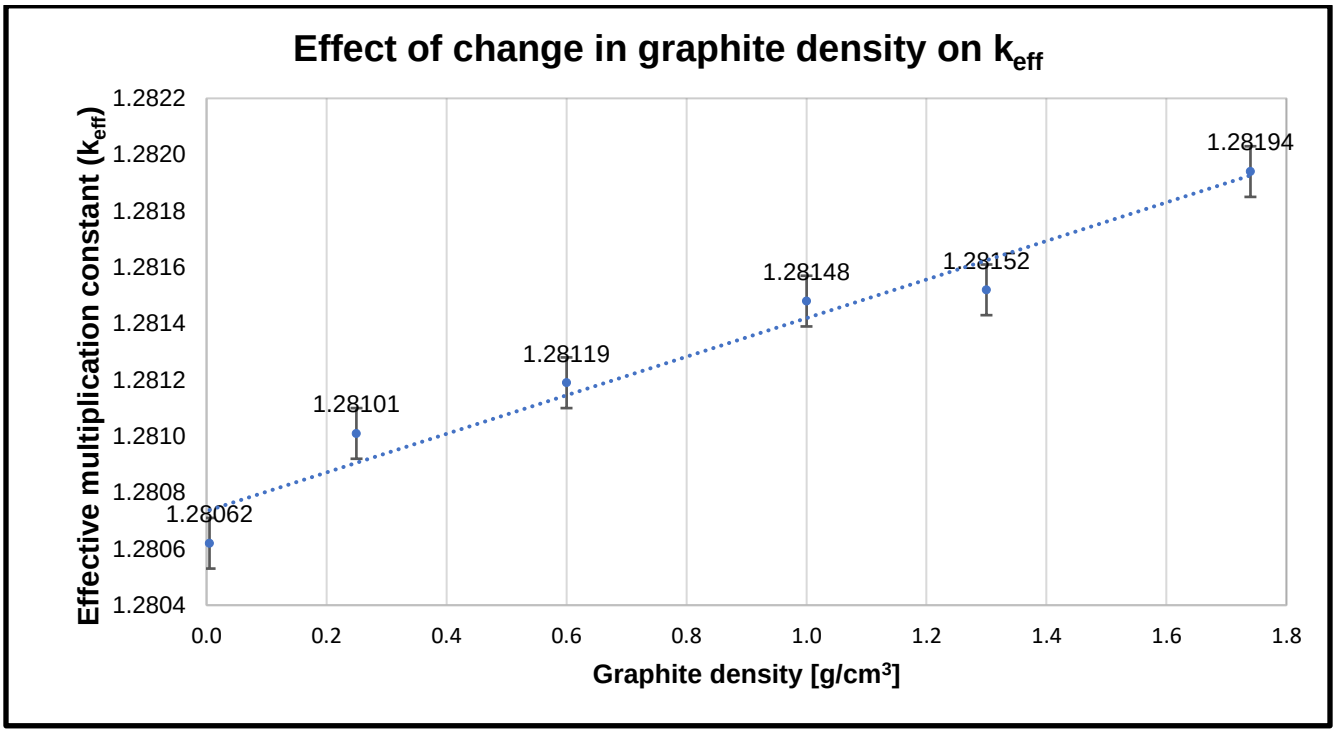

Figure 4-6: The study of the effect of the removal of top structures

In terms of the chosen reactor conditions, the multiplication factor increased with rising graphite densities. This was due to graphite's excellent neutron reflecting properties; implying that the higher the graphite density value, the greater the quantity of graphite present, resulting in more neutron reflection back into the core and thus higher values of k_{eff}. In other words, it was determined that the inclusion of the top and bottom structures reduces the neutron leakage from the core through the top and bottom of the reactor. This section also justifies the study done for model 2. Put simply, a difference in k_{eff} between the two density limits in Figure 4-6 of 132pcm in terms of neutron economy (i.e., equivalence in pebbles lost) is significant and it is therefore important that this structure be modelled in future studies on this reactor.

The flux profiles of the reactor setups at graphite densities of 1.74g/cm^3, 0.6g/cm^3 and 0.0005g/cm^3 are shown in Figure 4-7 below, with their corresponding multiplication factors given in Figure 4-6. It should be noted that the top and bottom structures for the real reactor are not solid structures because channels are necessary for coolant flow, pebble entry and exit etc.; hence, the density of graphite was varied. In principle, more material regions should be defined,

particularly these helium filled regions in the reflector structures. However, due to the low neutronic effect of low-density helium, it was not included in this study. Figure 4-7 shows that the flux profile of the reactor configuration with higher graphite density values flattens, in other words they have a lower flux peak value and greater flux values towards the reactor edges than those with lower graphite density values.

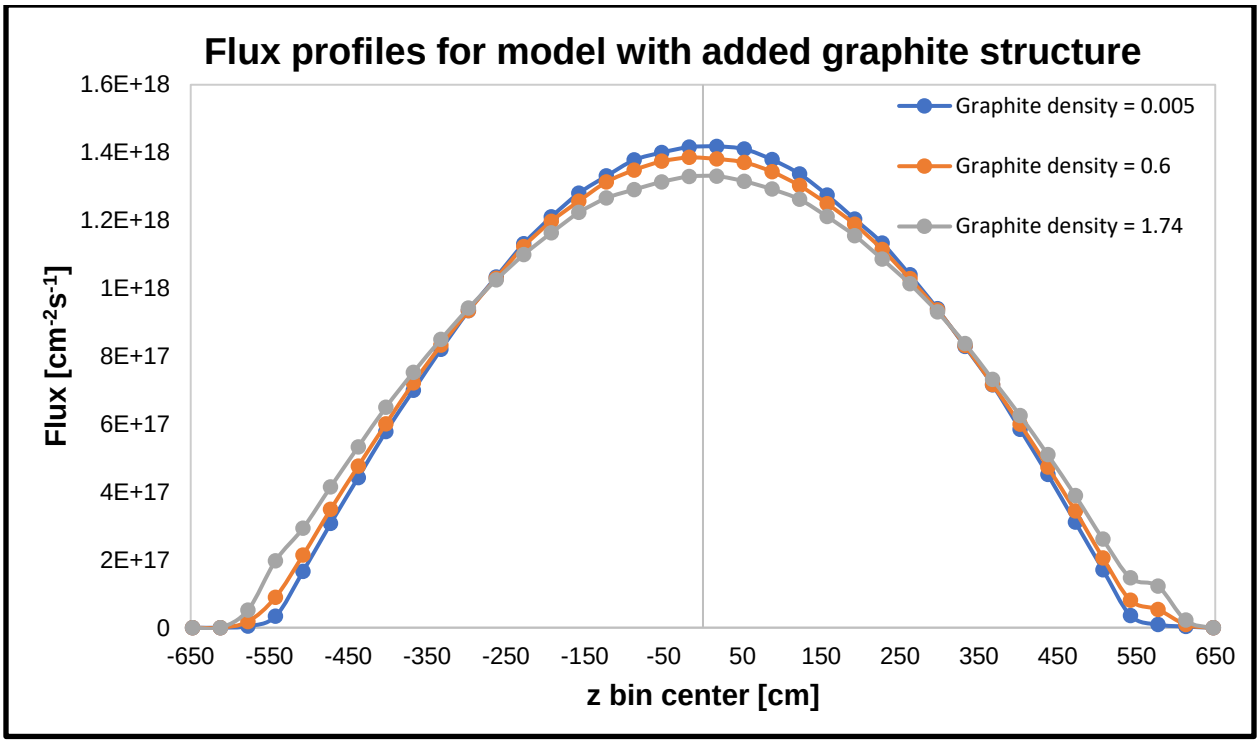

Figure 4-7: The flux profile for models at different top and bottom structure densities

4.2.2 Temperature coefficients

Moving on to the sensitivity analysis aspects of this study, the estimation of the temperature coefficient encompasses the Doppler, moderator, coolant, and isothermal temperature coefficients. Some previously calculated temperature coefficients for the HTGR are shown in Table 4-4 for a broad comparison of the findings presented in this section.

Table 4-4: Reactivity coefficients calculated for the HTGR

Reactivity coefficient	**HTGR**
Doppler ($\Delta k/k \times 10^{-6}K^{-1}$)	-7
Coolant void ($\Delta k/k \times 10^{-6}K^{-1}$)	_

Moderator ($\Delta k/k \times 10^{-6}\ K^{-1}$)	+1

Adopted from Stacey, (2018:167)

The calculation of the temperature coefficient for the developed model was carried out in the following order:

1. Moderator temperature coefficient;
2. Coolant temperature coefficient; and the
3. Doppler temperature coefficient.

To calculate the coefficients, we must define a few terms. Firstly, the deviation of the multiplication factor from the initial state is expressed in terms of reactivity. The reactivity coefficients α_ρ can be approximated in first order as :

$$\alpha_\rho = \frac{\Delta_\rho}{\Delta Tx} \qquad 4\text{-}2$$

Where

$\Delta_{\boldsymbol{\rho}}$ = reactivity changes because of changes in parameters such as fuel or moderator temperatures. It is given by:

$$\Delta_\rho = \frac{k_2 - k_1}{k_1 . k_2} \qquad 4\text{-}3$$

$\Delta \boldsymbol{Tx}$ = the change in reactor component temperature. It is important to note that Serpent includes a function (Doppler-broadening pre-processor routine) that lets the user alter the temperatures of ACE format cross-sections as the cross-section data libraries is just provided at 300K intervals (Leppänen, 2015:50).

k_i = multiplication factor before and after change.

Equation 4-3 is derived in Appendix B-3.

Lamarsh & Baratta, (2001:365) describe the temperature coefficient as $\alpha_\rho = \frac{\partial \rho}{\partial Tx}$ were infinitesimal changes of the temperature variables *T* and ρ are given in the expression. A small temperature change (ΔTx =5K) was then chosen which was not too small that changes would not be significant and observable. It was noted that the reactivity coefficient could be calculated using a derivation from the six-factor formula as proposed in a current master's study by A. Blennies,(2022). However, since the six-factor formula is in principle a two-energy group formula, it was not

appropriate to use such a formula derived from the six-factor formula as a graphite reactor shows more spectral heterogeneity than a two-group energy formalism would allow.

Model parameters for all the temperature coefficient calculations:

1. the enrichment of fuel was assumed to be 4%;
2. the core contained pebbles with fuel only;
3. the influence of control rods was not included; and
4. only BCC and FCC models were simulated.

4.2.2.1 Moderator temperature coefficient

To accurately evaluate and analyse the moderator temperature coefficient, the temperature of the fuel particles and coolant material had to be kept at a constant temperature, and since the PBR-250 is a graphite-moderated reactor, all the graphite structures temperatures were varied. Notably, this was a significant approximation because the temperature response of graphite is different when there is a change in reactor power. To illustrate, during reactor power changes, graphite structures embedded with coated fuel particles will display a temperature change earlier than graphite structures outside the fuel pebbles.

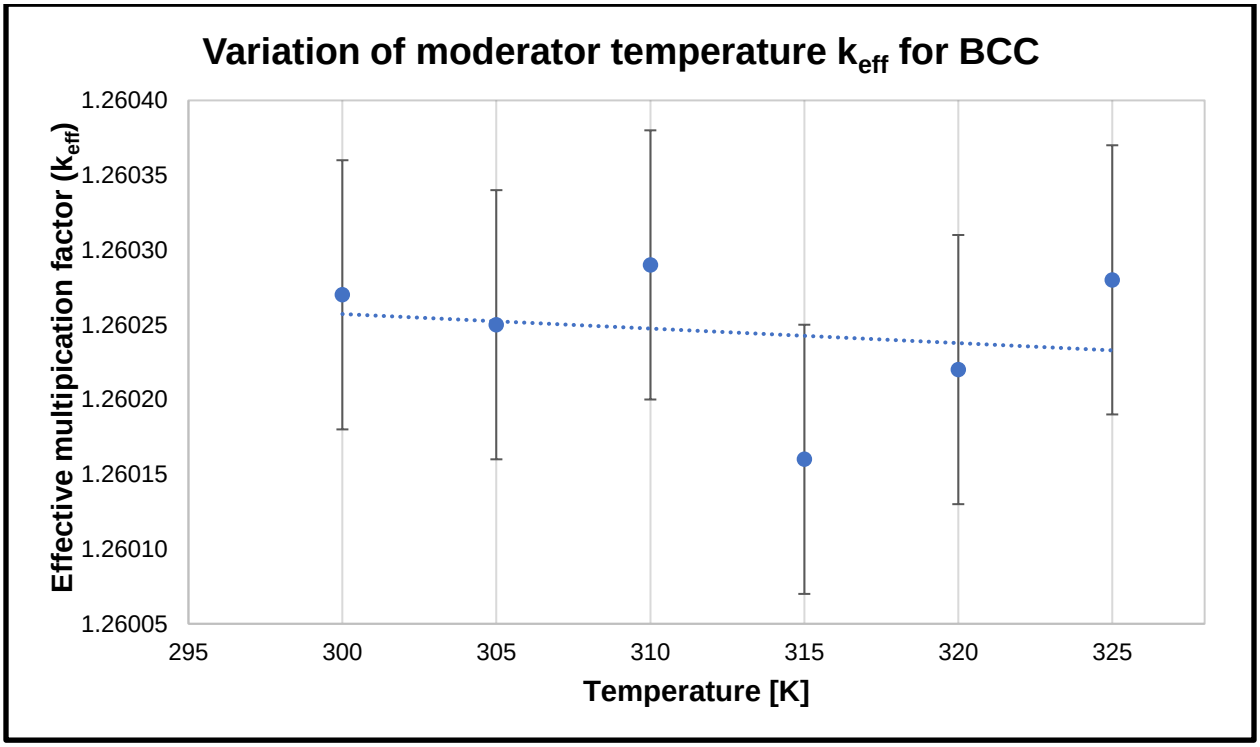

Figure 4-8: Variation of moderator temperature k_{eff} for BCC

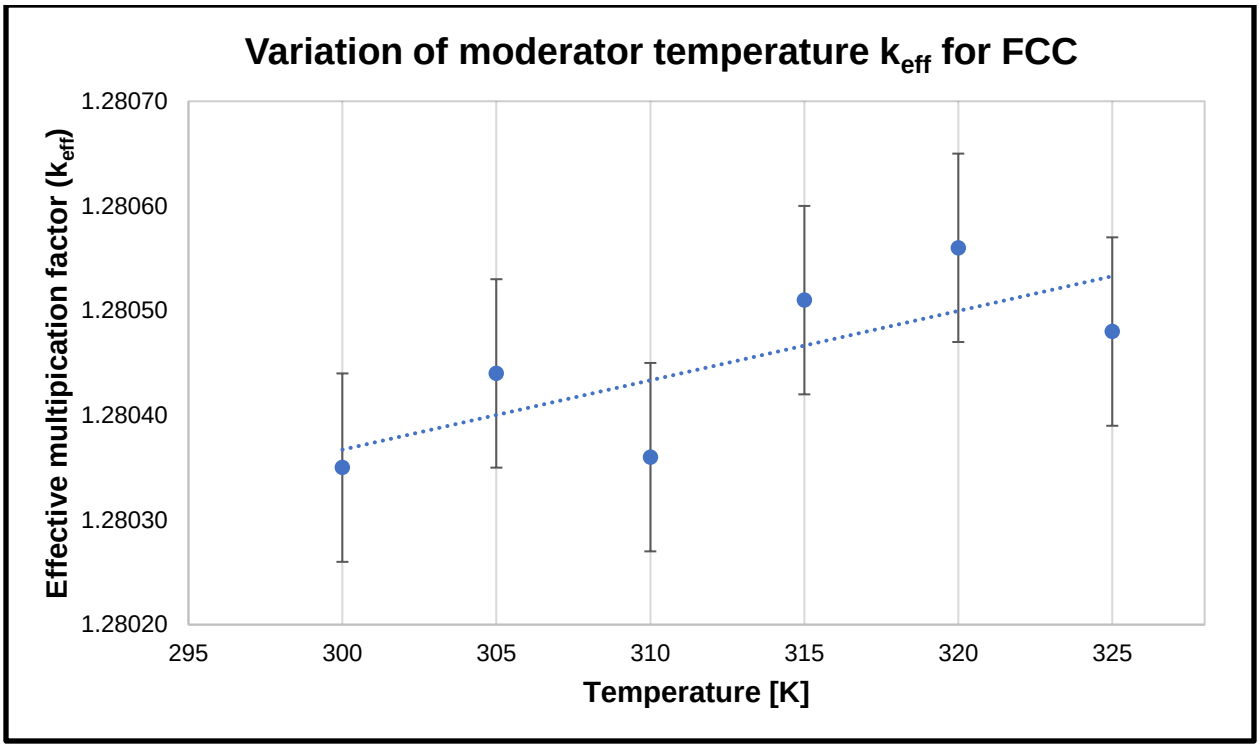

Figure 4-9: Variation of moderator temperature k_{eff} for FCC

Figure 4-8 and Figure 4-9 above show the effect of changing the moderator temperature on the effective multiplication factor for both the BCC and FCC setups in temperature increments of 5K i.e. ΔTx =5K, from 300K to 325K. Considering these figures, it is seen that some k_{eff} values lie within the statistical estimate of other k_{eff} values at different temperatures. To illustrate, in Figure 4-8 at temperatures of 300K and 325K, and in Figure 4-9 at temperatures of 300K and 310K, the k_{eff} value could statistically be the same in a different run (by changing the random number generator seed) as their values lie within the same statistical range. Therefore, it was determined that there was no clear correlation between the k_{eff} and the corresponding temperature describing the moderator temperature coefficient.

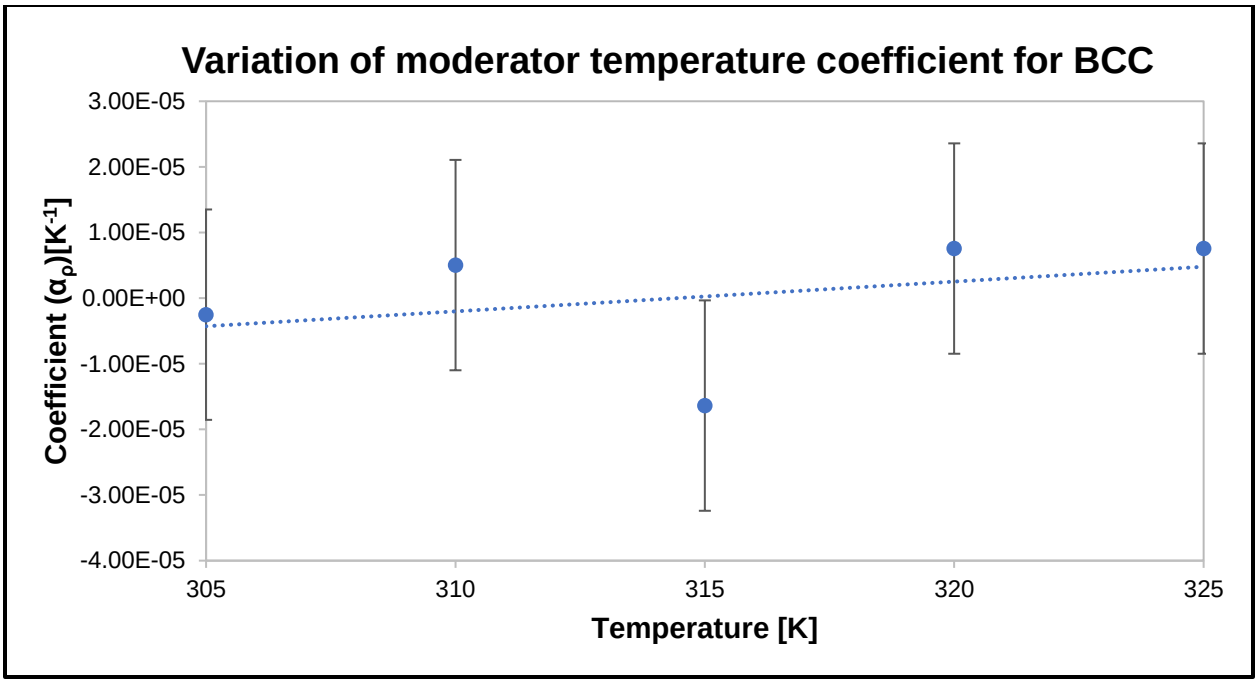

Figure 4-10: Variation of moderator temperature coefficient for BCC

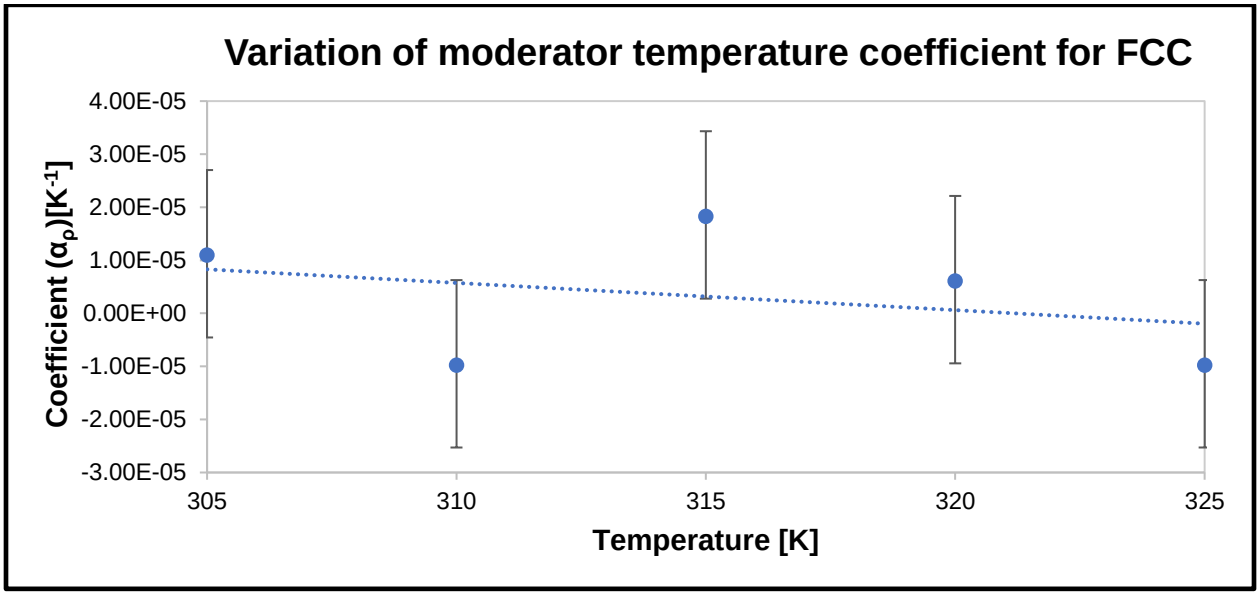

Figure 4-11: Variation of moderator temperature coefficient for FCC

Considering the Figure 4-11 and Figure 4-10 above, which show the variation of the moderator temperature coefficient (α_ρ), it was found that there was no clear correlation between the moderator temperature coefficient and the temperature.

4.2.2.2 Coolant temperature coefficient

To evaluate and analyse the coolant temperature coefficient, the temperature of all other materials that make up the reactor were kept constant, while the temperature of the helium coolant was varied. Firstly, we consider Figure 4-12 and Figure 4-13 which show the effect of variation of the coolant temperature with increments of 5K i.e., ΔTx=5K, from 300K to 325K on the effective multiplication factor for both the BCC and FCC setups. From the figures below, some multiplication factor values lie within the statistical estimate of other k_{eff} values at different temperatures. To illustrate, in Figure 4-12 at temperatures of 300K and 315K, and in Figure 4-13 at temperatures of 305K and 320K, the k_{eff} values could have been statistically be the same in a different run (by changing the random number generator seed) as their values lie within the same statistical range. Therefore, it can be concluded that there was no clear correlation between the k_{eff} and the corresponding temperature describing the coolant temperature coefficient.

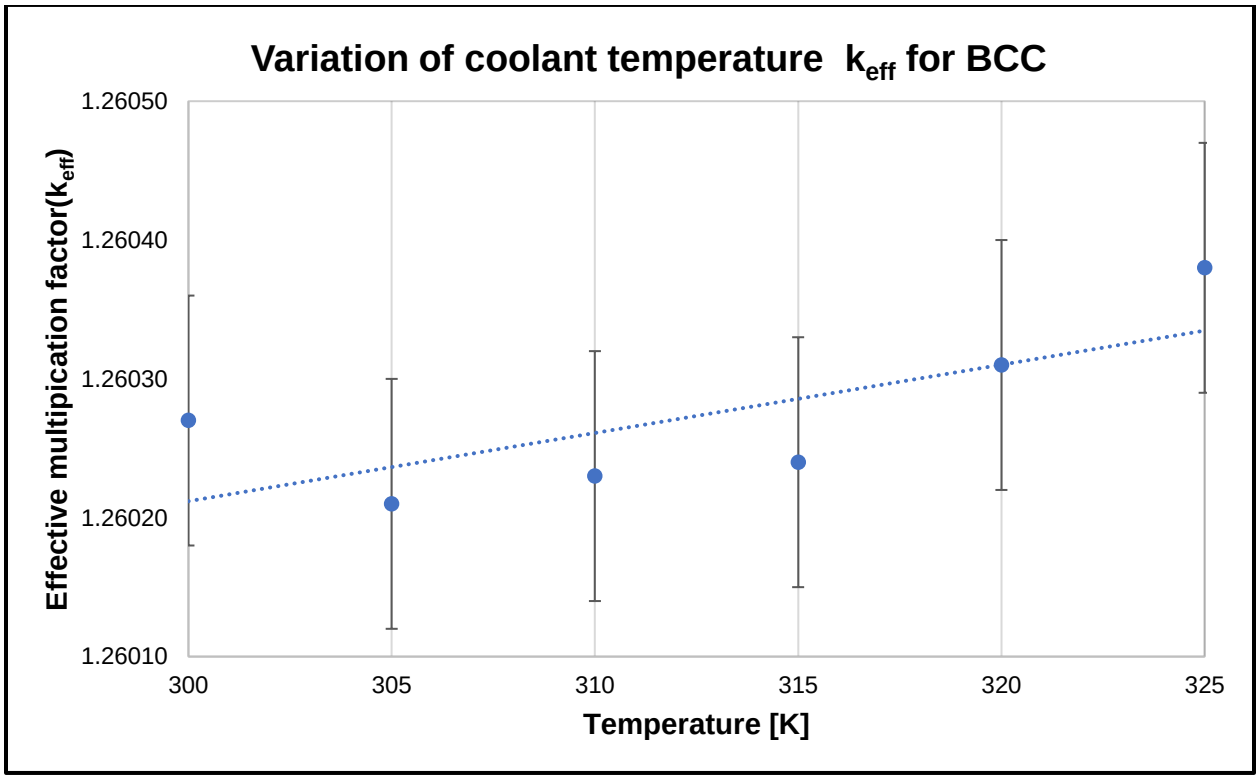

Figure 4-12: Variation of coolant temperature k_{eff} for BCC

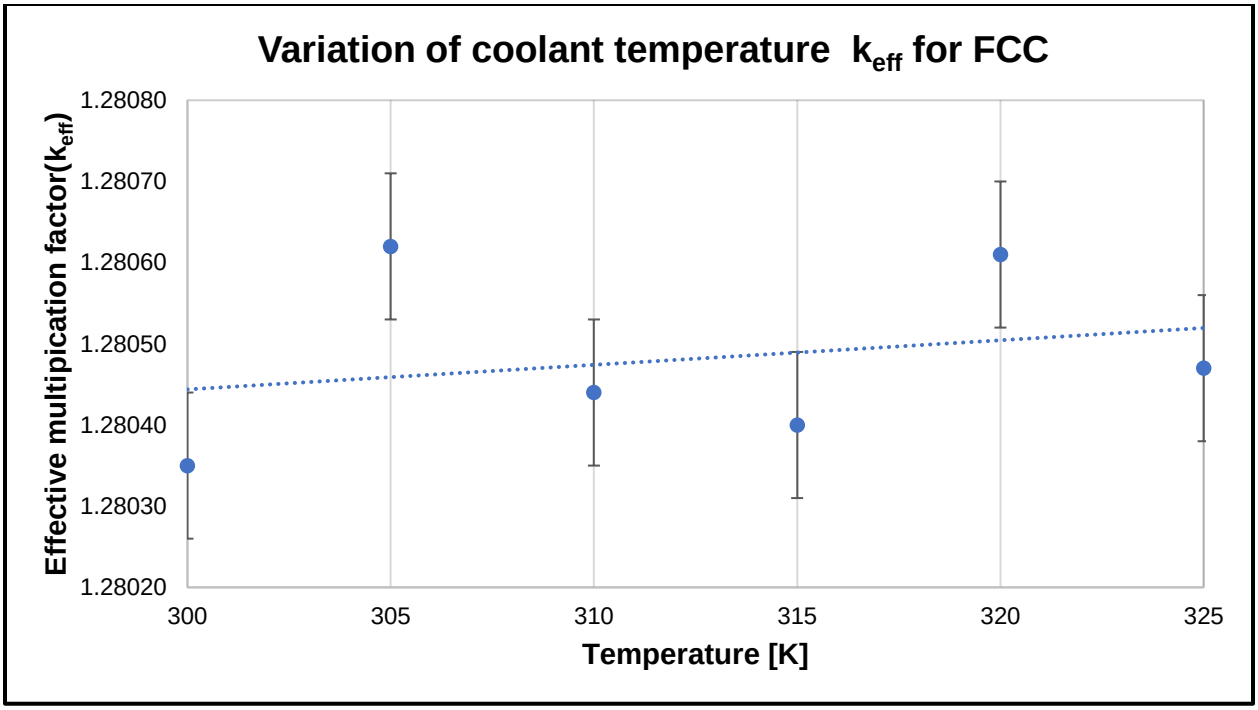

Figure 4-13: Variation of coolant temperature k_{eff} for FCC

Now considering Figure 4-14 and Figure 4-15, relative to the magnitude of values of the fuel temperature coefficient (Figure 4-18 and Figure 4-19), the coolant temperature coefficient values were low. This is due to helium having a generally low density and a low neutron absorption cross-section. For most reactor designs, the coolant temperature coefficient is not usually calculated because its contribution to the total temperature coefficient of the specific reactor is marginal, or, from the reasons highlighted, has no observable effect. There was no clear correlation between the coolant temperature coefficient and the temperature.

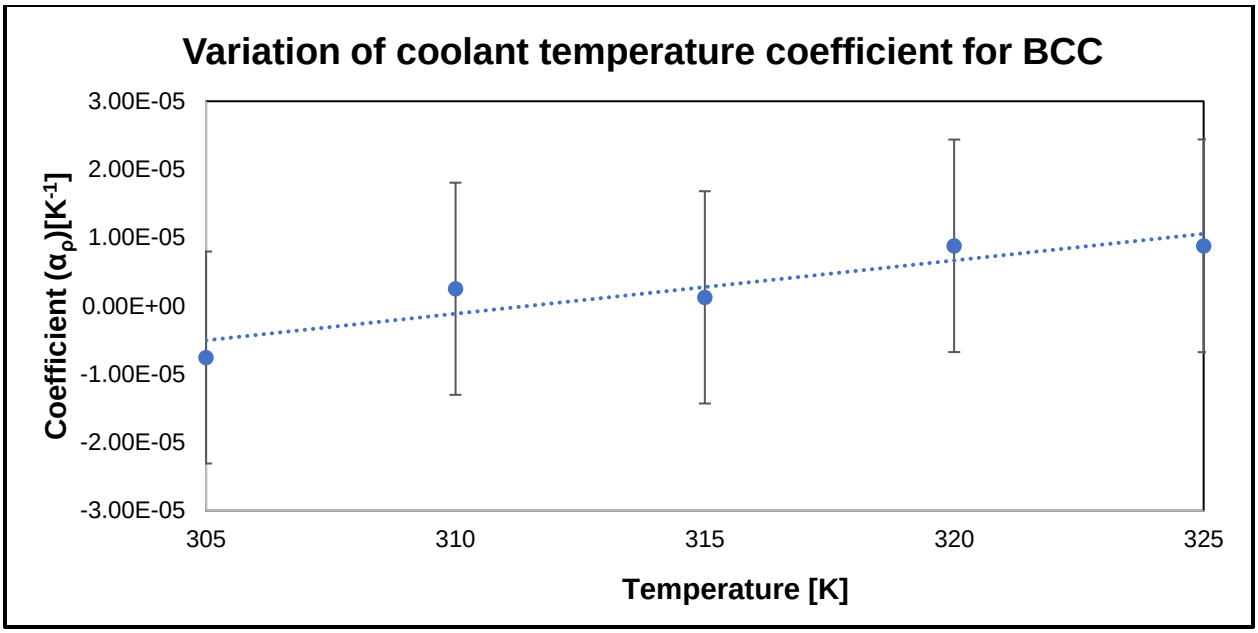

Figure 4-14: Variation of coolant temperature coefficient for BCC

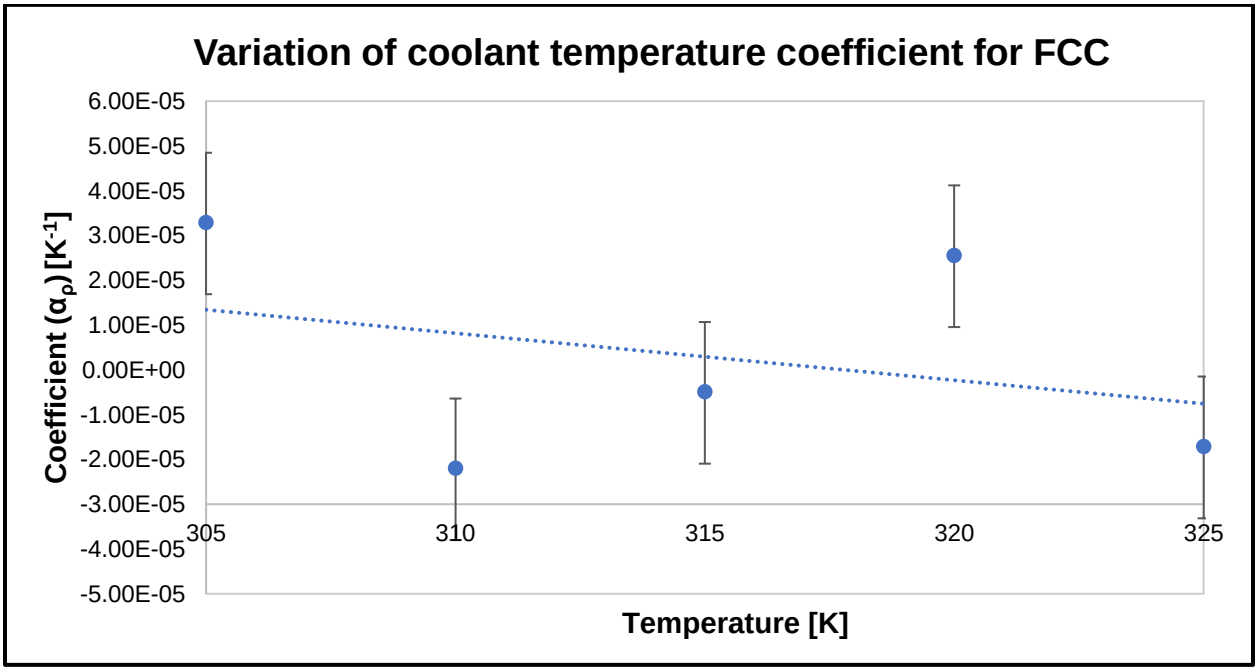

Figure 4-15: Variation of coolant temperature coefficient for FCC

4.2.2.3 Doppler temperature coefficient

Lastly we will consider the Doppler temperature coefficient. To evaluate and analyse the Doppler temperature coefficient, the temperature of the fuel particles were varied while the temperature of all the other reactor structures was kept constant. Considering the simulation outcome for the effect of variation of fuel particle temperature on k_{eff} shown in Figure 4-16 and Figure 4-17 below,

it is clear that the effective multiplication factor decreased with an increase in fuel particle temperature. The latter trend occurs because of the effect previously described in section 2.11, that is, the increase in temperature resulted in the Doppler broadening of the resonance capture cross-sections of ^{238}U. Consequently, the broadening caused more free neutrons to be absorbed by ^{238}U; thus, it decreased the value of k_{eff}.

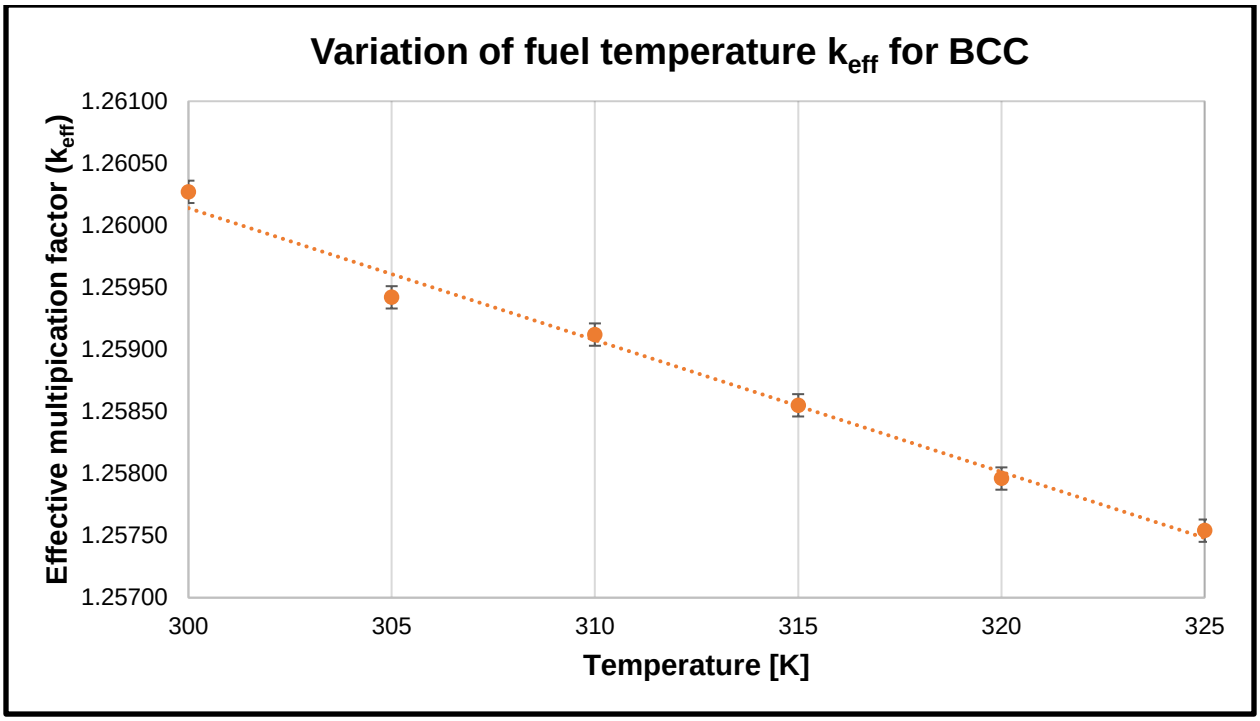

Figure 4-16: Variation of fuel temperature on the k_{eff} for BCC

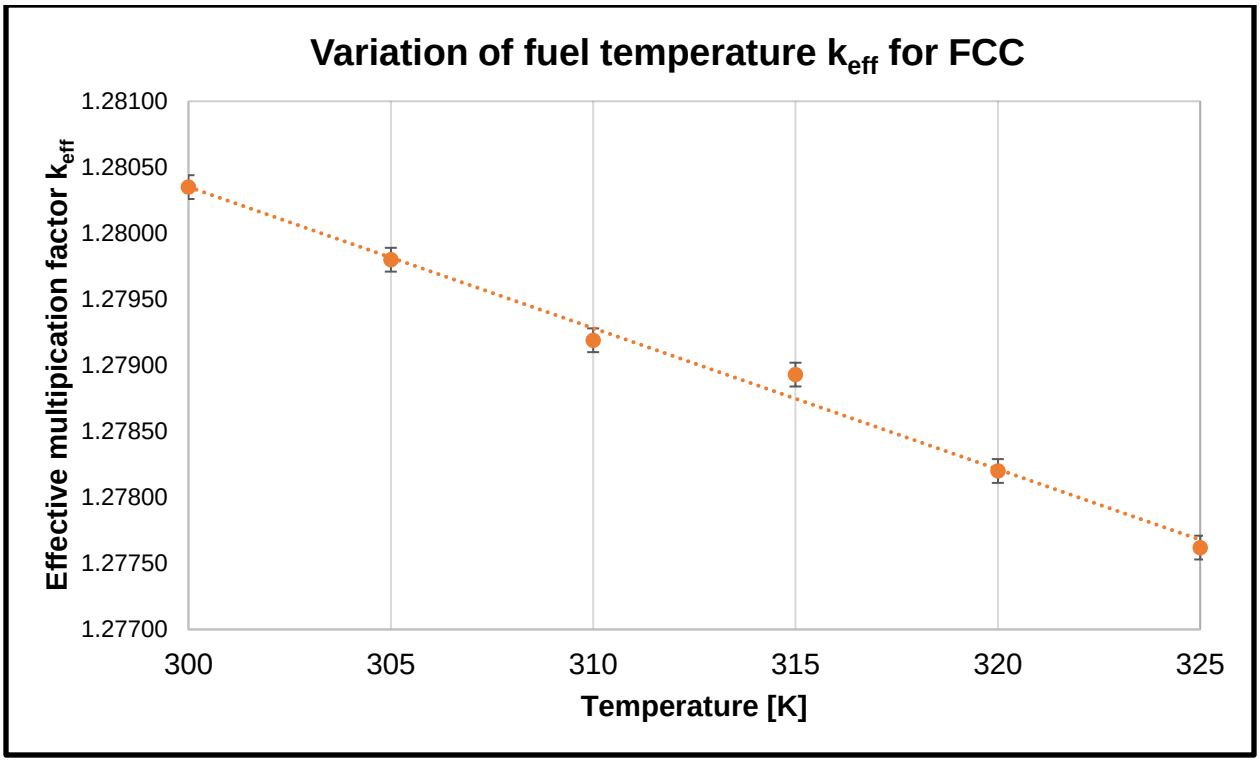

Figure 4-17: Variation of fuel temperature on the k_{eff} for FCC

We now consider Figure 4-18 and Figure 4-19, which show the variation of the fuel temperature coefficient with ΔTx=5K from 300K to 325K for both the BCC and FCC models. For both model setups, the temperature coefficient values were all negative and it can therefore be deduced that the reactor had a very strong negative temperature coefficient, which is the desired outcome.

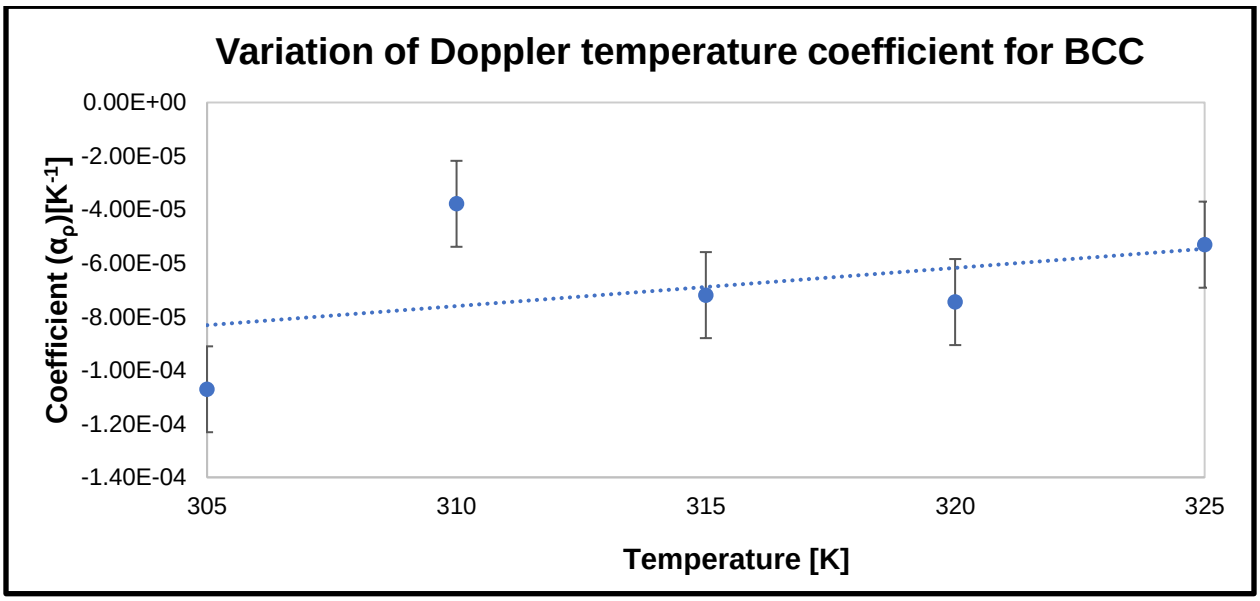

Figure 4-18: Variation of Doppler temperature coefficient for BCC

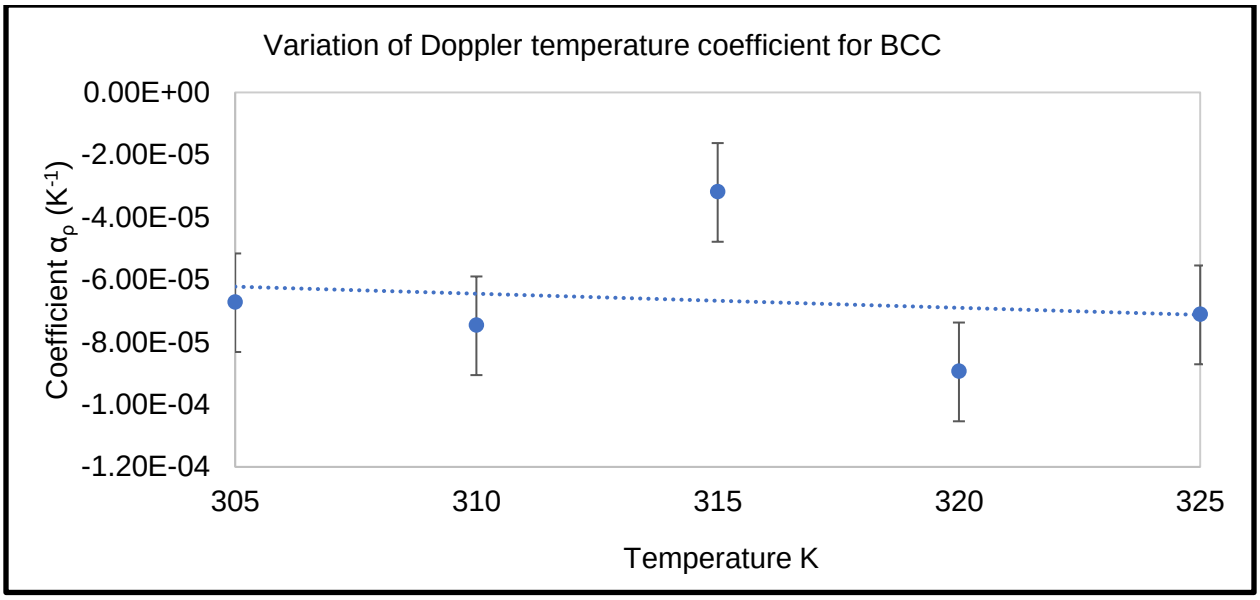

Figure 4-19: Variation of Doppler temperature coefficient for FCC

4.2.2.4 Calculated total temperature coefficient.

Having looked at the above individual temperature effects on the multiplication factor (k_{eff}), we will now consider the overall temperature effect on k_{eff}. The total temperature coefficient (α_T) was approximated by the equation given by Sihlangu (2016:77) in a study on the prismatic PMR200 HTGR, given by:

$$\alpha_T = \alpha_F + \alpha_C + \alpha_M \qquad 4\text{-}4$$

The equation assumes that each individual term on the right-hand side is independent of the other. The reactivity coefficient value results for the application of Equation 4-4 are shown in Table 4-5.

Table 4-5: Calculated reactivity coefficients

$T(K)$	α_F	α_C	α_M	α_T
305 (FCC)	-6.7 x10^{-5}	3.3 x10^{-5}	1.1 x10^{-5}	-2.3 x10^{-5}
305 (BCC)	-10.7 x10^{-5}	-0.8 x10^{-5}	-0.3 x10^{-5}	-11.7 x10^{-5}
310 (FCC)	-7.5 x10^{-5}	-2.2 x10^{-5}	-1.0 x10^{-5}	-10.6 x10^{-5}
310 (BCC)	-3.8 x10^{-5}	0.3 x10^{-5}	0.5 x10^{-5}	-3.0 x10^{-5}

315 (FCC)	-3.2 x10^{-5}	-0.5 x10^{-5}	1.8 x10^{-5}	-1.8 x10^{-5}
315 (BCC)	-7.2 x10^{-5}	0.1 x10^{-5}	-1.6 x10^{-5}	-8.7 x10^{-5}
320 (FCC)	-8.9 x10^{-5}	2.6 x10^{-5}	0.6 x10^{-5}	-5.8 x10^{-5}
320 (BCC)	-7.5 x10^{-5}	0.9 x10^{-5}	0.8 x10^{-5}	-5.8 x10^{-5}
325 (FCC)	-7.1 x10^{-5}	-1.7 x10^{-5}	-1.0 x10^{-5}	-9.8 x10^{-5}
325 (BCC)	-5.3 x10^{-5}	0.9 x10^{-5}	0.8 x10^{-5}	-3.7 x10^{-5}

An equivalent calculation was considered and carried out where all the material parameters were changed simultaneously by 5K increments from 300K to 325K. The results of the runs are indicated in Table 4-7. The percentage difference between the coefficients, α_T, shown in Table 4-5 and α_T shown in Table 4-6, is presented for the corresponding setups in Table 4-7. The percentage difference in the values of the calculated α_t for both setups is very significant, implying that equation 4-4 might not be the most accurate to use. It could be that a higher order approximation, or non-independence between the coefficients might be possible. However, sets of α_t values are negative, suggesting that the reactor is self-stabilising, which is desired.

Table 4-6-Results for isothermal change of reactor materials

$T(K)$	α_T **(Isothermal)**	
	FCC	**BCC**
305	-5.0 x10^{-5}	-10.7 x10^{-5}
310	-9.7 x10^{-5}	-5.3 x10^{-5}
315	-6.7 x10^{-5}	-3.8 x10^{-5}
320	-4.3 x10^{-5}	-6.3 x10^{-5}
325	-8.3 x10^{-5}	-16.6 x10^{-5}

The percentage difference was calculated using the adopted formulae from Cole *et al*. (2017:1) :

$$Percentage\ difference = \frac{|a-b|}{\left|\frac{a+b}{2}\right|} \times 100\% \qquad 4\text{-}5$$

Table 4-7: Percentage difference in α_T

$T(K)$	% Difference in α_T	
	FCC	**BCC**
305	73%	9%
310	10%	55%
315	114%	79%
320	29%	8%
325	16%	127%

4.2.3 Effect of isothermal temperature change of reactor components on the multiplication factor.

To assess the effect of the isothermal temperature change of all reactor components to the value of k_{eff}, all the reactor structures and materials were varied with equal temperature increments. The temperature range chosen was from 300K to 575K with temperature increments of 25K. It should be noted that this was not conducted to compute the reactivity coefficients since $\Delta \boldsymbol{Tx}$=25K for equation 4-2, was thought to be large for a meaningful k_{eff} estimate.

The model results for the effect of reactor isothermal temperature change on the effective multiplication factor are presented in Figure 4-20 and Figure 4-21, establishing that as the temperature of the material components increased for both BCC and FCC setups, the k_{eff} value decreased. The main contributor to these observations would be Doppler temperature coefficient, as established in section 4.2.2.3. During fission reactions, much higher temperatures are achieved in fuel particles with more pronounced effects on the value of k_{eff}. The results also complement model 3 in that the temperature defect, for example, must be considered in the safe design of nuclear reactors.

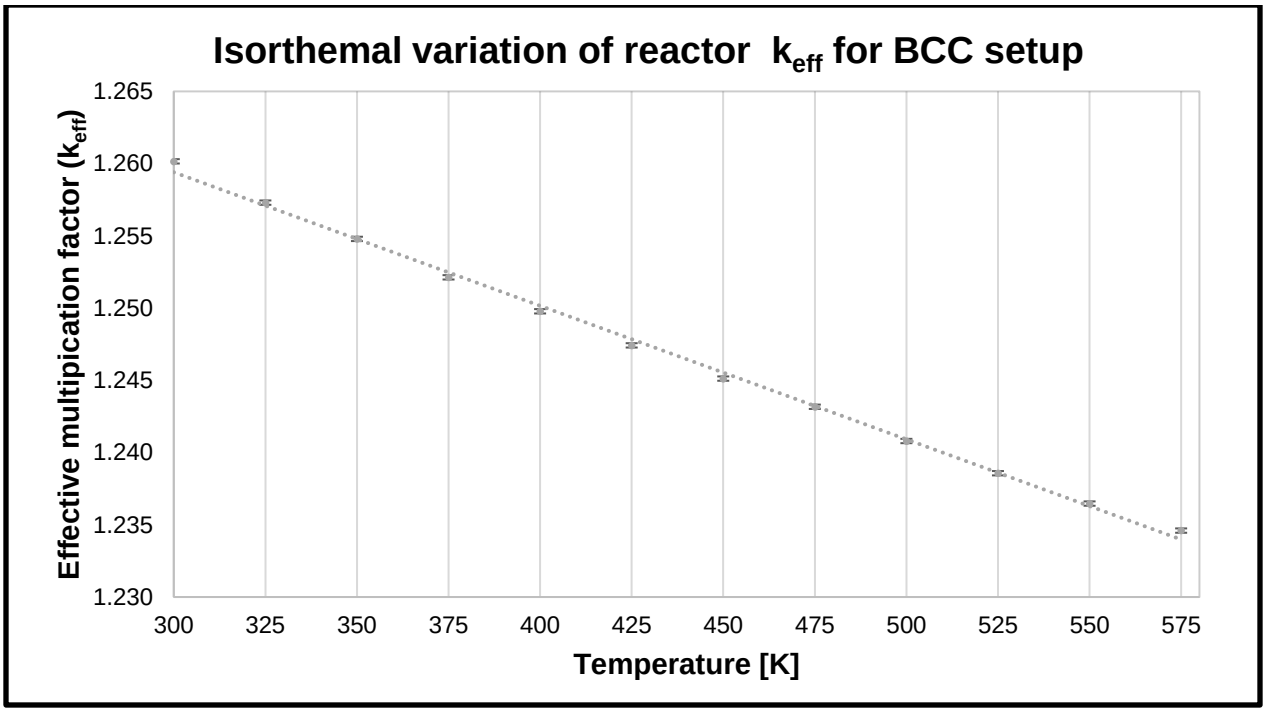

Figure 4-20: Isothermal variation of reactor components on k_{eff} for BCC setup

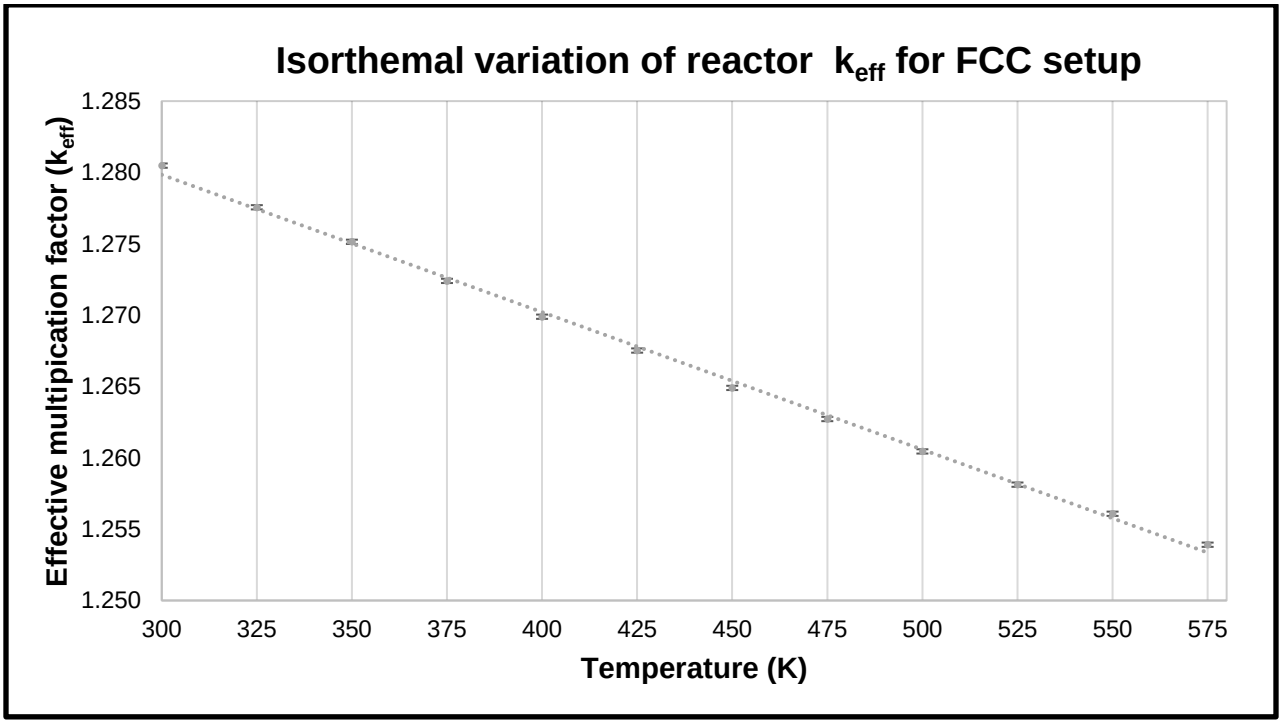

Figure 4-21: Isothermal variation of reactor components on k_{eff} for FCC setup

4.2.4 Control rods and the RSS

There are two independent shutdown systems in the PBR-250, namely the control rods and the RSS. It is important to note that the effectiveness of the control systems depends on the value of the neutron flux at the position of the control element since the reaction rate is a product of the cross-section and the flux. Because of this, the control rod has maximum effect when placed where the flux is maximal in a reactor while the variation of the worth depends on the axial flux shape of the reactor setup. Turning to the design aspects of the reactor, the control rods must be able to compensate for all reactivity changes. This section will evaluate the effectiveness of the shutdown systems, by examining the differential and integral rod worth and their effect on the flux.

According to Kugeler and Zhang (2019:38), for this reactor type, there is a reactivity demand for the control rods of around 2.2% and a reactivity demand of about 8.1% for the RSS. This follows from the fact that the control rod must compensate for all reactivity changes due to part-load operation and reactivity control due to accidents and at hot conditions. The RSS must have the capacity to allow the reactor to become cold-subcritical and guarantee this state.

4.2.4.1 Integral rod worth

The integral rod worth was calculated by measuring the change in reactivity when the rod was completely withdrawn from the reactor and inserted from the top of the reactor. A curve of the integral control rod worth against the control rod depth is shown in Figure 4-22 below for the BCC and FCC reactor setups. From this, it is evident that the BCC setup recorded higher integral rod worth values compared to the FCC setup as seen by the BCC points being above the FCC points. Knowing that the concentration of ^{10}B in the control rods was constant for the models, the difference in the values was thus due to the different setup of the fuel pebbles in the models. In view of this, the higher fissile material concentration in the FCC setup compared to the BCC setup resulted in different fissile material to ^{10}B concentration ratios between the models. In other words, with reference to the amount of fissile material between them, there is relatively more ^{10}B in the BCC setup than in the FCC setup; thus, when compared, there were larger integral rod worth drops in the BCC system than its FCC counterpart. Additionally, the more the neutron-absorbing material present, the higher the chance of neutron absorption.

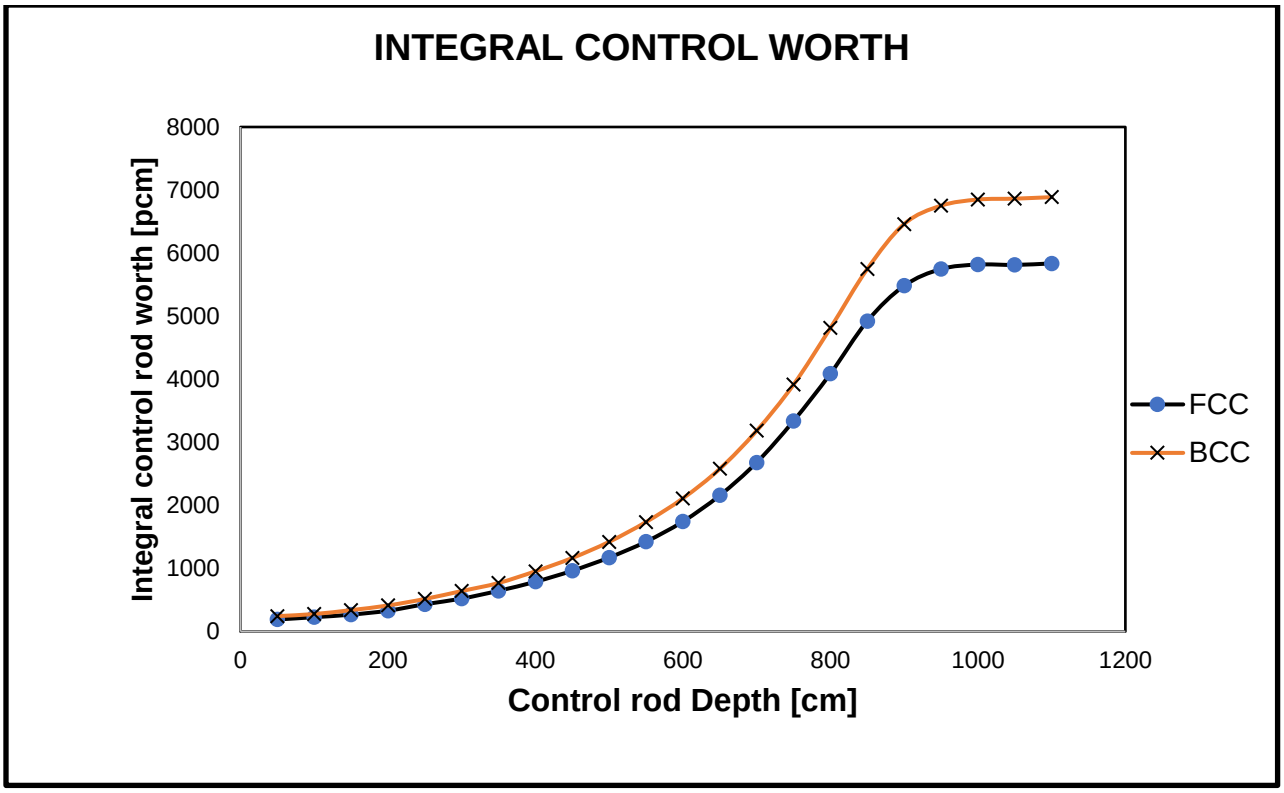

Figure 4-22: Integral control worth

The integral control rod worth for both configurations was found to be of a sigmoidal form. Furthermore, their worth per unit length of the control rod insertion at the bottom and top of the PBR-250, was less than that in the middle of the reactor suggesting that the amount of reactivity inserted per unit length of insertion, was the highest when the control rods were in the vicinity of the reactor axial centre. As mentioned above, the value of the flux contributes to the reaction rate, and hence larger values of the flux will contribute more to the reaction rate. This follows from the results of the findings in section 4.2.6.1, which show that fluxes peaked at the reactor's axial centre, thus neutron absorption was most significant and effective the closer it was to the axial centre of the reactor.

4.2.4.2 Differential rod worth

Having considered the integral rod-worth, we will now look at the differential rod worth which is the reactivity change per unit movement of the control rod.

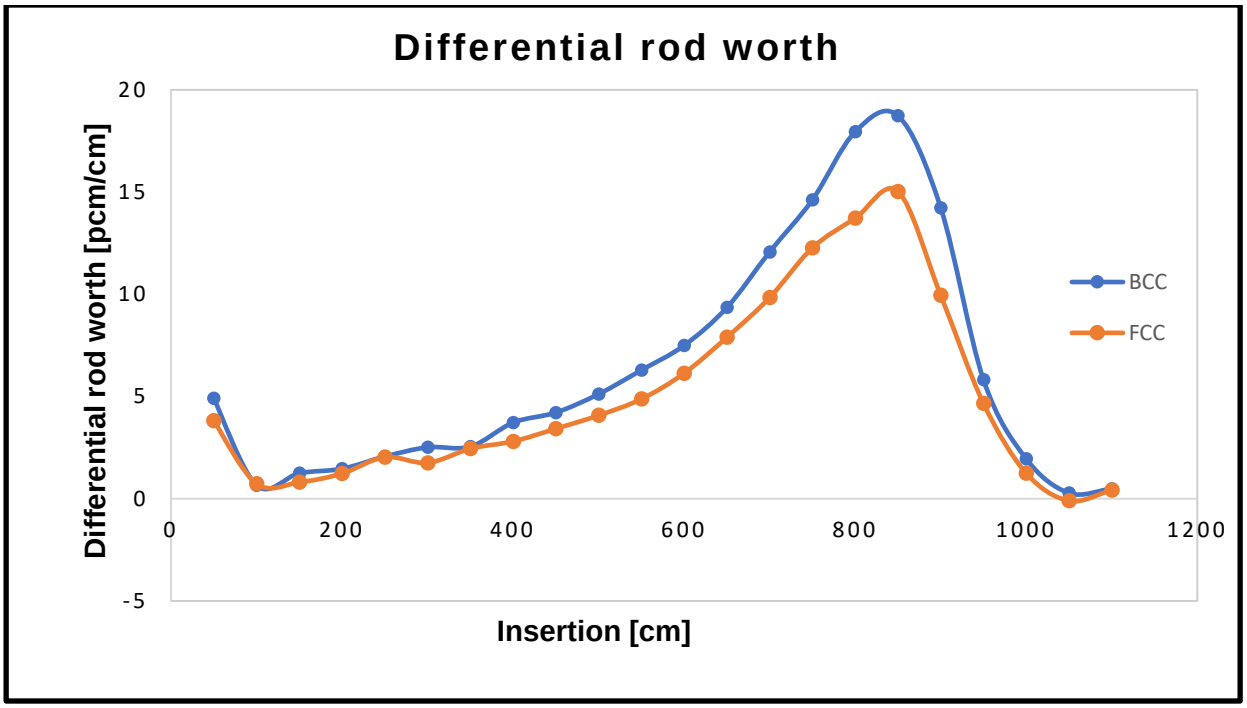

Figure 4-23: Differential control rod worth

Figure 4-23 above shows curves which peak in the lower half of the core rather than at the axial centre of the reactor despite that without control rods, the flux is axially symmetrical and peaks at the centre as shown later in Figure 4-24 and Figure 4-25. In other words, when the control rods were inserted at a certain distance from the top, the flux axial symmetry was no longer preserved as the rods effectively suppressed the neutron flux in their vicinity while also shifting the flux peak as shown clearly later in Figure 4-29. Therefore, with the reaction rate being a product of cross-section and flux, the maximum reaction rate due to control rod absorption got shifted towards the region of the core where the control rods were not present.

It was also observed that the bottom and top of the reactor core had lesser flux thus the movement of the control rods resulted in lower neutron absorption compared to the areas closer to the axial centre. The amount of reactivity inserted per unit of insertion was observed to be highest when the control rod is inserted in 2/3^{rds} of the core.

4.2.5 SCRAM reactivity

We will now consider the effectiveness of the reactor shutdown system as this is important when looking at reactor design. SCRAM is an emergency shutdown of a nuclear reactor by the termination of fission reactions. To assess the SCRAM reactivity, various models were set up to

simulate different scenarios of the control rod and RSS status. The model setups are indicated in Table 4-8 and Table 4-9 with the assumptions for this study outlined below.

Model assumptions

1. The ^{10}B in the boron carbide RSS is assumed to be 50w/o; and
2. The ^{10}B in the Boron Carbide control rods is assumed to be 90w/o.

Regarding the above model assumptions, concentration of the ^{10}B in the RSS was less than that in the control rods because both the RSS elements and control rods were modelled as distinct cylindrical channels despite that in real reactors, the control rods are short cylindrical-shaped segments (absorber pins) joined end-to-end to form a long control rod, and the RSS elements are made up of small absorber balls. The small absorber balls have void areas around them due to the spherical packing, while the control rods are cylindrical solid volumes. It follows then considering the void surrounding the absorber balls, that the ^{10}B concentration per unit volume in the RSS will be lower than that in the control rods; thus, the result is the difference in concentrations of the ^{10}B in the model assumptions. The sleeves were replaced with B_4C at 90w/o in config-4 given in Table 4-8, resulting in homogeneous control rod cylindrical channels. The model was used to determine the influence of the sleeve materials on the multiplication factor, and to confirm the model assumption given above that increasing the absorber concentration reduces the multiplication factor.

Table 4-8: k_{eff} for SCRAM

Config	Status of absorbers	BCC	FCC
1	None (RSS + control rods)	1.26019 +/- 0.00009	1.28049 +/- 0.00009
2	RSS only	1.16137 +/- 0.00009	1.19867 +/- 0.00009
3	Control Rods only, with sleeves	1.16342 +/- 0.00009	1.19976 +/- 0.00009
4	Control Rods only, without sleeves	1.16113 +/- 0.00009	1.19818 +/- 0.00009
5	RSS + control rods	1.12671 +/- 0.00009	1.17063 +/- 0.00009

Table 4-9: SCRAM reactivity

	$\% \left\lvert \frac{k_2 - k_1}{k_1 \times k_1} \right\rvert$	
	BCC	**FCC**

No (RSS + control rods)	Reference	Reference
RSS only	-6.75 %	-5.33%
Control Rods only with sleeves	-6.60%	-5.25%
Control Rods only without sleeves	-6.77%	-5.36%
RSS + control rods present	-9.40 %	-7.33%

Moving on to the data reported in the preceding tables, the percentage reactivity was determined using the equation given in Table 4-9 where k_1 is the multiplication factor of the model in which no neutron absorbers (control rods and RSS) are present in the reactor core. The difference in the k-values between the FCC and BCC setups with neutron absorbers in Table 4-8 was due to the difference in the fissile material to ^{10}B ratios as explained earlier in section 4.2.4.1. In terms of all the setups shown in Table 4-9, the control rods had an absolute reactivity of above 2.2%; this suggests that the designed control rods satisfy the reactivity demand for the HTR design, as described by Kugeler and Zhang (2019:38). The reactivity demand of 8.1% for the RSS is not satisfied in either the BCC or FCC setup.

In summary, it would be advantageous if further work is conducted in incorporating the modelling of random packing in the core, and modelling and optimising the placements of the spherical RSS elements rather than using homogenised volumes. The highlighted reasons would provide more accurate results and could possibly satisfy the required reactivity demand described by Kugeler and Zhang (2019).

4.2.6 Effect of neutron absorbers on the flux

This section will investigate the neutron flux profiles of various reactor model configurations, as well as the influence of neutron absorbers on the flux profiles. The reader is directed to section 3.2.3 for information on how the mesh detector functions and how the data was analysed. The neutron flux values in Serpent depend on how the neutron source rate was normalised and Serpent provides several options for source rate normalisation. For the computations in this study, unless specified, normalisation to a total heat produced of 250MW was set using the option described in Appendix A3-o.

4.2.6.1 Model flux profiles without absorbers

The axial flux profiles grouped in terms of neutron energy, for the BCC and FCC setups without any absorbers present are shown in Figure 4-24 and Figure 4-25 i.e., axial neutron flux profiles for model 2. The energy groups shown in the plots were described in Section 3.2.3. For the parameters used in the plots, 20 mesh bins were set, and the axial flux through the point (x;y) = (14;14) was plotted, where the values contained in the brackets are mesh bin numbers corresponding to spatial coordinates given in Appendix C-2.

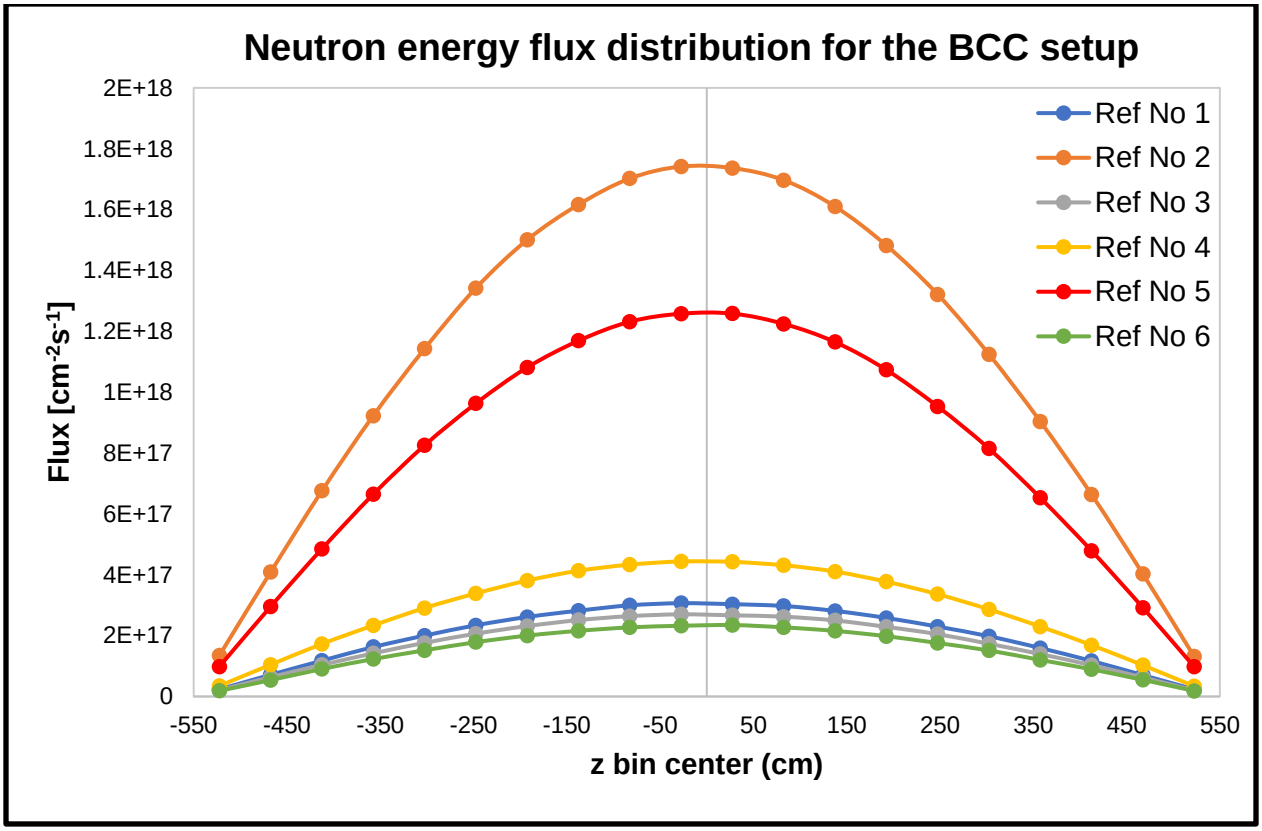

Figure 4-24: Neutron energy flux distribution for the BCC setup

With reference to Figure 4-24 and Figure 4-25, thermal neutrons contribute the most to the overall flux since they have the greatest flux values when compared to other neutron energy groups. Furthermore, the flux peaked towards the centre of the reactor model at z=0. Comparing the plots, the BCC setup had higher recorded flux values than the FCC setup, for instance, in terms of the thermal neutron flux values at z = 27.5cm, the percentage difference between the two setup values is 7%. This indicates that even though the multiplication factor is larger in the FCC setup than the BCC setup, the solution of the neutron transport does not necessarily mean the flux also exhibits the same trend.

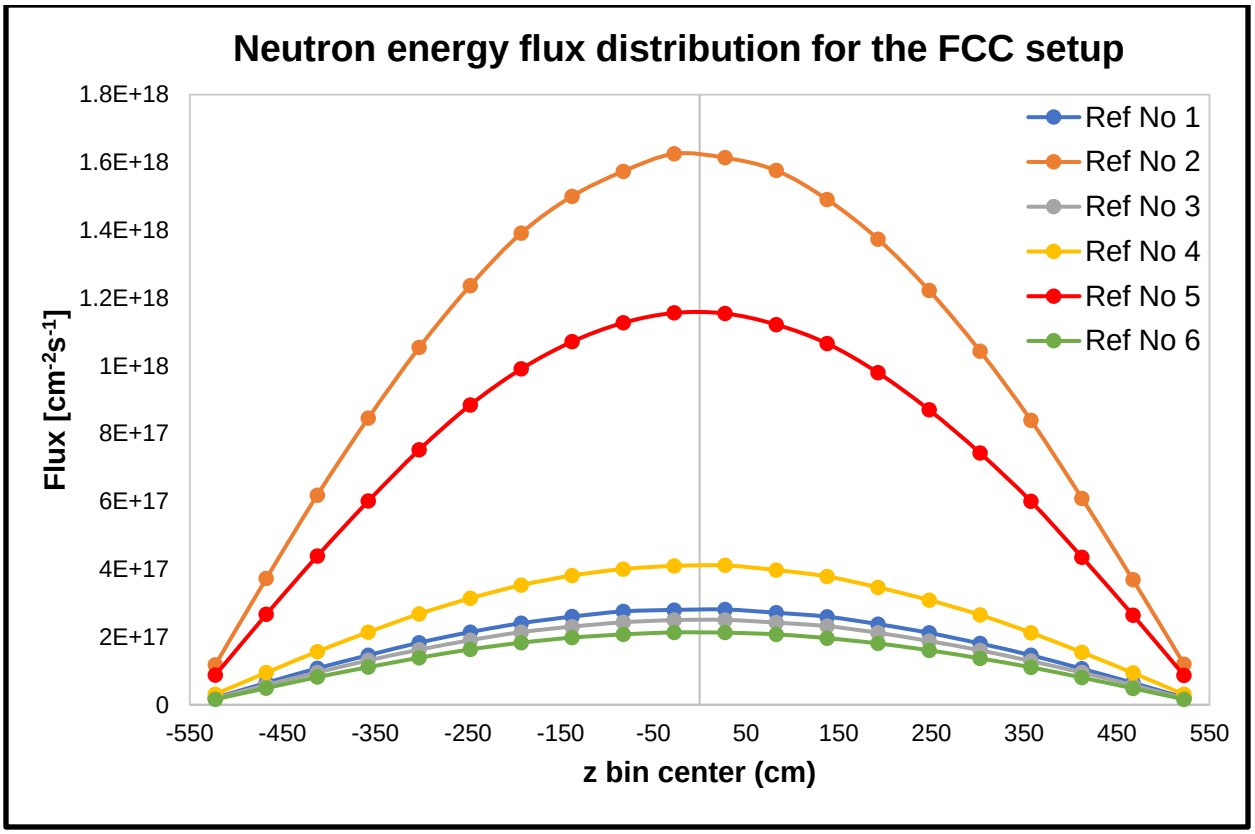

Figure 4-25: Neutron energy flux distribution for the FCC setup

Having considered the axial flux, the corresponding radial flux of the models are shown in Figure 4-26 and Figure 4-27. For the parameters used, 40 mesh bins were set and the radial flux through the point (y;z) = (20;20) was analysed for the thermal and fast neutron flux. The flux values peaked towards the radial centre, with the FCC flux values being lower than the BCC flux values for comparable neutron groups i.e., BCC vs FCC thermal flux, and BCC vs FCC fast neutron flux. As we move away from the radial centre of the reactor, the plots decrease in size, corresponding to decreasing flux values.

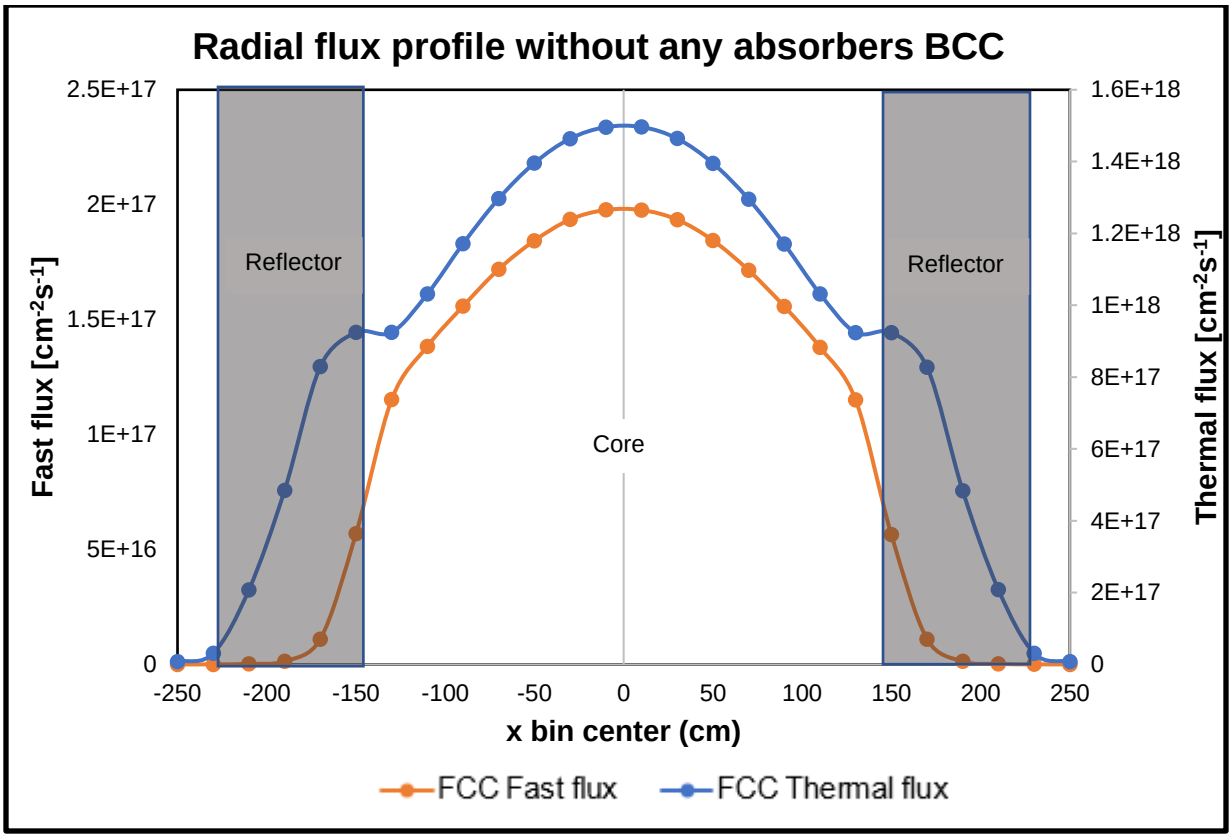

Figure 4-26: Radial neutron flux distribution for the BCC setup

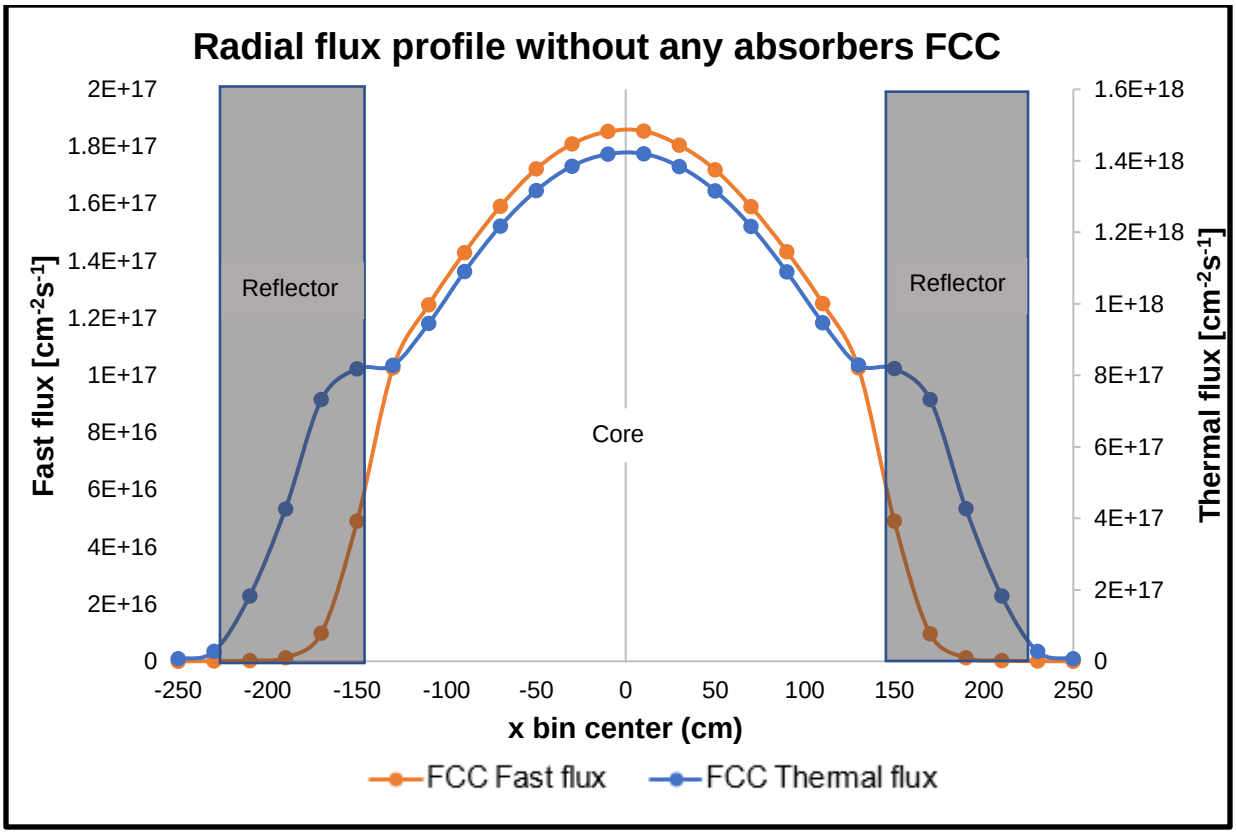

Figure 4-27: Radial neutron flux distribution for the FCC setup

4.2.6.2 Model Flux profiles with burnable poisons

For this section, we will now consider how the burnable poisons affect the flux. The model parameters for the study are as follows:

1. The enrichment of fuel is assumed to be 4%;
2. The configuration for the pebbles has a 50% ratio normal fuel pebbles to burnable poison pebbles;
3. The calculation was not normalised;
4. The burnable poison is B_4C particles; and
5. A total of 20 mesh bins were set and the axial flux through the bin point $[x;y]=[4;4]$ was analysed for the thermal neutron flux.

Figure 4-28 below shows the effect of varying the concentration of the ^{10}B in BCC and FCC reactor setups on the flux. These concentration variations were carried out for verification since one would expect the flux to be lowered as the boron concentration is increased, and the observation of such leads to the verification of the input models. The flux values of the FCC setup were lower than the flux values on the BCC setup. Furthermore, the flux values for all models peaked towards the

centre of the reactor. Continuing with the observations made in Figure 4-28, the maximum flux for the different setups was achieved by reactor models with 0% absorber concentration, and flux values for all reactor setups decreased with increasing absorber concentration. ^{10}B removes neutrons by absorption from the system. Therefore, as ^{10}B increased in concentration, the neutron density, and, subsequently, flux, decreased correspondingly with k (multiplication constant). To illustrate how the value of k is affected we will consider and assume that the value of k to be approximated using equation 5-2, where each model could be simplified to $k = C\frac{1}{\Sigma_a}$, where $C = \frac{\nu \Sigma_f}{1+L^2B_g^2}$ would be constant for this instance. As the concentration of the absorber increases, the value Σ_a increases, reducing k. The value of k for each model tested is shown in Table 4-10, and it is evident that k decreases as the ^{10}B concentration is increased.

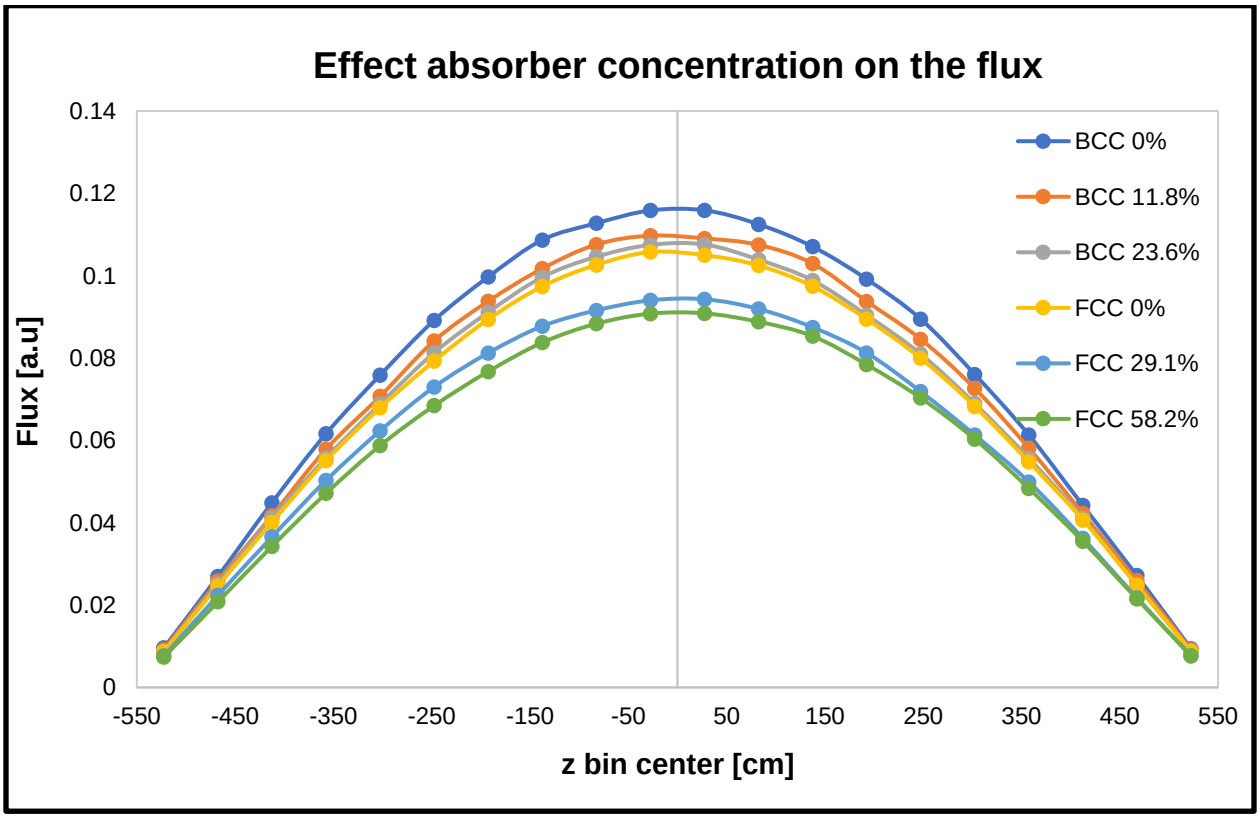

Figure 4-28: The effect of the presence of absorber material on the flux

Table 4-10: Corresponding multiplication factors for Figure 4-28

Setup	^{10}B Concentration %	k_{eff}
BCC	0	1.22937 +/- 0.00010

BCC	11.8	1.08850 +/- 0.00014
BCC	23.6	1.00479 +/- 0.00012
FCC	0	1.25728 +/- 0.00010
FCC	29.1	0.99385 +/- 0.00013
FCC	58.2	0.89878 +/- 0.00011

Having considered how the burnable poisons affect the neutron flux, verification as stated in the previous section continues with a study on the effect of the control rods on the flux. The model parameters for the study were as follows:

1. The enrichment of fuel is assumed to be 4%;
2. The core contained normal fuel pebbles only; and
3. A total of 20 mesh bins were set and the axial flux through the point (x;y) = (4;4) was analysed for the thermal neutron flux

Figure 4-29 below shows the effect of control rod position on the axial thermal neutron flux of the FCC and BCC setup.

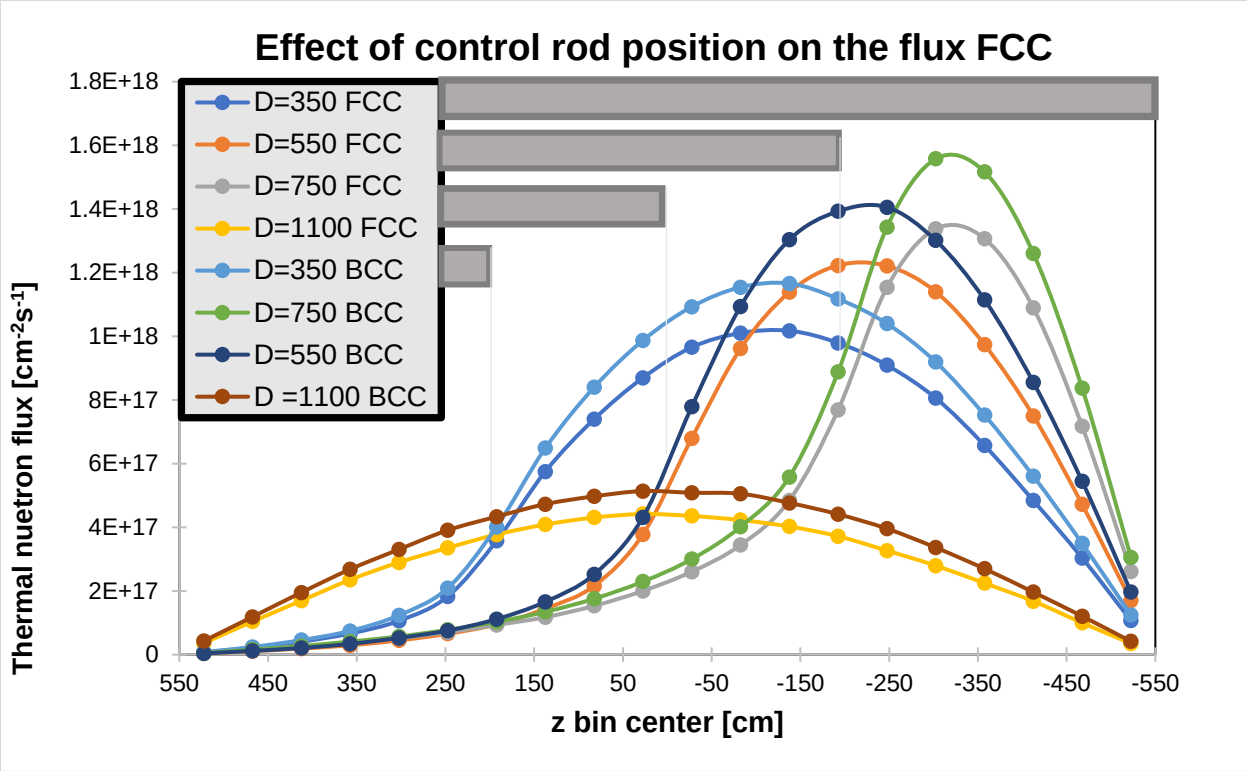

Figure 4-29: Comparison of the effect of the control rod position on flux

In Figure 4-29 above, the control rods were inserted from the top of the reactor (at position z=550cm in the figure) with insertion depths of 350cm; 550cm; 750cm and 1100cm. As discussed earlier, the control rods absorb neutrons in its vicinity, thereby creating a flux depression in the vicinity where the control rod is present. As a result, the movement of the control rods caused the flux profile to peak below the rod as shown in the figure above. Furthermore, it is noted from the figure that the deeper the control rod, the higher the peak flux value recorded which was offset away from the centre of the reactor. Results of similar nature are shown by Stacey (2018:76).

4.3 Model Verification Using NWURCS

This section covers the PBR-250 base core model verification using NWURCS, which modelled all core structures up to the particles. The particle location in the pebble employed in the NWURCS model was the same as in the manually developed model, with the particle location modelling in the pebble carried out explicitly.

The model parameters for both the manual base model and NWURCS-developed model were:

1. an SC pebble configuration was developed;
2. the enrichment of fuel was assumed to be 4%;

3. the core contained pebbles with fuel only;
4. the influence of control rods was not included; and
5. for fuel particle locations in the pebbles, the same file generated by the Serpent disperse function was employed.

The manually developed PBR-250 base core model was assessed and verified using NWURCS. The modelling methodology of the manually created model was different from the modelling methodology used in NWURCS, that is, the manual model placed the fuel pebbles individually in the core using calculated coordinates while the NWURCS model used lattices to place fuel pebbles in the core. Following from this, it was imperative that the variables defining the models were to equivalent to qualify the models for comparability. The following techniques were developed and used in this study for model verification:

1. All the dimensions of all reactor structures were compared and made similar, to illustrate with an example, both pebble radii for both models was set to 3cm and core radius to 150cm.
2. Pebbles were physically counted and compared between the models. This was carried out by firstly counting them manually and confirming that the pebble placement in the core was similar for each row and column using the graphical core image files developed using the plot function discussed in Appendix A3-i. The result of this exercise found the core to have the same number of pebbles across and down. The only difference would have been in the precision of placements since the pebble positions were calculated and rounded off to four decimal places.
3. Material compositions were calculated manually and confirmed for both models. This was done to confirm that the calculations done by NWURCS and those done manually were consistent.
4. Material compositions developed by NWURCS and those manually developed were compared matched and made similar (NWURCS calculated compositions compared to manually calculated compositions, checking if the same materials are used with same compositions between). After checking and matching the composition, the value of the multiplication factor was calculated to check the difference between the models. Table 4-11 shows the outcome of the exercise in which it was found that there was a 13 pcm difference. In view of the difference in values, since Serpent is a stochastic code, both models are statistically equal. For the two models to be statistically equal, one would expect that the difference would lie within three times the standard deviation, and, for this

comparison, the standard deviation taken to be equal to the difference. It was noted that a single value for both calculations will not arise, since the random walk in both models will be different. This is because the lattices of the NWURCS models produce additional planes in comparison with the manually built model, leading to additional surfaces that must be considered in the random walk. The geometry, however, remains the same.

Table 4-11: Model comparison

NWURCS model	MANUAL model
1.20752 +/- 0.00013	1.20739 +/- 0.00013

4.4 Verification and validation of the models

The verification of the models was carried out by means of visual inspections of the geometry plots, and the agreement of the results with expected physics arguments as discussed in the sections above. Validation was not carried out because it is not part of the scope of an Option B Masters programme. However, partial validation of the models can be assessed since Serpent is currently undergoing considerable validation in many aspects of modelling.

4.5 Computational time evaluation with Serpent

The time economy was assessed in this section and was not intended as an analysis of the performance of the computer software and hardware, but rather, as a record to ensure other users can assess how they can plan their calculations using Serpent with the NWU High-Performance Computing (HPC) facility. All calculations were carried out at the NWU using its HPC centre. The term “HPC” refers to supercomputers and computer clusters used to solve advanced computation problems.

Considering the study carried out in this section, only the FCC setup, specifically model 2, was assessed since it was the most densely packed; thus, it took the most time to calculate with respect to the base models which had no neutron absorbers. The set parameters were the number of source neutrons, the number of active cycles, and the number of cores used in a set calculation. Additionally, the number of inactive cycles was fixed at 80 for the reasons highlighted in section 4.1. Altogether, the results were obtained from the results file (_res.m) produced after a calculation and the parameters recorded included the memory usage, the error produced after

calculation, the total CPU time, and the total transport cycle time. Table 4-12 below shows the parameters used during several model calculations and their subsequent results.

Table 4-12: Assessed parameters for the time economy of Serpent.

Pebble setup	Number of source neutrons	Number of active cycles	Number of cores	Memory required [MB]	Error value	Total CPU time [hrs]	Total transport cycle time
FCC	20000	10000	32	1832.46	0.00007	2.311	0.075
FCC	20000	10000	48	2460.03	0.00007	2.208	0.049
FCC	10000	5000	48	2457.81	0.00014	0.584	0.013
FCC	5000	5000	48	2457.81	0.00020	0.302	0.007
FCC	2500	2500	48	2429.79	0.00039	0.095	0.003

The following was noted from this study and Table 4-12 :

1. The total CPU time taken to obtain a standard deviation of 0.00007 with 48 cores was 2.21 hrs. This is a reasonable amount of time for a calculation of this nature to this accuracy.
2. Decreasing the number of cores to 32 increased the time to 2.31 hrs which is not a significant increase in time. The NWU HPC has six nodes with 48 cores and four nodes with 32 cores. Therefore, even if all the six nodes with 48 cores were in use (by other users), one could still run the calculation with 32 cores if any are available, and not experience a significant increase in time.
3. There was a significant decrease in CPU time if an analysis accepted a higher statistical deviation (for example, 0.00014 or even 0.00039).
4. The higher the number of processes the more memory was required for the run.
5. The presence of absorbers in the models increased the total transport calculation time but this result is not shown in the table.

Chapter 5: Conclusion and recommendations

5.1 Conclusion

This dissertation provides a preliminary study on the PBR-250 with great emphasis being placed on the IAEA CRP reactor specifications. It was intended to develop and provide insight on various methodological aspects of reactor design and analysis using Serpent 2.1.31, and to further serve as a starting point for further uncertainty and sensitivity analysis studies; all on this reactor type. It very important to undertake neutronic studies on the design models and to verify them for further studies.

Firstly, before any simulation calculation was analysed, a source convergence study was carried out. This study established the appropriate number of inactive cycles required for the simulations, as running the simulation with inappropriate number of these cycles would lead to inaccurate k_{eff} values. The determination of the appropriate number of inactive cycles was established using the cycle-wise Shannon entropy plots, resulting in a value of 30 cycles as adequate, with a conservative 80 cycles chosen for all the simulations. Having established the number of skipped cycles, different pebble configurations were evaluated (i.e., SC, BCC, and FCC) for the developed reactor models. The explicit modelling feature of Serpent provides a reliable and flexible method to describe the pebble/particle locations in the reactor system. Flexibility was realised as any lattice developing program or method could be used to generate the pebble/particle locations with precision as demonstrated with the manual model i.e., using MS Excel for pebble location calculations. Modelling pebble configurations in Serpent could also be carried out using repeating units to form lattices as demonstrated by the model developed using NWURCS.

The initial base models, filled with 4% enriched fuel pebbles, were found to be supercritical for all pebble setups. For design purposes, this was a good result, as the supercriticality would offset some reactor phenomena, such as the temperature defect, and the increase in the concentration of xenon and samarium in the core, that bring down the k_{eff} after start-up. Other measures could then be taken that are able to bring the reactor closer to a critical state. The studies on the incorporation of burnable poison pebbles (the study varied neutron poison concentration to the fresh core state), provides an insight into a method that could potentially be used bring down the value of k_{eff} effectively and compensate for some excess reactivity associated with using fuel

pebbles. After reducing the k_{eff} to a suitable value for operation, control rods could then be used to bring the reactor to a critical state as their effect on the reactor can be easily controlled. The base model used in calculations in this dissertation had missing top and bottom structures, and it was found that the exclusion of these graphite structures reduced the neutron economy of the reactor significantly.

More onto the sensitivity analysis aspects, to realise the beneficial inherent safety features associated with this reactor type, the temperature coefficients for the PBR-250 were calculated with BCC and FCC configurations being studied. It was found that for all reactor setups, a very strong Doppler coefficient was realised, and its influence had a dominant effect on the total temperature coefficient. Furthermore, for the above-mentioned reactor configurations, the calculated total temperature coefficient, which was obtained by summing the individual temperature coefficients i.e., moderator, coolant, and fuel temperature coefficients, had a negative value. A study on the isothermal temperature change of all the reactor components with (ΔTx=25K) on the value of k_{eff} was also carried out and it was established that as the temperature of all reactor components increased, the value of k_{eff} decreased. These findings support the negative calculated total temperature coefficient with the main contributor to the findings being the Doppler coefficient. It was further established that the sum of individual temperature coefficients ($\alpha_F + \alpha_C + \alpha_M$) for a given temperature change (in this case ΔTx=5K), does not equal the total temperature coefficient (α_T) for the isothermal temperature change of the same components of the reactor with the same temperature increment.

To assess and verify the reactivity control system of the designed reactor model, the rod worth of the system was calculated, with the integral and differential control rod worth for the FCC and BCC setup analysed. For both the differential and integral control worth, the BCC setup recorded higher reactivity values compared to the FCC setup. The SCRAM reactivity was then calculated to assess the effectiveness of both the control rods and the RSS in stopping the fission reactions. It was found that the designed control rods satisfied the reactivity demand described by Kugeler and Zhang (2019:38), while the RSS on the other hand did not satisfy the reactivity demand required. Now considering neutron flux studies, the flux profiles of different reactor setups were assessed in this dissertation. The effect that neutron absorbers and control rods have on the shape of the flux was examined for different pebble setups. The importance of the flux profile evaluation was mainly associated with methodology development and as an additional model verification step. Different ways of analysing the flux profiles were explored, including characterising the flux radially, axially and in terms of the neutron energy.

Model verification was carried out using NWURCS, with the base model generated using it. NWURCS was also verified in the process with manual calculation of material specifications and visual verification of the NWURCS output files being compared to the manually developed core model output files. It was found that NWURCS produces a model statistically equal to the manually developed model with a 13pcm difference in the value of k_{eff}. The time economy for the transport calculations was reported by considering the error acceptable to the user in terms of k_{eff} . In conclusion, the work has successfully produced robust working models that can serve as base models for further work by the Nuclear Engineering Research group at the NWU.

5.2 Recommendations

This dissertation was used to address some methodology and design aspects, which are associated with the stochastic design of the PBR250, by using Serpent. The overall study of this dissertation provided a good estimate of the directions in which the design of the PBR-250 can be conducted. However, the following needs to be carried out to reach the goals of the Nuclear Engineering Research Group at the NWU:

1. More definite information and details are needed to fully describe the reactor for full core studies to be carried out. This includes information on the missing parts of the reactor, top and bottom structures of the reactor, and information on the actual positions of pebbles in a reactor etc.;
2. The SC system and the random packing system models must be developed with parallel studies as were performed for the BCC and FCC models in this current study;
3. Burn-up calculations should be carried out, together with algorithms, to predict the flow of the pebbles through the core;
4. Thermal fluid calculations should be carried out to characterise the temperature fields in the reactor. The neutronic calculations must, therefore, be coupled with thermal-hydraulic calculations using Serpent and a thermal fluid program that is compatible with Serpent, and;
5. NWURCS should be updated to include BCC packing and random packing of the spheres and to model the control rods and absorber spheres.

Further minor recommendations are:

1. A study should always be done to determine the error required for calculations to ensure that the results are consistent for an error of less than 15pcm. For starting values, the number of source neutrons should be >20000 and active cycles > 10000.

Bibliography

1. ˇZohar, A., ˇStancar, Z., Batistoni, P., Conroy, S., Snoj, L. & Lengar, S. 2021. *Validation of Serpent for fusion nuetronics analysis at JET*. Paper presented at the EPJ Web of Conferences. https://iopscience.iop.org/article/10.1088/1741-4326/ab2276
2. Ardiansyah, H., Seker, V., Downar, T., Skutnik, S. & Wieselquist, W. 2021. Evaluation of the PBMR-400 Core design Steady State Condition with Serpent and AGREE. *Jounal of Physics*, Conference series, 0.1088/1742-6596/2048/1/012024
3. Becker, B. 2010. *On the influence of the resonance scattering treatment in Monte Carlo codes on High Temperature Reactor Characteristics.* Stuttgart (Germany): University of Stuttgart. https://www.researchgate.net/publication/279382322_On_the_influence_of_the_resonance_scattering_treatment_in_Monte_Carlo_codes_on_high_temperature_reactor_characteristics
4. Blennies, A. 2022. The temperature reactivity coefficient of an in-rod heterogenous PWR thorium/uranium fuel design.
5. Bonakdarpour, M. 2021. *Inverse Transform Sampling*. https://stephens999.github.io/fiveMinuteStats/inverse_transform_sampling.html Date of access: 3 Aug.
6. Cole, T.J. & Altman, D.G. 2017. Statistics Notes: What is a percentage difference? *Bmj*, 358,
7. Cox, A.M.G., Harris, S.C., Horton, E.L. & Kyprianou, A.E. 2019. Multi-species Neutron Transport Equation. *Journal of Statistical Physics*, 176(2):425-455. 10.1007/s10955-019-02307-2
8. Du Toit, M.H. & Naicker, V.V. 2018. Developing a Full-Core MCNP6 and RELAP5 Model of the European Pressurized Reactor Using NWURCS. *Nuclear Science and Engineering*,
9. Ferng Y.M., Lin, K,. 2013. Investigating effects of BCC and FCC arrangements on flow and heat transfer characteristics in pebbles through CFD methodology. 66-75. 10.1016/j.nucengdes.2013.02.009
10. Flowers, P., Theopold, K., Langley, R. & William, R. 2012. Chemistry. In: Rice University.

11. Grimod, M. 2010. Neutronic Modeling of Pebble Bed Reactors in APOLLO2 https://inis.iaea.org/collection/NCLCollectionStore/_Public/43/116/43116811.pdf Date of access: 5 Oct 2021.
12. IAEA. 1996. *Absorber materials, control rods and designs of shutdown systems for advanced liquid metal fast reactors*. Austria. https://inis.iaea.org/collection/NCLCollectionStore/_Public/27/072/27072854.pdf
13. IAEA. 2010. Nuclear Energy development in the 21st Century:Global Scenarios and Regional Trends. NP-T-1.8:1.
14. IAEA. 2012. The High Temperature Gas Cooled Reactor Test Module Core Physics Benchmarks In. https://www-pub.iaea.org/MTCD/publications/PDF/te_1382_web/TE_1382_Part2.pdf Date of access: 30 Aug 2021.
15. info@nuclear-power.com. *nuclearpower.com*. https://www.nuclear-power.com/nuclear-power/reactor-physics/atomic-nuclear-physics/fundamental-particles/neutron/neutron-energy/ Date of access:
16. Kaltiaisenaho, T. 2014. Statistical Tests and the Underestimation of Variance in Serpent 2. http://montecarlo.vtt.fi/download/VTT-R-00371-14.pdf Date of access: 24 Jul 2021
17. Kameyama, Y. 2021. Climate Change Policy: Can New Actors Affect Japan's Policy-Making in the Paris Agreement Era? *Social Science Japan Journal*, 24(1):67-84. 10.1093/ssjj/jyaa051
18. Kugeler, K. & Zhang, Z. 2019. *Modular High-temperature Gas-cooled Reactor Power Plant*. 1st. Berlin, Heidelberg: Springer Berlin Heidelberg : Imprint: Springer,. Date of access: 3 Jun 2021. 10.1007/978-3-662-57712-7
19. Kugeler, K., Nathalie, P. & Tragsdorf, I. 2021. *Reactor Safety*.
20. Lamarsh, J.R. & Baratta, A.J. 2001. *Introduction to nuclear engineering*. 3rd. Upper Saddle River, N.J.: Prentice Hall. (Addison-Wesley series in nuclear science and engineering).
21. Larsen, E.W. 2008. An Overview of Neutron Transport Problems and Simulation Techniques.
22. Leppänen, J. 2009. Two practical methods for unionized energy grid construction in continuous-energy Monte Carlo neutron transport calculation. *Annals of Nuclear Energy*, 36(7):878-885. 10.1016/j.anucene.2009.03.019
23. Leppänen, J. 2010. Performance of Woodcock delta-tracking in lattice physics applications using the Serpent Monte Carlo reactor physics burnup calculation code. *Annals of Nuclear Energy*, 37(5):715-722.

24. Leppänen, J. 2015. *Serpent – a Continuous-energy Monte Carlo Reactor Physics Burnup Calculation Code*. Finland: VTT Technical Research Centre of Finland. (User's Manual).
25. Leppänen, J. 2021. *Delta- and surface-tracking - Serpent Wiki*. http://serpent.vtt.fi/mediawiki/index.php/Delta-_and_surface-tracking Date of access: 30 May
26. Leppänen, J., Pusa, M., Viitanen, T., Valtavirta, V. & Kaltiaisenaho, T. 2015. The Serpent Monte Carlo code: Status, development and applications in 2013. *Annals of Nuclear Energy*, 82:142-150. 10.1016/j.anucene.2014.08.024
27. Lohnert, G.H. 1990. Technical design features and essential safety-related properties of the HTR-module. *Nuclear Engineering and Design*, 121(2):259-275.
28. Massimi, L. 1976. *Physics of high temperature reactors*. 1st. Pergamon Press.
29. Mokhtari, O. & Mazrou, H. 1994. *Convergence assessment of the MCNP5 model for NUR research reactor*. Paper presented at the AIP Conference5 Jun 2021. https://doi.org/10.1063/1.5048158 Date of access.
30. Muellner, N., Arnold, N., Gufler, K., Kromp, W., Renneberg, W. & Liebert, W. 2021. Nuclear energy - The solution to climate change? *Energy Policy*, 155, 10.1016/j.enpol.2021.112363
31. NEA. 2017. *JEFF-3.3*. https://www.oecd-nea.org/dbdata/jeff/jeff33/index.html Date of access: 28 July 2021.
32. Nyalunga, G., Naicker, V.V. & Du Toit, M. 2016. Developing skills for neutronic modelling of nuclear power reactors in South Africa. *Journal of Energy in Southern Africa*, 27(4):64-76. 10.17159/2413-3051/2016/v27i4a1496
33. PBMR-SA. 2011. Status report 70 - Pebble Bed Modular Reactor (PBMR).
34. PBMR-SA. 2012. The PBMR's Safety features. https://www.nrc.gov/docs/ML0310/ML031000208.pdf Date of access: 6 July 2021.
35. Rahgoshay, M. & Noori-Kalkhoran, O. 2013. Calculation of control rod worth and temperature reactivity coefficient of fuel and coolant with burn-up changes for VVRS-2MWth nuclear reactor. *Nuclear Engineering and Design*, 256:322-331. 10.1016/j.nucengdes.2012.08.033
36. Reitsma , F., Strydom, G., Tyobeka, B. & Ivanov, K. 2012. The IAEA Coordantes Research program on HTGR Reactor Physics, Thermal-hydraulic and depletion Uncertainty Analysis. *Description of the Benchmark Test Cases and Phases*,

37. Reitsma, F., Ivanov, K., Downar, T., de Haas, H. & Gougar, H.D. 2006. The OECD/NEA/NSC PBMR coupled neutronics/thermal hydraulics transient benchmark: The PBMR-400 core design. In. Proceedings of PHYSOR. pp. 10-14.
38. Rosales, J., Munoz, A., Garcia, C., Garcia, L., Brayner, C., Perez, J. & Abanades, A. 2014. Computational model for the neutronic simulation of
39. pebble bed reactor's core using MCNPX. *International Journal of Nuclear Energy*, 2014:12. http://dx.doi.org/10.1155/2014/279073
40. Serpent.vtt.fi. 2021. *A continuous-energy Monte Carlo Reactor Physics Burnup Calculation Code*. https://serpent.vtt.fi/serpent Date of access:
41. Serpent.vtt.fi. 2022. *Delta- and surface-tracking*. https://serpent.vtt.fi/mediawiki/index.php/Delta-_and_surface-tracking Date of access: 7 April
42. Sihlangu, S.F. 2016. A neutronic model of the PMR200 prismatic modular reactor using MCNP5.
43. Stacey, W.M. 2018. *Nuclear reactor physics*. 3rd. Weinheim: Wiley-VCH.
44. Taylor, J.R. 1997. *An Introduction to Error Analysis: The Study of Uncertainties in Physical Measurements*. 2. University Science Books.
45. Tran, H.N. & Hoang, V.K. 2012. Core characteristics of an OTTO refueling pebble bed reactor and comparison with a multi-pass scheme. In. Proc. 6th Int. Topical Meeting on High Temperature Reactor Technology HTR2012.
46. Van Heerden, G., Sen, R.S. & Reitsma, F. 2006. *Calculational Approach and Results of the Safe Shutdown Earthquake Event for the Pebble Bed Modular Reactor*. Paper presented at the PHYSOR-2006, Vancouver, Canada. https://www.researchgate.net/publication/265821402_Calculational_Approach_and_Results_of_the_Safe_Shutdown_Earthquake_Event_for_the_Pebble_Bed_Modular_Reactor Date of access.
47. Vaz, P. 2009. Neutron transport simulation (selected topics). *Radiation Physics and Chemistry*, 78(10):829-842. 10.1016/j.radphyschem.2009.04.022
48. Wolters, E.R. 2011. *Hybrid Monte Carlo-Deterministic Neutron Transport Methods Using Nonlinear Functionals.* University of Michigan.

Appendix A: Serpent input files

This section gives the Serpent input file that was used to model the PBR-250. This could be used as a template for further design of the pebble bed reactor using Serpent. The syntax definition used in the code is shown in appendix A-3.The data can be directly copied and run. The additional files that are needed can be requested from Prof V Naicker/Olvidio Lunga or developed by the user. The additional files contain the coordinates of the missing cells.

A-1: Manual input file

```
% ----------------------------------------------------------------------------% ----------------------------------------------------------
%include “cores/Control_rods12.inp”
include “cores/withoutCR.inp”
%include “cores/RSS12.inp”
include “cores/noRSS12.inp”
% ----------------------------------------------------------------------------
% --- Coated particle:
particle 1
fuel    0.0250
buffer  0.0345
PyC     0.0385
SiC     0.0420
PyC     0.0460
matrix

% --- Universe surrounding particles:
surf 11 inf
cell particles 5 matrix  -11

% --- Read particles:
%pbed 10 5 “cores/particlesfinal.inp”
%pbed 10 5 “cores/Scparticles.inp”
pbed 10 5 “cores/Nwurcsrandompart.inp”

% --- Pebble with particles
particle 100
fill 10 2.5
matrix 3.0
```

helium

% --

%Burnable poison particles

particle 2

B4CP 0.0070

matrix

% --- Universe surrounding particles:

surf 12 inf

cell BPP 4 matrix -12

pbed 11 4 “cores/BPP.inp”

% --- Pebble with no particles

particle 1001

fill 11 2.5

matrix 3.0

helium

% --

%% --- Universe surrounding pebble:

surf 20 inf

cell 20 3 helium -20

% --- Read pebbles:

pbed 20 3 “cores/part3_SC.inp”

% --

% “reactor components”

cell core 0 fill 20 -Core

cell Carbonring 0 helium -Carbonringouter Carbonringinner

cell graphitering 0 matrix Core -Carbonringinner Rodhole1 Rodhole2 Rodhole3 Rodhole4 Rodhole5 Rodhole6 Rodhole7 Rodhole8 Rodhole9 Rodhole10 Rodhole11 Rodhole12 Rodhole13 Rodhole14 Rodhole15 Rodhole16 Rodhole17 Rodhole18 Rodhole19 Rodhole20 Rodhole21 Rodhole22 Rodhole23 Rodhole24 FlowChannel1 FlowChannel2 FlowChannel3 FlowChannel4 FlowChannel5 FlowChannel6 FlowChannel7 FlowChannel8 FlowChannel9 FlowChannel10 FlowChannel11 FlowChannel12 FlowChannel13 FlowChannel14 FlowChannel15 FlowChannel16 FlowChannel17 FlowChannel18 FlowChannel19 FlowChannel20 FlowChannel21 FlowChannel22 FlowChannel23 FlowChannel24

cell reactoroutside 0 outside Carbonringouter

/******** Radial boundaries of the core **********/

```
% --- Outer radius and core

surf Carbonringouter cylz 0.0 0.0 250 -550 550
surf Carbonringinner cylz 0.0 0.0 225 -550 550
surf Core cylz 0.0 0.0 150 -550 550

% ------------------------------------------------------------------------
% :RCS(Reactivity control system)

surf    Rodhole1    cylz    153.5822064     41.15222817     6.5     -550    550
surf    Rodhole2    cylz    137.6980392     79.5    6.5     -550    550
surf    Rodhole3    cylz    112.4299782     112.4299782     6.5     -550    550
surf    Rodhole4    cylz    79.5    137.6980392     6.5     -550    550
surf    Rodhole5    cylz    41.15222817     153.5822064     6.5     -550    550
surf    Rodhole6    cylz    9.73993E-15     159     6.5     -550    550
surf    Rodhole7    cylz    -41.15222817    153.5822064     6.5     -550    550
surf    Rodhole8    cylz    -79.5   137.6980392     6.5     -550    550
surf    Rodhole9    cylz    -112.4299782    112.4299782     6.5     -550    550
surf    Rodhole10   cylz    -137.6980392    79.5    6.5     -550    550
surf    Rodhole11   cylz    -153.5822064    41.15222817     6.5     -550    550
surf    Rodhole12   cylz    -159    1.94799E-14     6.5     -550    550
surf    Rodhole13   cylz    -153.5822064    -41.15222817    6.5     -550    550
surf    Rodhole14   cylz    -137.6980392    -79.5   6.5     -550    550
surf    Rodhole15   cylz    -112.4299782    -112.4299782    6.5     -550    550
surf    Rodhole16   cylz    -79.5   -137.6980392    6.5     -550    550
surf    Rodhole17   cylz    -41.15222817    -153.5822064    6.5     -550    550
surf    Rodhole18   cylz    -2.92198E-14    -159    6.5     -550    550
surf    Rodhole19   cylz    41.15222817     -153.5822064    6.5     -550    550
surf    Rodhole20   cylz    79.5    -137.6980392    6.5     -550    550
surf    Rodhole21   cylz    112.4299782     -112.4299782    6.5     -550    550
surf    Rodhole22   cylz    137.6980392     -79.5   6.5     -550    550
surf    Rodhole23   cylz    153.5822064     -41.15222817    6.5     -550    550
surf    Rodhole24   cylz    159     -3.89597E-14    6.5     -550    550



% ------------------------------------------------------------------------
% Flow Channels

surf    FlowChannel1    cylz    201.8784977     54.09318043     9       -550    550
```

```
surf    FlowChannel2    cylz    180.9993094     104.5   9       -550    550
surf    FlowChannel3    cylz    147.7853173     147.7853173     9       -550    550
surf    FlowChannel4    cylz    104.5   180.9993094     9       -550    550
surf    FlowChannel5    cylz    54.09318043     201.8784977     9       -550    550
surf    FlowChannel6    cylz    1.28028E-14     209     9       -550    550
surf    FlowChannel7    cylz    -54.09318043    201.8784977     9       -550    550
surf    FlowChannel8    cylz    -104.5  180.9993094     9       -550    550
surf    FlowChannel9    cylz    -147.7853173    147.7853173     9       -550    550
surf    FlowChannel10   cylz    -180.9993094    104.5   9       -550    550
surf    FlowChannel11   cylz    -201.8784977    54.09318043     9       -550    550
surf    FlowChannel12   cylz    -209    2.56056E-14     9       -550    550
surf    FlowChannel13   cylz    -201.8784977    -54.09318043    9       -550    550
surf    FlowChannel14   cylz    -180.9993094    -104.5  9       -550    550
surf    FlowChannel15   cylz    -147.7853173    -147.7853173    9       -550    550
surf    FlowChannel16   cylz    -104.5  -180.9993094    9       -550    550
surf    FlowChannel17   cylz    -54.09318043    -201.8784977    9       -550    550
surf    FlowChannel18   cylz    -3.84084E-14    -209    9       -550    550
surf    FlowChannel19   cylz    54.09318043     -201.8784977    9       -550    550
surf    FlowChannel20   cylz    104.5   -180.9993094    9       -550    550
surf    FlowChannel21   cylz    147.7853173     -147.7853173    9       -550    550
surf    FlowChannel22   cylz    180.9993094     -104.5  9       -550    550
surf    FlowChannel23   cylz    201.8784977     -54.09318043    9       -550    550
surf    FlowChannel24   cylz    209     -5.12112E-14    9       -550    550

cell    fC1     0       void    -FlowChannel1
cell    fC2     0       void    -FlowChannel2
cell    fC3     0       void    -FlowChannel3
cell    fC4     0       void    -FlowChannel4
cell    fC5     0       void    -FlowChannel5
cell    fC6     0       void    -FlowChannel6
cell    fC7     0       void    -FlowChannel7
cell    fC8     0       void    -FlowChannel8
cell    fC9     0       void    -FlowChannel9
cell    fC10    0       void    -FlowChannel10
cell    fC11    0       void    -FlowChannel11
cell    fC12    0       void    -FlowChannel12
cell    fC13    0       void    -FlowChannel13
cell    fC14    0       void    -FlowChannel14
cell    fC15    0       void    -FlowChannel15
cell    fC16    0       void    -FlowChannel16
```

```
cell        fC17      0          void       -FlowChannel17
cell        fC18      0          void       -FlowChannel18
cell        fC19      0          void       -FlowChannel19
cell        fC20      0          void       -FlowChannel20
cell        fC21      0          void       -FlowChannel21
cell        fC22      0          void       -FlowChannel22
cell        fC23      0          void       -FlowChannel23
cell        fC24      0          void       -FlowChannel24


% --------------------------------------------------------------------------
% Material data:
% -- Fuel:
mat fuel   -10.4                       tmp 300

92238.03c    -0.846598
92235.03c    -0.034830
 8016.03c    -0.118571

% --- Carbon buffer layer:
mat buffer  -1.05         moder grph 6000 tmp 300
6000.03c    -1

% --- Pyrolytic carbon layer:
mat PyC     -1.90         moder grph 6000 tmp 300
6000.03c    -1

% --- Silicon carbide layer:
mat SiC     -3.18                      tmp 300
14000.03c    -0.70000
 6000.03c    -0.30000

% --- Graphite matrix:
mat matrix  -1.74         moder grph 6000 tmp 300
 6000.03c    -1


mat helium   2.65156E-05                tmp 300
2004.03c    2.65156E-05
```

```
mat sleeves -7.8                        tmp 300
24000.03c   0.180  %Chemical composition
26000.03c   0.681
28000.03c   0.100
14000.03c   0.010
25055.03c   0.020
 6000.03c   0.001
22000.03c   0.008

% 90 enrichment of boron carbide
Mat B4C -1.8
5010.03c  -0.687109
5011.03c  -0.083940
6012.03c  -0.228951

% 90 enriched boron carbide
Mat B4CP -1.8
5010.03c  -0.370472
5011.03c  -0.407327
6012.03c  -0.222200

 % --- Thermal scattering data:
therm grph gre7.00 t
% ------------------------------------------------------------------------
%options
set bc 1
set his 1
set acelib “xs/sss_endfb68u.xsdata”
% --- Neutron population: 10000 neutrons per cycle, 280 active / 50 inactive cycles
set pop 10000 280 80
% ------------------------------------------------------------------------

% --- Geometry plots
%plot 3 5000 5000 -550 -300 300 -300 300
%plot 2 5000 5000 0 -300 300 -600 600
% ------------------------------------------------------------------------

% ------------------------------------------------------------------------

plot 2 5000 5000 125 -300 300 -600 600
```

```
plot 2 5000 5000 75.3 -300 300 -600 600
plot 2 5000 5000 25 -300 300 -600 600
plot 2 5000 5000 25 -300 300 -600 600
plot 2 5000 5000 -50 -300 300 -600 600
plot 2 5000 5000 -100 -300 300 -600 600
plot 2 5000 5000 -125 -300 300 -600 600
% --------------------------------------------------------------------------

mesh 3 1000 1000
mesh 2 1000 1000
% --------------------------------------------------------------------------
%ene 1 1 1E-11 2.50E-08 2.5001E-08 1.00E-06 1.0001E-06 1.00E-05 1.0001E-05 0.0003 0.000301 1 1.01 2.00E+01
%de 1
det 3
dx -200.0 200.0 20      % 20 bins in x-direction
dy -200.0 200.0 20      % 20 bins in y-direction
dz -550.0 550.0 20      % 20 bins in z-direction
% --------------------------------------------------------------------------
```

A-2: NWURCS-developed input file.

```
% input generated using NWURCS: lc_jul2020
set title “PB4”
% ------------------------------------------------------------------
%set acelib “/home/naicker/test/sss_jef22u.xsdata”
set acelib “/home/27136183/Serpent/Serpent_2020_download/Serpent2/xs/sss_endfb68u.xsdata”

% ------------------------------------------------------------------
set pop 20000 5000 80
% ------------------------------------------------------------------
set bc 1
% ------------------------------------------------------------------
cell 100001     0 fill     2     -2
cell 100002     0 fill     3     -3
cell 100003     0 m_00001     -1    2    3
cell 100004     0 outside      1
% ------------------------------------------------------------------
lat    2  1   0.000000   0.000000 51 51   6.000000
         4    4    4    4    4    4    4    4    4    4
         4    4    4    4    4    4    4    4    4    4
         4    4    4    4    4    4    4    4    4    4
         4    4    4    4    4    4    4    4    4    4
         4    4    4    4    4    4    4    4    4    4
         4
         4    4    4    4    4    4    4    4    4    4
         4    4    4    4    4    4    4    4    4    4
         4    5    5    5    5    5    5    5    5    5
         4    4    4    4    4    4    4    4    4    4
         4    4    4    4    4    4    4    4    4    4
         4
         4    4    4    4    4    4    4    4    4    4
         4    4    4    4    4    4    4    5    5    5
         5    5    5    5    5    5    5    5    5    5
         5    5    5    5    4    4    4    4    4    4
         4    4    4    4    4    4    4    4    4    4
         4
         4    4    4    4    4    4    4    4    4    4
         4    4    4    4    4    5    5    5    5    5
```

5 5 5 5 5 5 5 5 5 5
5 5 5 5 5 5 4 4 4 4
4 4 4 4 4 4 4 4 4 4
4
4 4 4 4 4 4 4 4 4 4
4 4 4 5 5 5 5 5 5 5
5 5 5 5 5 5 5 5 5 5
5 5 5 5 5 5 5 5 4 4
4 4 4 4 4 4 4 4 4 4
4
4 4 4 4 4 4 4 4 4 4
4 5 5 5 5 5 5 5 5 5
5 5 5 5 5 5 5 5 5 5
5 5 5 5 5 5 5 5 5 5
4 4 4 4 4 4 4 4 4 4
4
4 4 4 4 4 4 4 4 4 4
5 5 5 5 5 5 5 5 5 5
5 5 5 5 5 5 5 5 5 5
5 5 5 5 5 5 5 5 5 5
5 4 4 4 4 4 4 4 4 4
4
4 4 4 4 4 4 4 4 4 5
5 5 5 5 5 5 5 5 5 5
5 5 5 5 5 5 5 5 5 5
5 5 5 5 5 5 5 5 5 5
5 5 4 4 4 4 4 4 4 4
4
4 4 4 4 4 4 4 4 5 5
5 5 5 5 5 5 5 5 5 5
5 5 5 5 5 5 5 5 5 5
5 5 5 5 5 5 5 5 5 5
5 5 5 4 4 4 4 4 4 4
4
4 4 4 4 4 4 4 5 5 5
5 5 5 5 5 5 5 5 5 5
5 5 5 5 5 5 5 5 5 5
5 5 5 5 5 5 5 5 5 5
5 5 5 5 4 4 4 4 4 4
4

4 4 4 4 4 4 5 5 5 5
5 5 5 5 5 5 5 5 5 5
5 5 5 5 5 5 5 5 5 5
5 5 5 5 5 5 5 5 5 5
5 5 5 5 5 4 4 4 4 4
4
4 4 4 4 4 5 5 5 5 5
5 5 5 5 5 5 5 5 5 5
5 5 5 5 5 5 5 5 5 5
5 5 5 5 5 5 5 5 5 5
5 5 5 5 5 5 4 4 4 4
4
4 4 4 4 4 5 5 5 5 5
5 5 5 5 5 5 5 5 5 5
5 5 5 5 5 5 5 5 5 5
5 5 5 5 5 5 5 5 5 5
5 5 5 5 5 5 4 4 4 4
4
4 4 4 4 5 5 5 5 5 5
5 5 5 5 5 5 5 5 5 5
5 5 5 5 5 5 5 5 5 5
5 5 5 5 5 5 5 5 5 5
5 5 5 5 5 5 5 4 4 4
4
4 4 4 4 5 5 5 5 5 5
5 5 5 5 5 5 5 5 5 5
5 5 5 5 5 5 5 5 5 5
5 5 5 5 5 5 5 5 5 5
5 5 5 5 5 5 5 4 4 4
4
4 4 4 5 5 5 5 5 5 5
5 5 5 5 5 5 5 5 5 5
5 5 5 5 5 5 5 5 5 5
5 5 5 5 5 5 5 5 5 5
5 5 5 5 5 5 5 5 4 4
4
4 4 4 5 5 5 5 5 5 5
5 5 5 5 5 5 5 5 5 5
5 5 5 5 5 5 5 5 5 5
5 5 5 5 5 5 5 5 5 5

```
5   5   5   5   5   5   5   5   4   4
4
4   4   5   5   5   5   5   5   5   5
5   5   5   5   5   5   5   5   5   5
5   5   5   5   5   5   5   5   5   5
5   5   5   5   5   5   5   5   5   5
5   5   5   5   5   5   5   5   5   4
4
4   4   5   5   5   5   5   5   5   5
5   5   5   5   5   5   5   5   5   5
5   5   5   5   5   5   5   5   5   5
5   5   5   5   5   5   5   5   5   5
5   5   5   5   5   5   5   5   5   4
4
4   4   5   5   5   5   5   5   5   5
5   5   5   5   5   5   5   5   5   5
5   5   5   5   5   5   5   5   5   5
5   5   5   5   5   5   5   5   5   5
5   5   5   5   5   5   5   5   5   4
4
4   4   5   5   5   5   5   5   5   5
5   5   5   5   5   5   5   5   5   5
5   5   5   5   5   5   5   5   5   5
5   5   5   5   5   5   5   5   5   5
5   5   5   5   5   5   5   5   5   4
4
4   5   5   5   5   5   5   5   5   5
5   5   5   5   5   5   5   5   5   5
5   5   5   5   5   5   5   5   5   5
5   5   5   5   5   5   5   5   5   5
5   5   5   5   5   5   5   5   5   5
4
4   5   5   5   5   5   5   5   5   5
5   5   5   5   5   5   5   5   5   5
5   5   5   5   5   5   5   5   5   5
5   5   5   5   5   5   5   5   5   5
5   5   5   5   5   5   5   5   5   5
4
4   5   5   5   5   5   5   5   5   5
5   5   5   5   5   5   5   5   5   5
```

5	5	5	5	5	5	5	5	5	5
5	5	5	5	5	5	5	5	5	5
5	5	5	5	5	5	5	5	5	5
4									
4	5	5	5	5	5	5	5	5	5
5	5	5	5	5	5	5	5	5	5
5	5	5	5	5	5	5	5	5	5
5	5	5	5	5	5	5	5	5	5
5	5	5	5	5	5	5	5	5	5
4									
4	5	5	5	5	5	5	5	5	5
5	5	5	5	5	5	5	5	5	5
5	5	5	5	5	5	5	5	5	5
5	5	5	5	5	5	5	5	5	5
5	5	5	5	5	5	5	5	5	5
4									
4	5	5	5	5	5	5	5	5	5
5	5	5	5	5	5	5	5	5	5
5	5	5	5	5	5	5	5	5	5
5	5	5	5	5	5	5	5	5	5
5	5	5	5	5	5	5	5	5	5
4									
4	5	5	5	5	5	5	5	5	5
5	5	5	5	5	5	5	5	5	5
5	5	5	5	5	5	5	5	5	5
5	5	5	5	5	5	5	5	5	5
5	5	5	5	5	5	5	5	5	5
4									
4	5	5	5	5	5	5	5	5	5
5	5	5	5	5	5	5	5	5	5
5	5	5	5	5	5	5	5	5	5
5	5	5	5	5	5	5	5	5	5
5	5	5	5	5	5	5	5	5	5
4									
4	5	5	5	5	5	5	5	5	5
5	5	5	5	5	5	5	5	5	5
5	5	5	5	5	5	5	5	5	5
5	5	5	5	5	5	5	5	5	5
5	5	5	5	5	5	5	5	5	5
4									

```
4   4   5   5   5   5   5   5   5   5
5   5   5   5   5   5   5   5   5   5
5   5   5   5   5   5   5   5   5   5
5   5   5   5   5   5   5   5   5   5
5   5   5   5   5   5   5   5   5   4
4
4   4   5   5   5   5   5   5   5   5
5   5   5   5   5   5   5   5   5   5
5   5   5   5   5   5   5   5   5   5
5   5   5   5   5   5   5   5   5   5
5   5   5   5   5   5   5   5   5   4
4
4   4   5   5   5   5   5   5   5   5
5   5   5   5   5   5   5   5   5   5
5   5   5   5   5   5   5   5   5   5
5   5   5   5   5   5   5   5   5   5
5   5   5   5   5   5   5   5   5   4
4
4   4   5   5   5   5   5   5   5   5
5   5   5   5   5   5   5   5   5   5
5   5   5   5   5   5   5   5   5   5
5   5   5   5   5   5   5   5   5   5
5   5   5   5   5   5   5   5   5   4
4
4   4   4   5   5   5   5   5   5   5
5   5   5   5   5   5   5   5   5   5
5   5   5   5   5   5   5   5   5   5
5   5   5   5   5   5   5   5   5   5
5   5   5   5   5   5   5   5   4   4
4
4   4   4   5   5   5   5   5   5   5
5   5   5   5   5   5   5   5   5   5
5   5   5   5   5   5   5   5   5   5
5   5   5   5   5   5   5   5   5   5
5   5   5   5   5   5   5   5   4   4
4
4   4   4   4   5   5   5   5   5   5
5   5   5   5   5   5   5   5   5   5
5   5   5   5   5   5   5   5   5   5
5   5   5   5   5   5   5   5   5   5
```

5 5 5 5 5 5 5 4 4 4
4
4 4 4 4 5 5 5 5 5 5
5 5 5 5 5 5 5 5 5 5
5 5 5 5 5 5 5 5 5 5
5 5 5 5 5 5 5 5 5 5
5 5 5 5 5 5 5 4 4 4
4
4 4 4 4 4 5 5 5 5 5
5 5 5 5 5 5 5 5 5 5
5 5 5 5 5 5 5 5 5 5
5 5 5 5 5 5 5 5 5 5
5 5 5 5 5 5 4 4 4 4
4
4 4 4 4 4 5 5 5 5 5
5 5 5 5 5 5 5 5 5 5
5 5 5 5 5 5 5 5 5 5
5 5 5 5 5 5 5 5 5 5
5 5 5 5 5 5 4 4 4 4
4
4 4 4 4 4 4 5 5 5 5
5 5 5 5 5 5 5 5 5 5
5 5 5 5 5 5 5 5 5 5
5 5 5 5 5 5 5 5 5 5
5 5 5 5 5 4 4 4 4 4
4
4 4 4 4 4 4 4 5 5 5
5 5 5 5 5 5 5 5 5 5
5 5 5 5 5 5 5 5 5 5
5 5 5 5 5 5 5 5 5 5
5 5 5 5 4 4 4 4 4 4
4
4 4 4 4 4 4 4 4 5 5
5 5 5 5 5 5 5 5 5 5
5 5 5 5 5 5 5 5 5 5
5 5 5 5 5 5 5 5 5 5
5 5 5 4 4 4 4 4 4 4
4
4 4 4 4 4 4 4 4 4 5
5 5 5 5 5 5 5 5 5 5

5 5 5 5 5 5 5 5 5 5
5 5 5 5 5 5 5 5 5 5
5 5 4 4 4 4 4 4 4 4
4
4 4 4 4 4 4 4 4 4 4
5 5 5 5 5 5 5 5 5 5
5 5 5 5 5 5 5 5 5 5
5 5 5 5 5 5 5 5 5 5
5 4 4 4 4 4 4 4 4 4
4
4 4 4 4 4 4 4 4 4 4
4 5 5 5 5 5 5 5 5 5
5 5 5 5 5 5 5 5 5 5
5 5 5 5 5 5 5 5 5 5
4 4 4 4 4 4 4 4 4 4
4
4 4 4 4 4 4 4 4 4 4
4 4 4 5 5 5 5 5 5 5
5 5 5 5 5 5 5 5 5 5
5 5 5 5 5 5 5 5 4 4
4 4 4 4 4 4 4 4 4 4
4
4 4 4 4 4 4 4 4 4 4
4 4 4 4 4 5 5 5 5 5
5 5 5 5 5 5 5 5 5 5
5 5 5 5 5 5 4 4 4 4
4 4 4 4 4 4 4 4 4 4
4
4 4 4 4 4 4 4 4 4 4
4 4 4 4 4 4 4 5 5 5
5 5 5 5 5 5 5 5 5 5
5 5 5 5 4 4 4 4 4 4
4 4 4 4 4 4 4 4 4 4
4
4 4 4 4 4 4 4 4 4 4
4 4 4 4 4 4 4 4 4 4
4 5 5 5 5 5 5 5 5 5
4 4 4 4 4 4 4 4 4 4
4 4 4 4 4 4 4 4 4 4
4

4 4 4 4 4 4 4 4 4 4
4 4 4 4 4 4 4 4 4 4
4 4 4 4 4 4 4 4 4 4
4 4 4 4 4 4 4 4 4 4
4 4 4 4 4 4 4 4 4 4
4
% ----------
lat 3 1 0.000000 0.000000 51 51 6.000000
6 6 6 6 6 6 6 6 6 6
6 6 6 6 6 6 6 6 6 6
6 6 6 6 6 6 6 6 6 6
6 6 6 6 6 6 6 6 6 6
6 6 6 6 6 6 6 6 6 6
6
6 6 6 6 6 6 6 6 6 6
6 6 6 6 6 6 6 6 6 6
6 7 7 7 7 7 7 7 7 7
6 6 6 6 6 6 6 6 6 6
6 6 6 6 6 6 6 6 6 6
6
6 6 6 6 6 6 6 6 6 6
6 6 6 6 6 6 6 7 7 7
7 7 7 7 7 7 7 7 7 7
7 7 7 7 6 6 6 6 6 6
6 6 6 6 6 6 6 6 6 6
6
6 6 6 6 6 6 6 6 6 6
6 6 6 6 6 7 7 7 7 7
7 7 7 7 7 7 7 7 7 7
7 7 7 7 7 7 6 6 6 6
6 6 6 6 6 6 6 6 6 6
6
6 6 6 6 6 6 6 6 6 6
6 6 6 7 7 7 7 7 7 7
7 7 7 7 7 7 7 7 7 7
7 7 7 7 7 7 7 7 6 6
6 6 6 6 6 6 6 6 6 6
6
6 6 6 6 6 6 6 6 6 6
6 7 7 7 7 7 7 7 7 7

7 7 7 7 7 7 7 7 7 7
7 7 7 7 7 7 7 7 7 7
6 6 6 6 6 6 6 6 6 6
6
6 6 6 6 6 6 6 6 6 6
7 7 7 7 7 7 7 7 7 7
7 7 7 7 7 7 7 7 7 7
7 7 7 7 7 7 7 7 7 7
7 6 6 6 6 6 6 6 6 6
6
6 6 6 6 6 6 6 6 6 7
7 7 7 7 7 7 7 7 7 7
7 7 7 7 7 7 7 7 7 7
7 7 7 7 7 7 7 7 7 7
7 7 6 6 6 6 6 6 6 6
6
6 6 6 6 6 6 6 6 7 7
7 7 7 7 7 7 7 7 7 7
7 7 7 7 7 7 7 7 7 7
7 7 7 7 7 7 7 7 7 7
7 7 7 6 6 6 6 6 6 6
6
6 6 6 6 6 6 6 7 7 7
7 7 7 7 7 7 7 7 7 7
7 7 7 7 7 7 7 7 7 7
7 7 7 7 7 7 7 7 7 7
7 7 7 7 6 6 6 6 6 6
6
6 6 6 6 6 6 7 7 7 7
7 7 7 7 7 7 7 7 7 7
7 7 7 7 7 7 7 7 7 7
7 7 7 7 7 7 7 7 7 7
7 7 7 7 7 6 6 6 6 6
6
6 6 6 6 6 7 7 7 7 7
7 7 7 7 7 7 7 7 7 7
7 7 7 7 7 7 7 7 7 7
7 7 7 7 7 7 7 7 7 7
7 7 7 7 7 7 6 6 6 6
6

6 6 6 6 6 7 7 7 7 7
7 7 7 7 7 7 7 7 7 7
7 7 7 7 7 7 7 7 7 7
7 7 7 7 7 7 7 7 7 7
7 7 7 7 7 7 6 6 6 6
6
6 6 6 6 7 7 7 7 7 7
7 7 7 7 7 7 7 7 7 7
7 7 7 7 7 7 7 7 7 7
7 7 7 7 7 7 7 7 7 7
7 7 7 7 7 7 7 6 6 6
6
6 6 6 6 7 7 7 7 7 7
7 7 7 7 7 7 7 7 7 7
7 7 7 7 7 7 7 7 7 7
7 7 7 7 7 7 7 7 7 7
7 7 7 7 7 7 7 6 6 6
6
6 6 6 7 7 7 7 7 7 7
7 7 7 7 7 7 7 7 7 7
7 7 7 7 7 7 7 7 7 7
7 7 7 7 7 7 7 7 7 7
7 7 7 7 7 7 7 7 6 6
6
6 6 6 7 7 7 7 7 7 7
7 7 7 7 7 7 7 7 7 7
7 7 7 7 7 7 7 7 7 7
7 7 7 7 7 7 7 7 7 7
7 7 7 7 7 7 7 7 6 6
6
6 6 7 7 7 7 7 7 7 7
7 7 7 7 7 7 7 7 7 7
7 7 7 7 7 7 7 7 7 7
7 7 7 7 7 7 7 7 7 7
7 7 7 7 7 7 7 7 7 6
6
6 6 7 7 7 7 7 7 7 7
7 7 7 7 7 7 7 7 7 7
7 7 7 7 7 7 7 7 7 7
7 7 7 7 7 7 7 7 7 7

```
7   7   7   7   7   7   7   7   7   6
6
6   6   7   7   7   7   7   7   7   7
7   7   7   7   7   7   7   7   7   7
7   7   7   7   7   7   7   7   7   7
7   7   7   7   7   7   7   7   7   7
7   7   7   7   7   7   7   7   7   6
6
6   6   7   7   7   7   7   7   7   7
7   7   7   7   7   7   7   7   7   7
7   7   7   7   7   7   7   7   7   7
7   7   7   7   7   7   7   7   7   7
7   7   7   7   7   7   7   7   7   6
6
6   7   7   7   7   7   7   7   7   7
7   7   7   7   7   7   7   7   7   7
7   7   7   7   7   7   7   7   7   7
7   7   7   7   7   7   7   7   7   7
7   7   7   7   7   7   7   7   7   7
6
6   7   7   7   7   7   7   7   7   7
7   7   7   7   7   7   7   7   7   7
7   7   7   7   7   7   7   7   7   7
7   7   7   7   7   7   7   7   7   7
7   7   7   7   7   7   7   7   7   7
6
6   7   7   7   7   7   7   7   7   7
7   7   7   7   7   7   7   7   7   7
7   7   7   7   7   7   7   7   7   7
7   7   7   7   7   7   7   7   7   7
7   7   7   7   7   7   7   7   7   7
6
6   7   7   7   7   7   7   7   7   7
7   7   7   7   7   7   7   7   7   7
7   7   7   7   7   7   7   7   7   7
7   7   7   7   7   7   7   7   7   7
7   7   7   7   7   7   7   7   7   7
6
6   7   7   7   7   7   7   7   7   7
7   7   7   7   7   7   7   7   7   7
```

```
7   7   7   7   7   7   7   7   7   7
7   7   7   7   7   7   7   7   7   7
7   7   7   7   7   7   7   7   7   7
6
6   7   7   7   7   7   7   7   7   7
7   7   7   7   7   7   7   7   7   7
7   7   7   7   7   7   7   7   7   7
7   7   7   7   7   7   7   7   7   7
7   7   7   7   7   7   7   7   7   7
6
6   7   7   7   7   7   7   7   7   7
7   7   7   7   7   7   7   7   7   7
7   7   7   7   7   7   7   7   7   7
7   7   7   7   7   7   7   7   7   7
7   7   7   7   7   7   7   7   7   7
6
6   7   7   7   7   7   7   7   7   7
7   7   7   7   7   7   7   7   7   7
7   7   7   7   7   7   7   7   7   7
7   7   7   7   7   7   7   7   7   7
7   7   7   7   7   7   7   7   7   7
6
6   7   7   7   7   7   7   7   7   7
7   7   7   7   7   7   7   7   7   7
7   7   7   7   7   7   7   7   7   7
7   7   7   7   7   7   7   7   7   7
7   7   7   7   7   7   7   7   7   7
6
6   6   7   7   7   7   7   7   7   7
7   7   7   7   7   7   7   7   7   7
7   7   7   7   7   7   7   7   7   7
7   7   7   7   7   7   7   7   7   7
7   7   7   7   7   7   7   7   7   6
6
6   6   7   7   7   7   7   7   7   7
7   7   7   7   7   7   7   7   7   7
7   7   7   7   7   7   7   7   7   7
7   7   7   7   7   7   7   7   7   7
7   7   7   7   7   7   7   7   7   6
6
```

6 6 7 7 7 7 7 7 7 7
7 7 7 7 7 7 7 7 7 7
7 7 7 7 7 7 7 7 7 7
7 7 7 7 7 7 7 7 7 7
7 7 7 7 7 7 7 7 7 6
6
6 6 7 7 7 7 7 7 7 7
7 7 7 7 7 7 7 7 7 7
7 7 7 7 7 7 7 7 7 7
7 7 7 7 7 7 7 7 7 7
7 7 7 7 7 7 7 7 7 6
6
6 6 6 7 7 7 7 7 7 7
7 7 7 7 7 7 7 7 7 7
7 7 7 7 7 7 7 7 7 7
7 7 7 7 7 7 7 7 7 7
7 7 7 7 7 7 7 7 6 6
6
6 6 6 7 7 7 7 7 7 7
7 7 7 7 7 7 7 7 7 7
7 7 7 7 7 7 7 7 7 7
7 7 7 7 7 7 7 7 7 7
7 7 7 7 7 7 7 7 6 6
6
6 6 6 6 7 7 7 7 7 7
7 7 7 7 7 7 7 7 7 7
7 7 7 7 7 7 7 7 7 7
7 7 7 7 7 7 7 7 7 7
7 7 7 7 7 7 7 6 6 6
6
6 6 6 6 7 7 7 7 7 7
7 7 7 7 7 7 7 7 7 7
7 7 7 7 7 7 7 7 7 7
7 7 7 7 7 7 7 7 7 7
7 7 7 7 7 7 7 6 6 6
6
6 6 6 6 6 7 7 7 7 7
7 7 7 7 7 7 7 7 7 7
7 7 7 7 7 7 7 7 7 7
7 7 7 7 7 7 7 7 7 7

7 7 7 7 7 7 6 6 6 6
6
6 6 6 6 6 7 7 7 7 7
7 7 7 7 7 7 7 7 7 7
7 7 7 7 7 7 7 7 7 7
7 7 7 7 7 7 7 7 7 7
7 7 7 7 7 7 6 6 6 6
6
6 6 6 6 6 6 7 7 7 7
7 7 7 7 7 7 7 7 7 7
7 7 7 7 7 7 7 7 7 7
7 7 7 7 7 7 7 7 7 7
7 7 7 7 7 6 6 6 6 6
6
6 6 6 6 6 6 6 7 7 7
7 7 7 7 7 7 7 7 7 7
7 7 7 7 7 7 7 7 7 7
7 7 7 7 7 7 7 7 7 7
7 7 7 7 6 6 6 6 6 6
6
6 6 6 6 6 6 6 6 7 7
7 7 7 7 7 7 7 7 7 7
7 7 7 7 7 7 7 7 7 7
7 7 7 7 7 7 7 7 7 7
7 7 7 6 6 6 6 6 6 6
6
6 6 6 6 6 6 6 6 6 7
7 7 7 7 7 7 7 7 7 7
7 7 7 7 7 7 7 7 7 7
7 7 7 7 7 7 7 7 7 7
7 7 6 6 6 6 6 6 6 6
6
6 6 6 6 6 6 6 6 6 6
7 7 7 7 7 7 7 7 7 7
7 7 7 7 7 7 7 7 7 7
7 7 7 7 7 7 7 7 7 7
7 6 6 6 6 6 6 6 6 6
6
6 6 6 6 6 6 6 6 6 6
6 7 7 7 7 7 7 7 7 7

```
      7   7   7   7   7   7   7   7   7   7
      7   7   7   7   7   7   7   7   7   7
      6   6   6   6   6   6   6   6   6   6
      6
      6   6   6   6   6   6   6   6   6   6
      6   6   6   7   7   7   7   7   7   7
      7   7   7   7   7   7   7   7   7   7
      7   7   7   7   7   7   7   7   6   6
      6   6   6   6   6   6   6   6   6   6
      6
      6   6   6   6   6   6   6   6   6   6
      6   6   6   6   6   7   7   7   7   7
      7   7   7   7   7   7   7   7   7   7
      7   7   7   7   7   7   6   6   6   6
      6   6   6   6   6   6   6   6   6   6
      6
      6   6   6   6   6   6   6   6   6   6
      6   6   6   6   6   6   6   7   7   7
      7   7   7   7   7   7   7   7   7   7
      7   7   7   7   6   6   6   6   6   6
      6   6   6   6   6   6   6   6   6   6
      6
      6   6   6   6   6   6   6   6   6   6
      6   6   6   6   6   6   6   6   6   6
      6   7   7   7   7   7   7   7   7   7
      6   6   6   6   6   6   6   6   6   6
      6   6   6   6   6   6   6   6   6   6
      6
      6   6   6   6   6   6   6   6   6   6
      6   6   6   6   6   6   6   6   6   6
      6   6   6   6   6   6   6   6   6   6
      6   6   6   6   6   6   6   6   6   6
      6   6   6   6   6   6   6   6   6   6
      6
cell 100009    4 m_00002    -5
cell 100011    5 fill    8    -5
cell 100013    6 m_00002    -6
cell 100015    7 fill    9    -6
% --------------------------------------------------------------------
lat    8 11    0.000000    0.000000  305.999987
```

1 1 92
6.000000 6.000000 6.000000
10
10
10
10
10
10
10
10
10
10
10
10
10
10
10
10
10
10
10
10
10
10
10
10
10
10
10
10
10
10
10
10
10
10
10
10
10
10

10
10
10
10
10
10
10
10
10
10
10
10
10
10
10
10
10
10
10
10
10
10
10
10
10
10
10
10
10
10
10
10
10
10
10
10
10
10
10
10

```
        10
        10
        10
        10
        10
        10
        10
        10
        10
        10
        10
        10
        10
% ------------------------------------------------------------------
lat    9 11    0.000000    0.000000  857.999913
            1  1  92
           6.000000   6.000000   6.000000
        11
        11
        11
        11
        11
        11
        11
        11
        11
        11
        11
        11
        11
        11
        11
        11
        11
        11
        11
        11
        11
        11
        11
        11
        11
        11
        11
        11
        11
        11
        11
        11
```

11
11
11
11
11
11
11
11
11
11
11
11
11
11
11
11
11
11
11
11
11
11
11
11
11
11
11
11
11
11
11
11
11
11
11
11
11
11
11
11

```
        11
        11
        11
        11
        11
        11
        11
        11
        11
        11
        11
        11
        11
        11
        11
        11
        11
        11
        11
        11
        11
        11
        11
        11
        11
        11
        11
cell 100021    10 m_00002     -8    7
cell 100022    10 fill    12     -9
cell 100023    10 m_00001     -7    9
cell 100025    11 m_00002     -8    7
cell 100026    11 fill    12     -9
cell 100027    11 m_00001     -7    9
% ------------------------------------------------------------------------
pbed     12     14  “/home/27136183/Serpent/Serpent_2020_download/Serpent2/cores/particlesfinal.inp”
cell particles     14  m_00001    -10
% ------------------------------------------------------------------------
```

```
particle      1
m_00005    0.025000
m_00006    0.034500
m_00007    0.038500
m_00008    0.042000
m_00009    0.046000
m_00001



% ------------------------------------------------------------------------
surf   1 cyl          0.000000    0.000000  225.000000   30.000000 1133.999900
surf   2 cyl          0.000000    0.000000  150.000000   30.000000  581.999950
surf   3 cyl          0.000000    0.000000  150.000000  581.999950 1133.999900
surf   4 cyl          0.000000    0.000000  250.000000   30.000000 1133.999900
surf   5 cuboid       -3.000000    3.000000   -3.000000    3.000000
                  30.000000  581.999975
surf   6 cuboid       -3.000000    3.000000   -3.000000    3.000000
                 581.999925 1133.999900
surf   7 sph          0.000000    0.000000    0.000000    3.000000
surf   8 cuboid       -3.000000    3.000000   -3.000000    3.000000
                 -3.000000    3.000000
surf   9 sph          0.000000    0.000000    0.000000    2.500000
surf  10 inf



% ------------------------------------------------------------------------
%mat  m_00001  0.08725570 moder  grph  6000  tmp= 300.00  % inputmat id  53
   %6000.03c  1.0000E+00
mat m_00001 -1.74         moder grph 6000 tmp 300
 6000.03c    -1




%mat  m_00002  0.10068448  tmp= 300.00                  % inputmat id   2
  % 2003.03c  1.0100E-06
  % 2004.03c  1.0000E+00

mat m_00002   2.65156E-05               tmp 300
 2004.03c    2.65156E-05
```

```
%mat  m_00003  0.08725570  tmp= 300.00                % inputmat id  52
  %6000.03c  1.0000E+00
%mat  m_00004  0.08725570  tmp= 300.00  moder  grph  6000  % inputmat id  51
  %6000.03c  1.0000E+00

%mat  m_00005  0.06961980  tmp= 300.00                % inputmat id  21
 % 8016.03c  6.6641E-01
 %  8017.03c  2.5333E-04
 % 92235.03c  1.3497E-02
%  92238.03c  3.1984E-01


mat  m_00005   -10.4                    tmp 300

92238.03c    -0.846598
92235.03c    -0.034830
8016.03c    -0.118571



%mat  m_00006  0.05265430  tmp= 300.00                % inputmat id   7
  %6000.03c  1.0000E+00
mat m_00006  -1.05         moder grph 6000 tmp 300
 6000.03c    -1


%mat  m_00007  0.09527920  tmp= 300.00                % inputmat id   8
 % 6000.03c  1.0000E+00
 mat m_00007     -1.90         moder grph 6000 tmp 300
 6000.03c    -1



%mat  m_00008  0.09553600  tmp= 300.00                % inputmat id   9
  %6000.03c  5.0000E-01
```

```
 %14028.03c  4.6111E-01
 %14029.03c  2.3425E-02
 %14030.03c  1.5460E-02
mat m_00008      -3.18                    tmp 300
14000.03c    -0.70000
 6000.03c    -0.30000

%mat  m_00009  0.09527920  tmp= 300.00                % inputmat id  10
 % 6000.03c  1.0000E+00
mat m_00009    -1.90         moder grph 6000 tmp 300
 6000.03c    -1
therm grph  grj3.00 t
% ---------------------------------------------------------------------
plot 3 5000 5000
plot 3 5000 5000
plot 2 5000 5000
plot 2 5000 5000

mesh 3 1000 1000
mesh 2 1000 1000
```

A-3: General serpent syntax details

This section describes the syntax used in the Serpent code shown in Appendix A-2 and A-3 and the interested reader is directed to the Leppänen (2015).

A3-a: Surf card

Serpent has several elementary and derived surfaces. A “derived” surface type is one that is made up of two or more elementary surfaces, such as a cube made up of six planes (Leppänen *et al.,* 2015:19). It has a total of 20 surface types as listed in Table 5-1.

The syntax of the surface card is:
surf <id> <type> <param 1> <param 2> …

where:

<id> – surface identifier;
<type> – surface type;
<param 1> <param 2> ... – surface parameters;

Table 5-1:Surface type in Serpent code

Type	**Description**
Inf	all space
px; py; pz	plane perpendicular to x-axis; y-axis; z-axis
Sph	sphere
cylx; cyly;cylz	circular cylinder parallel to x-axis; y-axis; z-axis
Sqc	square cylinder parallel to z-axis
Cube	cube
Cuboid	cuboid
hexxc; hexyc	x-type; y-type hexagonal cylinder;
hexxprism; hexyprism	x-type; y-type; hexagonal prism;
Cross	cruciform cylinder parallel to z-axis
conx; cony	cone oriented in the x-axis; y-axis

Dode	dodecagonal cylinder parallel to z-axis
Octa	octagonal cylinder parallel to z-axis
Plane	general plane
quadratic	general quadratic surface

A3-b: Cell card

The geometry description in Serpent is made up of three-dimensional spaces known as cells. These cells are volumes enclosed by the intersections of elementary or defined surfaces. The code can handle surface boundary intersections, which means that the neutron is within the cell if and only if it is on the same side of each boundary surface as specified in the surface list (Leppänen et al., 2015:24). On the other hand, Serpent lacks a union operator, making the generation of custom surfaces challenging. Surfaces such as the elliptical KLAK channels seen on the HTR-10 (elliptical shapes set at varying angles around a centre) are difficult to define as they require manual coding in Serpent.

134yntaxntax of the cell card is:

cell <name> <u0> <mat> <surf 1> <surf 2> ...
where:
<name> – the cell name;
<u0> – the universe number of the cell;
<mat> – the cell material;
<surf 1> <surf 2> ... – the boundary surfaces.

Each cell is characterised by a collection of positive and negative surface numbers that correspond to the surface identifiers specified in the surface cards. Positive entries correspond to the surf’ce's outer space, whereas negative entries refer to the surf’ce's inner space.

A3-c: Include card

An input file can be divided into separate files which is very useful if input files are too long. This card is used when reading additional files, which are needed by the program during calculations, from the main file. The format for the include command is:

Inclu“e "<filena”e>"

<filename> – is the file path for the file to be included.

An example of use of this card in the generated input files is demonstrated with the nuclear data file, and the particle and pebble location files.

A3-d: Mat card

Cells may have materials inside them. The Mat Card is used to define the materials which are contained in the cells.

The basic syntax of the material card is:

mat <name> <dens> [<options>]
<iso 1> <frac 1>
<iso 2> <frac 2>
...
where:
<name> - the material name;
<dens> - density (mass or atomic);
<options> - options (depending on case);
<iso 1> <iso 2> .–. - names of the constituent nuclides; and
<frac 1> <frac 2> .–. - corresponding fractions (mass or atomic).

The nuclide names correspond to the cross-section library identifiers which define the cross-section data used in the calculation. For the mat card, atomic fractions, and densities (in units of $10^{24}/cm^3$) are assigned positive values, while mass fractions and densities (g/cm^3) are assigned negative values.

A3-e: Mesh card

The Serpent programme has a feature for visualising neutronics in thermal systems. This is accomplished by plotting and displaying a PNG graphic files of the system fission power and thermal fluxes. A hot area is represented on the plots by shades of red and yellow, whereas a cold area is represented by shades of blue. The plots can be shown on a yz-plane (1), xz-plane (2) and xy-plane (3) orientation. The Mesh Plots for the PBR-250 (SC-setup) are shown in Appendix D.

The parameters for a reaction rate mesh plotter are defined as:

mesh <or> <nx> <ny> [<sym> <x0> <x1> <y0> <y1> <z0> <z1>]

where:

<or> - orientation of the plot plane (1, 2 or 3);

<nx> - width of the plot in pixels;

<ny> - height of the plot in pixels;

<sym> - symmetry option (0, 2, 4 or 8);

<x0> - minimum value of the x-coordinate;

<x1> - maximum value of the x-coordinate;

<y0> - minimum value of the y-coordinate;

<y1> - maximum value of the y-coordinate;

<z0> - minimum value of the z-coordinate; and

<z1> - maximum value of the z-coordinate.

A3-f: Particle card

As discussed in Section 3.1.9, HTGR's consist of fuel particles that are made up of many layers of different materials (TRISO/BISO fuel particles). The fuel pebble also consists of two layers of materials (fuel particles dispersed in a graphite matrix, and an enclosing graphite-only layer). The particle card addresses the problem of defining these different layers in both the pebble and the fuel particles.

The multi-layer fuel particles or pebbles can be defined as:

particle <id>

<mat 1> <r1>

<mat 2> <r2>

...

<mat n>

where:

<id> - particle identifier (universe number);

<mat 1> <mat 2> ... – materials; and

<r1> <r2> ... - outer radii of the material regions.

A3-g: Pbed card

The geometries of pebble bed reactors can be modelled implicitly or explicitly, and this dissertation focuses on the latter, which was the best choice, as implicit modelling functions best

for low packing fractions. Explicit modelling involves reading particle/pebble positions from a separate file. This can be used to place pebbles in a reactor and fuel particles in the pebble's graphite matrix. The input syntax is:

pbed <u0> <uf> "<inputfile>" [<options>]

where:

<u0> - universe number of the dispersed medium;
<uf> - universe filling the space between the particles / pebbles;
<inputfile- input file containing the particle / pebble coordinates; and
<options> - options (the only options available is ‘pow’ options).

The particle/pebble is placed at a specific location therefore there is no estimation of particle/pebble locations. The particle/pebble location coordinates are described in a different file with an unlimited number of coordinate descriptions. The format in the file is:

<x> <y> <z> <r> <u>
where:
<x> - x-coordinate of the coated particle / pebble;
<y> - y-coordinate of the coated particle / pebble;
<z> - z-coordinate of the coated particle / pebble;
<r> - radius of the coated particle / pebble; and
<u> - universe number of the coated particle / pebble.

A3-h: Disperse option.

This option generates a random distribution of objects in each volume. The option was used to generate coordinates for the particles scattered throughout the graphite matrix. The generator requests volume; dimension and packing fraction information from the user. The method then generates a distribution inside the specified volume without any overlap.

A3-i: Plot option

Serpent uses the GD open-source graphics library, which is compiled with the Serpent code, to produce geometry plots in PNG format. The plots can be shown on a yz-plane (1), xz-plane (2) and xy-plane (3) orientation. The resolution of the output image is described by the width and height parameters and the material is randomly given a colour (void regions are in black, geometry errors bright green or red) unless specified. All the surfaces are given a solid black line and the space between overlapping surfaces is given a red colour. The syntax of the plotter command is:

plot <or> <nx> <ny> [<p> <min1> <max1> <min2> <max2>]

where:
<or> - orientation of the plot plane (1, 2 or 3);
<nx> - width of the plot in pixels;
<ny> - height of the plot in pixels;
<p> - position on the axis perpendicular to the plot plane;
<min1> - minimum value of the first coordinate;
<max1> - maximum value of the first coordinate;
<min2> - minimum value of the second coordinate; and
<max2> - maximum value of the second coordinate.

A3-j: Set card.

Serpent sets different calculation parameters using this command:
The syntax is given as:
set <param> <value 1> <value 2> ...
where:
<param> is the parameter name; and
<value 1> <value 2> ... are the parameter values.

This command was used to set the parameters covered in sections A3-k, A3-l, A3-o, and A3-p below.

A3-k: Pop

Serpent uses the k-eigenvalue criticality source method during criticality calculations, in which the simulation is undertaken in cycles and the distribution of the source in each cycle is formed by

the fission reaction distribution of the preceding cycle simulation. The parameters for criticality source calculation are set using:

set pop <npop> <cycles> <skip> [<keff0> <int>]

where:
<npop> - number of source neutrons per cycle;
<cycles> - number of active cycles run;
<skip> - number of inactive cycles run;
<keff0> - initial guess for k_{eff}; and
<int> - collection interval.

The number of source neutrons per cycle is fixed by npop. During a run, there are inactive cycles and active cycles. The inactive cycles allow the initial fission source distribution to converge before the results of the run are collected. The importance of the fission source distribution convergence is discussed in Section 2.12. Source points are initially randomly distributed in the geometry and the initial k_{eff} is set to unity. The statistical accuracy of the simulation depends on the number of active neutron histories.

A3-l: Acelib

A single directory file is utilised in Serpent for the cross-sections used in the transport simulation. The cross-section library directory file path is set using:

set acelib "<file>"

where
<file> - file path for the ACE directory file.

A3-m: Therm card

In simulated nuclear systems, low-energy free-gas elastic scattering processes are replaced by thermal scattering cross-sections for some important bound moderator nuclides, such as hydrogen in water or carbon in graphite. Thermal systems cannot be modelled using free-atom cross-sections without introducing significant inaccuracies in the spectrum and results. Thermal scattering data is defined using:

therm <thname> <lib>

where
<thname> - name of the data library; and
<lib> - library identifier as defined in the directory file.

The percentage sign (%) is used to define a comment line and anything after the character is ignored until the end of the line.

A3-n: Det

The collision estimate of neutron flux is used in the Serpent routine for calculating user-defined reaction rates integrated over space and energy. The response function, spatial, and energy domains are set by the detector parameters using

det <name> <param 1> <param 2> ...

where <name> is the detector name; and

<param 1> <param 2> ... are the detector parameter sets.

An example of a parameter that was used during the modelling process was:

de - Detector energy grid which defines the energy bins for the response function.

A3-o: Power

The calculations were normalised using total heating power in the system, set using this option. The syntax for is option is:

set power <P>
where <P> is the total heating power (W)

A3-p:His

This option is used to call for batch history records. When set, batch-wise history data on k_{eff}, fission source (Shannon) entropy etc., is calculated and recorded. The syntax for the option is:

set his <opt>

where;

opt: option to switch batch history record on (1/yes) or off (0/no)
When set, the output is a MATLAB compatible file, with tables of different parameters e.g., cycle-wise k_{eff}, transport cycle time, cycle-wise Shannon entropy etc.

A3-q: Output file (_res.m)

This is the main default output file that has all the results from the transport cycle. Significant output parameters used in this dissertation obtained from the file include the:

1. TOT_CPU_TIME - Total CPU time
2. TRANSPORT_CYCLE_TIME - Wall-clock time spent for transport simulation
3. CPU_USAGE - Total CPU usage fraction
4. MEMSIZE - Used memory size

Appendix B: Supplementary literature review

B-1: Neutron transport equation

One of the tasks in the design and analysis of nuclear reactors is the accurate and detailed prediction of neutron interactions (space, angle, energy, time-dependence) in all components of the reactor core and reflectors. The calculation of the transport of neutrons and their interactions with matter is perhaps the fundamental topic in reactor physics. The neutron transport equation describes the neutron flux across a directional planar cross-section in an inhomogeneous fissile medium (typically measured in the number of neutrons per cm^2 per second (Cox *et al.*, 2019:426) and it stems from the neutron balance equation which has its origin in the Boltzmann equation. The Boltzmann equation describes the statistical behaviour of neutrons in a fluid. Each term in the neutron transport equation corresponds to a physical process that changes a neutron's phase space: birth, collisions and leakage (Wolters., 2011:2).

The neutron transport equation is summarised as follows: In each volume the rate of change of neutrons = net rate of generation of neutrons in collisions + rate of introduction of source neutrons – net rate of outflow of neutrons.

The neutron transport equation is as follows (Stacey, 2018:307):

$$\begin{aligned}\frac{\partial \mathrm{N}}{\partial \mathrm{t}}(\vec{r},\hat{\Omega},\mathrm{t})\mathrm{d}\vec{r}\mathrm{d}\vec{\Omega} = {} & \mathrm{v}[N(\vec{r},\hat{\Omega},\mathrm{t}) - N(\vec{r}+\hat{\Omega}dl,\hat{\Omega},t)]\mathrm{dA}\mathrm{d}\hat{\Omega} \\ & + \int_0^{4\pi} \mathrm{d}\hat{\Omega}'\Sigma_s\left(\vec{r},\hat{\Omega}'\to\hat{\Omega}\right)\mathrm{vN}\left(\left(\vec{r},\hat{\Omega}',\mathrm{t}\right)\right)\mathrm{d}\vec{r}\mathrm{d}\hat{\Omega} \\ & + \frac{1}{4\pi}\int_0^{4\pi} \mathrm{d}\hat{\Omega}'\mathrm{v}\Sigma\mathrm{f}(\vec{r})\mathrm{vN}\left(\left(\vec{r},\hat{\Omega}',\mathrm{t}\right)\right)\mathrm{d}\vec{r}\mathrm{d}\hat{\Omega} + S_{ex}(\vec{r},\hat{\Omega})\mathrm{d}\vec{r}\mathrm{d}\hat{\Omega} \\ & - [\Sigma_a(\vec{r}) + \Sigma_s(\vec{r})]\mathrm{vN}\left((\vec{r},\hat{\Omega},\mathrm{t})\right)\mathrm{d}\vec{r}\mathrm{d}\hat{\Omega}\end{aligned} \qquad 5\text{-}1$$

where:

r - position vector

v - neutron velocity

Ω -neutron direction of motion

t – time

Σ_s - the macroscopic neutron scattering cross-section.

Σ_t - the macroscopic neutron total cross-section

$\frac{\partial N}{\partial t}\left(\vec{r},\hat{\Omega},t\right)\mathrm{d}\vec{r}\mathrm{d}\hat{\Omega}$ – rate of change of $N\left(\vec{r},\hat{\Omega},t\right)$ in the differential volume.

$\mathrm{v}\left[N\left(\vec{r},\hat{\Omega},\mathrm{t}\right)-N\left(\vec{r}+\hat{\Omega}dl,\hat{\Omega},t\right)\right]\mathrm{dAd}\hat{\Omega}$ is the net rate at which neutrons are flowing into the volume in the direction $\hat{\Omega}$;

$\int_0^{4\pi}\mathrm{d}\hat{\Omega}'\Sigma_s\left(\vec{r},\hat{\Omega}'\rightarrow\hat{\Omega}\right)\mathrm{vN}\left(\left(\vec{r},\hat{\Omega}',\mathrm{t}\right)\right)\mathrm{d}\vec{r}\mathrm{d}\hat{\Omega}$ is the rate at which neutrons travelling in the direction Ω′, integrated over all solid angles, are scattered into the volume and travel in the direction Ω;

$\frac{1}{4\pi}\int_0^{4\pi}\mathrm{d}\hat{\Omega}'\mathrm{v}\Sigma\mathrm{f}(\vec{r})\mathrm{vN}\left(\left(\vec{r},\hat{\Omega}',\mathrm{t}\right)\right)\mathrm{d}\vec{r}\mathrm{d}\hat{\Omega}$ is the rate at which neutrons initially travelling in the direction Ω′, integrated over all solid angles, result in fission in the differential volume;

$S_{ex}\left(\vec{r},\hat{\Omega}\right)\mathrm{d}\vec{r}\mathrm{d}\hat{\Omega}$ is the rate at which neutrons are being introduced into the volume element by an external source;

$[\Sigma_a(\vec{r})+\Sigma_s(\vec{r})]\mathrm{vN}\left(\left(\vec{r},\hat{\Omega}',\mathrm{t}\right)\right)\mathrm{d}\vec{r}\mathrm{d}\hat{\Omega}$ is the rate at which neutrons within the volume element, travelling in the direction Ω are being absorbed or scattered into a different direction Ω′;

Assumptions

- Particles may be considered as points;
- Particles travel in straight lines between points;
- Particle-particle interactions may be neglected;
- Collisions may be considered instantaneous;
- The material properties are isotropic;
- The properties of nuclei and the composition of materials under consideration are assumed to be known and time-independent unless explicitly stated; and
- Only the expected or mean value of the particle density distribution is represented.

B-2: Multiplication constant

The multiplication constant k can be given by

$$\mathrm{k}=\frac{\mathrm{v}\Sigma_\mathrm{f}/\Sigma_\mathrm{a}}{1+\mathrm{L}^2\mathrm{B}_\mathrm{g}^2}=\eta\mathrm{f}\varepsilon\mathrm{p}\mathrm{P}_{\mathrm{NL}}=\mathrm{k}_\infty\mathrm{P}_{\mathrm{NL}} \qquad 5\text{-}2$$

η = average number of neutrons released per fission

f = thermal utilisation

ε = fast fission factor

p = resonance escape probability

P_{NL} = non-leakage probability

k_{∞} = multiplication constant for an infinite assembly

B_g = Geometric buckling

The multiplication constant gives the average number of fission neutrons produced by a single neutron from a previous fission event. A system is critical (k = 1) if a single neutron on average survives from the current fission generation to cause another, the neutron population remains the same and does not change on average. If less than one fission neutron on average survives (k < 1), the neutron population in the system will decrease with time, and then the system is said to be subcritical. If more than one fission neutron on average survives (k > 1), the neutron population in the system will increase with time, and then the system is said to be supercritical (Larsen, 2008:12). Criticality can be achieved by the manipulation of the geometry of the reactor. Although it is possible to achieve criticality from a modelled geometry, control rods are usually used to achieve criticality. Criticality problems are usually formulated as eigenvalue problems, where a parameter is artificially modified until criticality is reached (α-time absorption eigenvalue).

B-3: Reactivity Calculation Derivation

Reactivity can be defined to show the deviation of the multiplication factor from unity. It follows from Stacey (2018:161) that the reactivity is given as:

$$\rho_i = \frac{k_i - 1}{k_i} \qquad 5\text{-}3$$

Where k_i = multiplication factor before and after change

The change in reactivity is given by:

$$\Delta_\rho = [(\rho \text{ After}) - (\rho \text{ Before})] = \rho_2 - \rho_1 \qquad 5\text{-}4$$

It follows that

$$\Delta_\rho = \frac{k_2 - 1}{k_2} - \frac{k_1 - 1}{k_1}$$

$$\Delta_\rho = \frac{k_1(k_2 - 1) - k_2(k_1 - 1)}{K_1 . K_2}$$

$$\Delta_\rho = \frac{k_1 k_2 - k_1 - k_2 k_1 + k_2}{k_1 . k_2}$$

$$\Delta_\rho = \frac{k_2 - k_1}{k_1 k_2}$$

5-5

B-4: Probability distribution function

Assume that x is a random variable representing a particular property of a neutron history, which could take up values over an interval, such that $a \leq x \leq b$ and there exists a probability distribution function, $f(x)$ such that $f(x)dx$ is the probability that a variable takes on a value within dx about x. It is normalised such that

$$\int_a^b f(x)\, dx = 1 \qquad 5\text{-}6$$

- where $f(x) \geq 0$ will not necessarily be a monotonically increasing function of x

The cumulative distribution function $F(x)$ is defined as the probability that the variable x takes on a value less than or equal to x:

$$F(x) = \int_a^x f(x')\, dx' \qquad 5\text{-}7$$

- and is a monotonically increasing function of x.

B-5: Nuclear data libraries

Nuclear data represents measured (or evaluated) probabilities of various physical interactions involving the nuclei of atoms. Serpent uses continuous-energy interaction data from ACE format cross-section libraries (Leppänen, 2015:11). ACE format data libraries are available publicly through the OECD/NEA Data Bank (http://www.nea.fr/html/databank/).

This Serpent installation package comes with libraries based on JEF-2.2, JEFF-3.1, ENDF/B-VI.8, and ENDF/B-VII evaluated data files. The JEFF library (Joint Evaluated Fission and Fusion

File) is an evaluated library produced through an international collaboration of NEA Data Bank-participating countries (NEA, 2017). The ENDF (Evaluated Nuclear Data File) was released by the Cross-Section Evaluation Working Group (CSEWG) and a collaboration between the National Nuclear Data Organization of the United States and Canada.

Continuous-energy neutron, dosimetry, and thermal scattering cross-sections are cross-sections available in the data files. Cross-sections are discussed in Section 2.9. Continuous-energy neutron cross-sections are utilised in the transport simulation and contain reaction cross-sections, energy and angular distributions, fission neutron yields, and delayed neutron parameters. The dosimetry cross-section includes derived reaction modes not commonly encountered in transport calculations and partial cross-sections. Thermal scattering cross-sections are used to replace the low-energy, free-gas elastic scattering reactions for several important bound-moderator nuclides, such as hydrogen in water or carbon in graphite, since thermal systems cannot be modelled using free-atom cross-sections without introducing significant errors in the spectrum and the results. The thermal scattering cross-sections are used for the graphite moderator in the Serpent models.

B-6: Inverse transform sampling

This section assumes the reader has basic knowledge of probability theory (Appendix B-4) and provides a summary of the inverse transform sampling discussed in section 2.7. After a neutron is born, the neutron path distance is sampled. According to Bonakdarpour (2021), distributions in algorithms can be sampled using the inverse transform method. The inverse sampling method generates random numbers from a probability distribution by using the inverse cumulative distribution $F^{-1}(x)$. The cumulative distribution for a random variable X is $F_x(x) = P(X \leq x)$.

- Algorithm for Continuous Distributions

  Assume the goal is to generate a random variable X using the cumulative distribution function $F_x(x)$. To begin, the inverse transform sampling procedure generates a random variable U that is evenly distributed in the range $[0;1]$. We let $X = F_x^{-1}(U)$. It happens that X will follow a distribution governed by the cumulative distribution function F_x.

- Algorithm for Discrete Distributions

  Assume that X is a discrete random variable such that $P(X = x_i) = p_i$. We generate a random variable U uniformly distributed in a range $[0;1]$. We then determine the index k such that

$\sum_{j=1}^{k-1} p_j \leq U < \sum_{j-1}^{k} p_j$, and return $X=x_k$. This step requires a search computer algorithm and processing.

B-7: Energy grid construction in Serpent

Continuous-energy Monte Carlo neutron transport codes use cross-section libraries, in which the cross-section values at each energy point are calculated through linear interpolation given by:

$$\sigma(E) = \frac{E - E_{j-1}}{E_j - E_{j-1}}(\sigma_j - \sigma_{j-1}) + \sigma_{j-1} \qquad 5\text{-}8$$

where

E_j and E_{j-1} are tabulated energy grids;

σ_j and σ_{j-1} are the corresponding tabulated cross-sections; and

j is the grid index such that $E_{j-1} < E < E_j$.

Each energy grid is constructed to within the maximum precision allowed by the user-given fractional reconstruction tolerance for each nuclide (Leppänen, 2009:879). This makes the grid points nuclide-specific distributed, in the sense that the grid index j must be found using an iterative search algorithm. This has the impact of repeated grid searches every time the energy of the neutron changes and when a particle enters a new material area.

The Serpent code is a lattice physics calculation code which is optimised for performance. A very significant amount of time is saved in the Serpent routine, which uses the unionised energy grid for all pointwise reaction cross-sections (Leppänen, 2009:879). The unionised energy grid refers to a grid that is used for tabulating the cross-sections of all nuclides in the continuous-energy Monte Carlo calculation. The unionised grid is made by merging the nuclide-specific grids in the cross-section data. The utilisation of a single-energy grid accelerates the calculations as the number of time-consuming grid search iterations is decreased. Macroscopic cross-sections for individual materials are pre-generated before the transport simulation. Instead of calculating the cross-sections by adding up all the constituent nuclides during tracking, the values are read from pre-generated tables, which also improves the performance of the Serpent code. Many grid generation routine methods have been used and developed. The Serpent code uses double indexing either independently, or in combination with the grid thinning method covered in the following subsections.

1. **Grid Thinning**

The method used in Serpent involves four steps:

1. Collect all energy grid points of all nuclides in array;
2. Collect all important energy grid points of all nuclides in array;
3. Perform grid thinning for array; and
4. Construct the final grid by merging arrays.

Steps 1 and 2 make sure that resonance peaks and small changes in the curves are reproduced and that threshold cross-sections are cut to zero below the threshold energy.

Important energy grid points include:

* Local cross-section minima and maxima;

* Minimum energies of threshold reactions e.g., inelastic scattering; and

All energy grid *points in* S *(*α*,* β*)* thermal scattering data.

Grid thinning is done by merging two adjacent energy points for the array if

$$\frac{E_j - E_{j-1}}{E_{j-1}} < \tau \qquad 5\text{-}9$$

Where

$\boldsymbol{\tau}$ = user-specified fractional grid thinning tolerance.

The simple average is computed for the combination of the two points as:

$$\mathrm{E}'_{\mathrm{j}-1} = \frac{\mathrm{E}_{\mathrm{j}-1} - \mathrm{E}_{\mathrm{j}}}{2} \qquad 5\text{-}10$$

After the four steps are completed, all the cross-sections of all nuclides are reconstructed using the new grid (Leppänen, 2009:880).

2. **Double Indexing**

This method involves storing and the use of all the cross-section data without reconstruction. A register of the original grid indexes on the unionised energy grid is made for each nuclide by the code so that each interval on the unionised grid has a direct reference to the corresponding interval on the original grid (Leppänen, 2009:880). The index is valid for all material for a given geometry and the iterative grid search for each neutron energy is done once. The double indexing method preserves all the original data points without any loss in memory from the storage of redundant data. It is not complicated to implement in a calculation code not made for a unionised energy grid, as no reconstructions of cross-sections are needed.

Appendix C: Supplementary section for results and discussion

C-1: Cycle-wise Shannon entropy plots for FCC and BCC setups

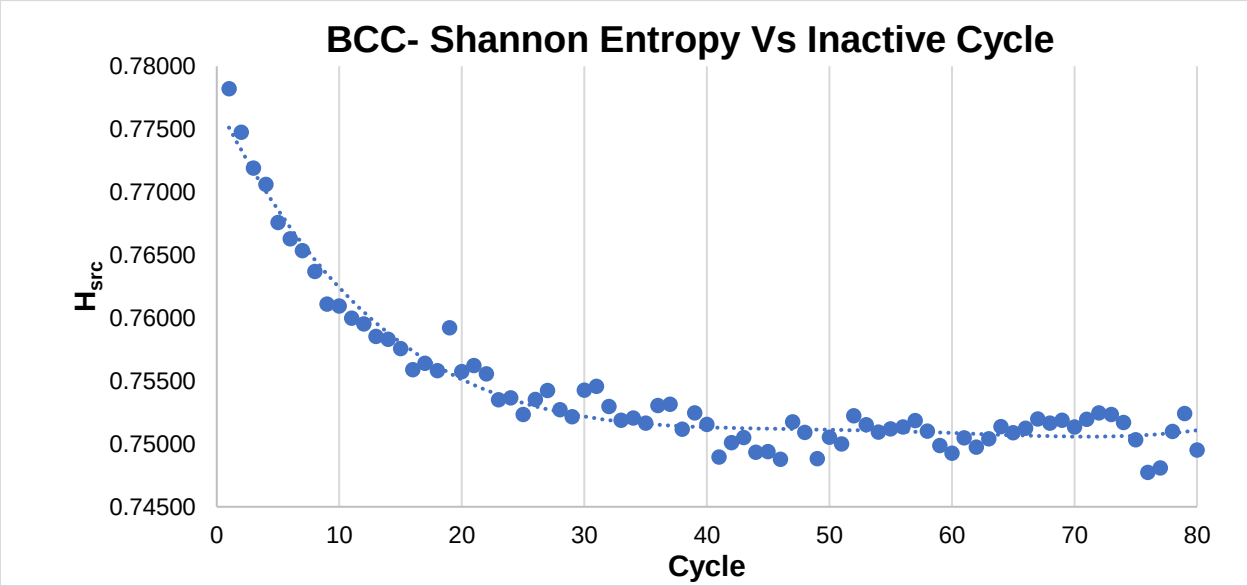

Figure 5-1: Shannon Entropy Vs Inactive Cycle for the BCC setup

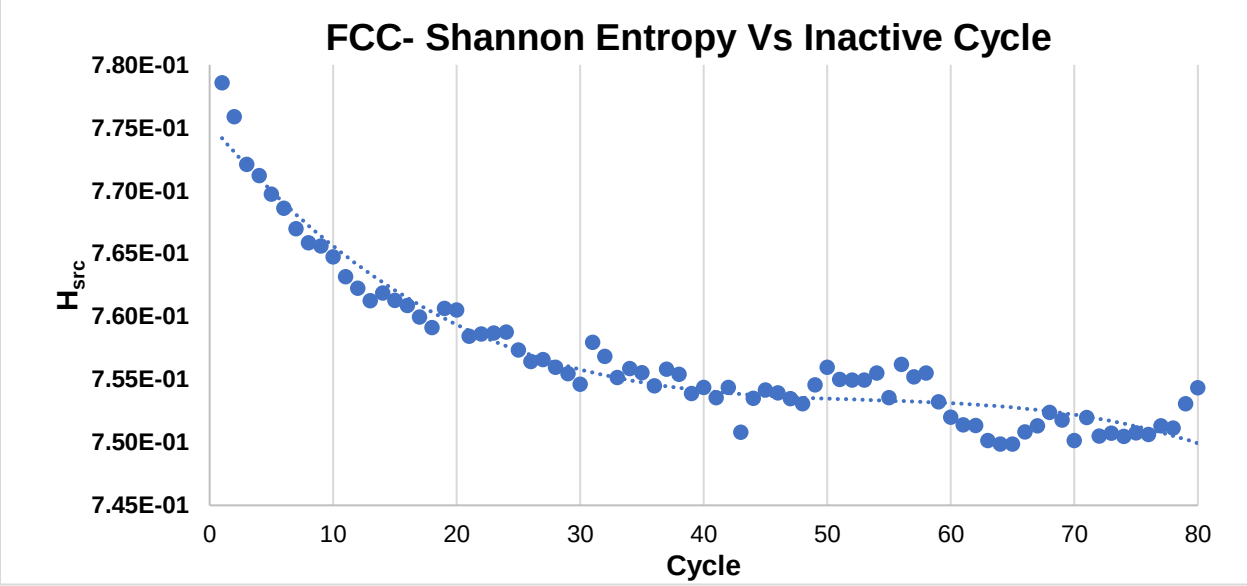

Figure 5-2: Shannon Entropy Vs Inactive Cycle for the FCC setup

C-2:: Mesh bin centre coordinates

Table 5-2: Bin centre coordinates

	20 mesh bins centre		40 mesh bins centre	
Mesh bin no	**Radial (x or y) coordinates**	**Vertical (z) coordinates**	**Radial (x or y) coordinates**	**Vertical (z) coordinates**
1	-190.00	-522.5	-390	-682.5
2	-170.00	-467.5	-370	-647.5
3	-150.00	-412.5	-350	-612.5
4	-130.00	-357.5	-330	-577.5
5	-110.00	-302.5	-310	-542.5
6	-90.00	-247.5	-290	-507.5
7	-70.00	-192.5	-270	-472.5
8	-50.00	-137.5	-250	-437.5
9	-30.00	-82.5	-230	-402.5
10	-10.00	-27.5	-210	-367.5
11	10.00	27.5	-190	-332.5
12	30.00	82.5	-170	-297.5
13	50.00	137.5	-150	-262.5
14	70.00	192.5	-130	-227.5
15	90.00	247.5	-110	-192.5
16	110.00	302.5	-90	-157.5
17	130.00	357.5	-70	-122.5
18	150.00	412.5	-50	-87.5
19	170.00	467.5	-30	-52.5
20	190.00	522.5	-10	-17.5
21			10	17.5
22			30	52.5

23			50	87.5
24			70	122.5
25			90	157.5
26			110	192.5
27			130	227.5
28			150	262.5
29			170	297.5
30			190	332.5
31			210	367.5
32			230	402.5
33			250	437.5
34			270	472.5
35			290	507.5
36			310	542.5
37			330	577.5
38			350	612.5
39			370	647.5
40			390	682.5

Appendix D: PBR-250 Mesh plots & core dimensions

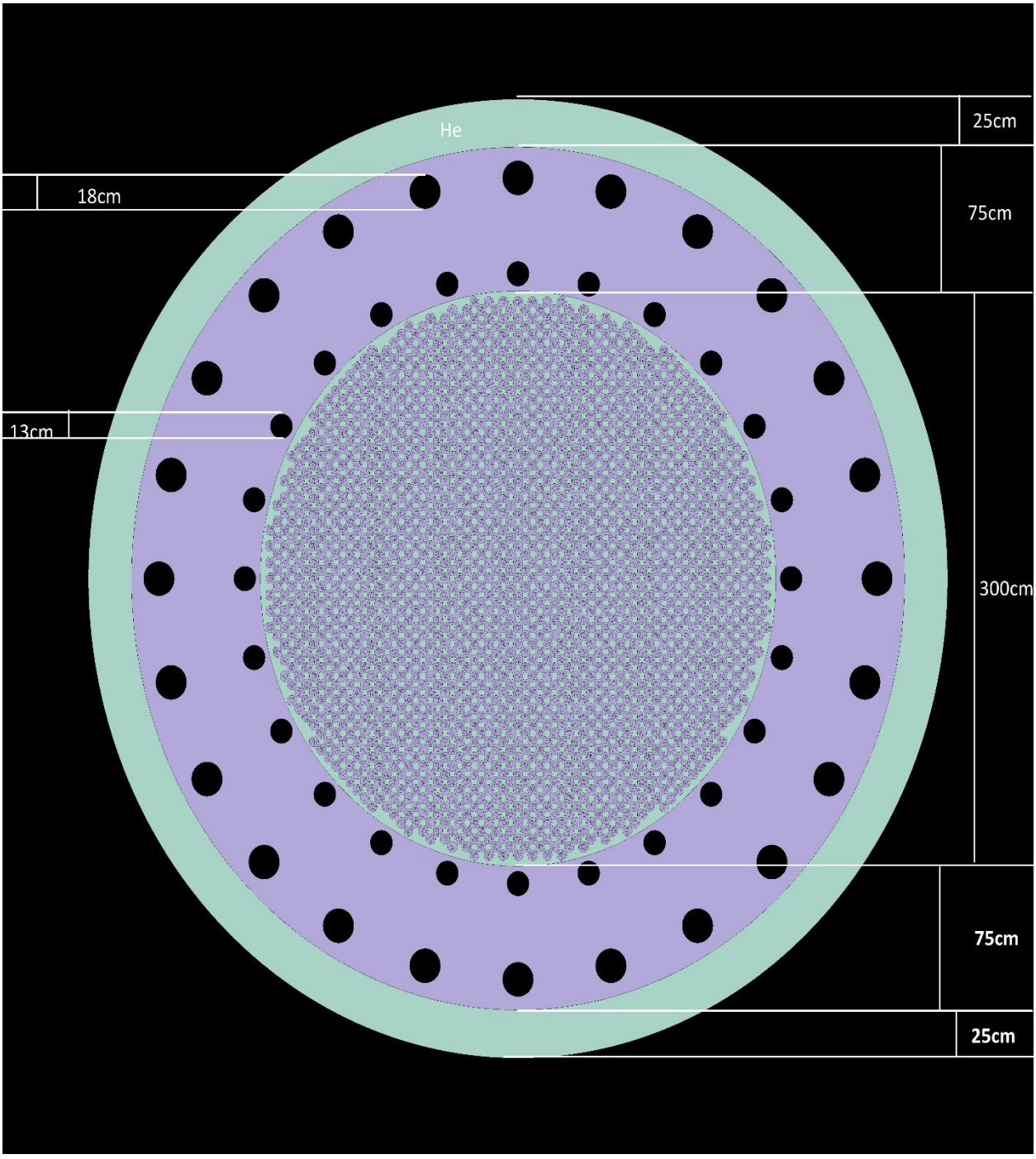

Figure 5-3: Top view dimensions for PBR-250

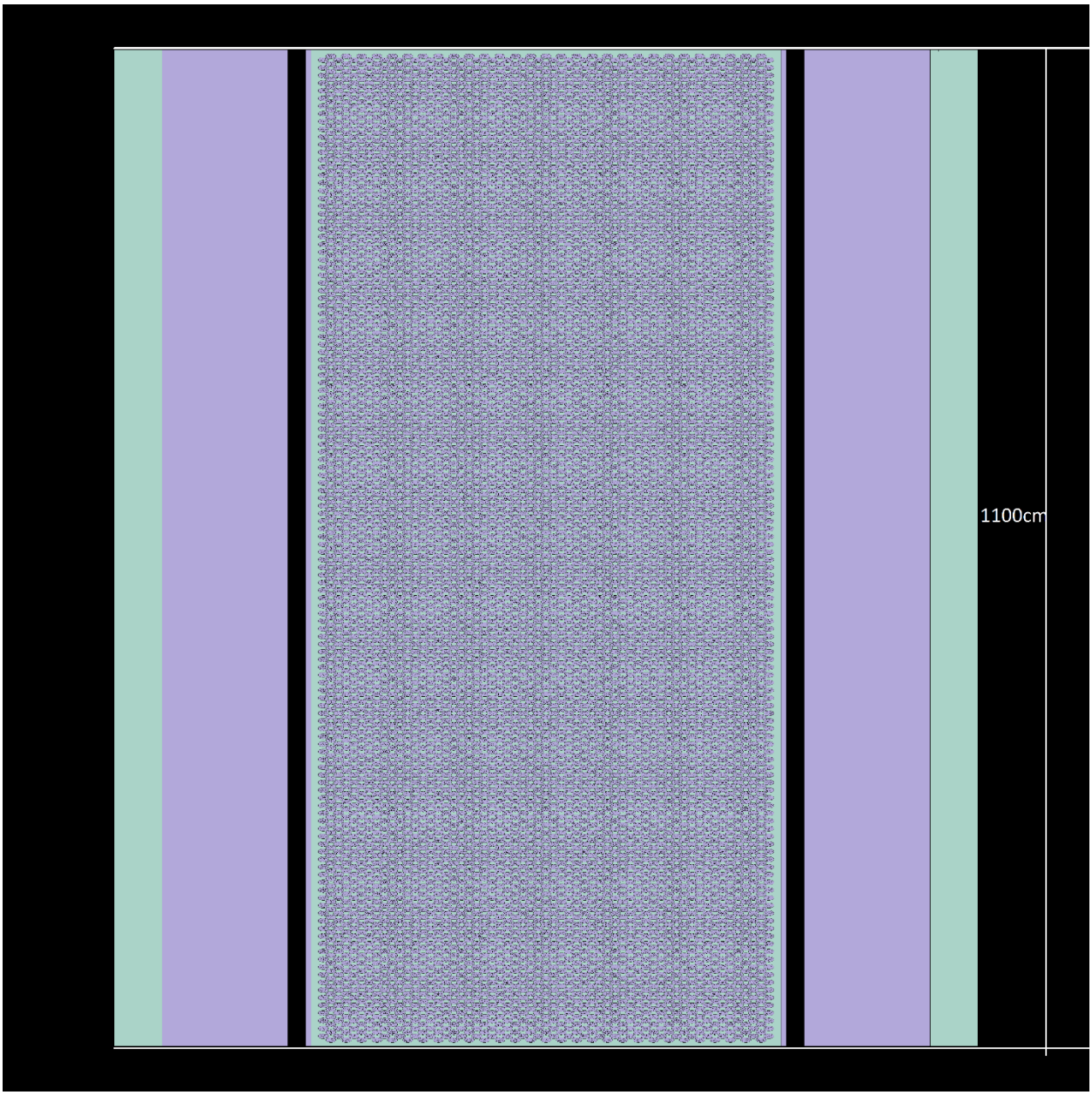

Figure 5-4: Side view dimensions for the PBR-250

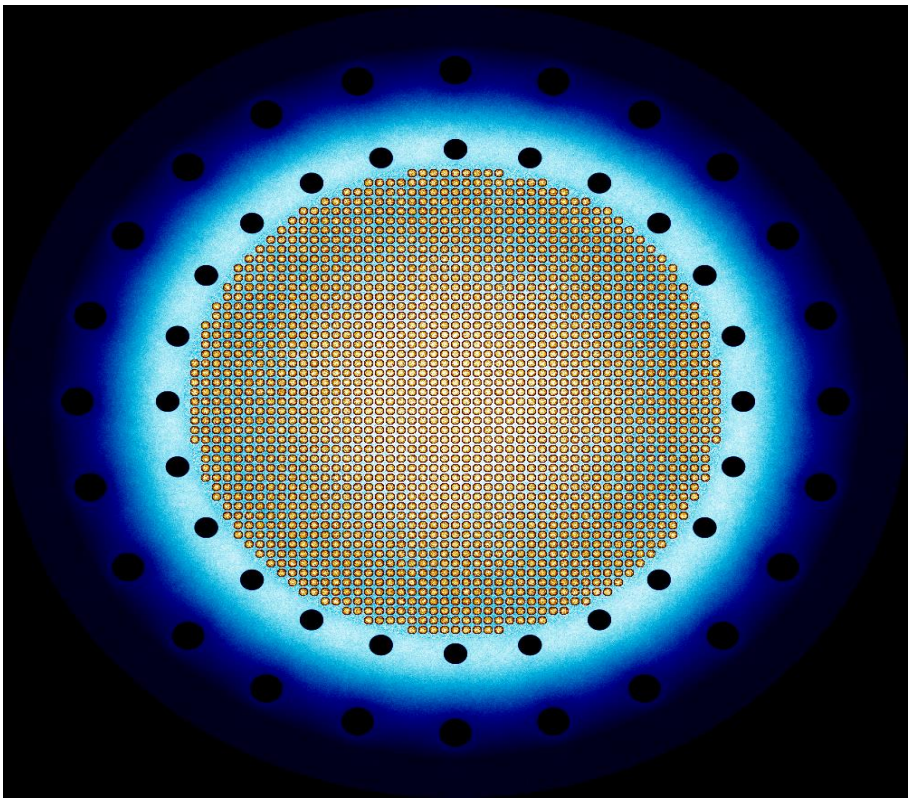

Figure 5-5: Mesh plot of Type 1

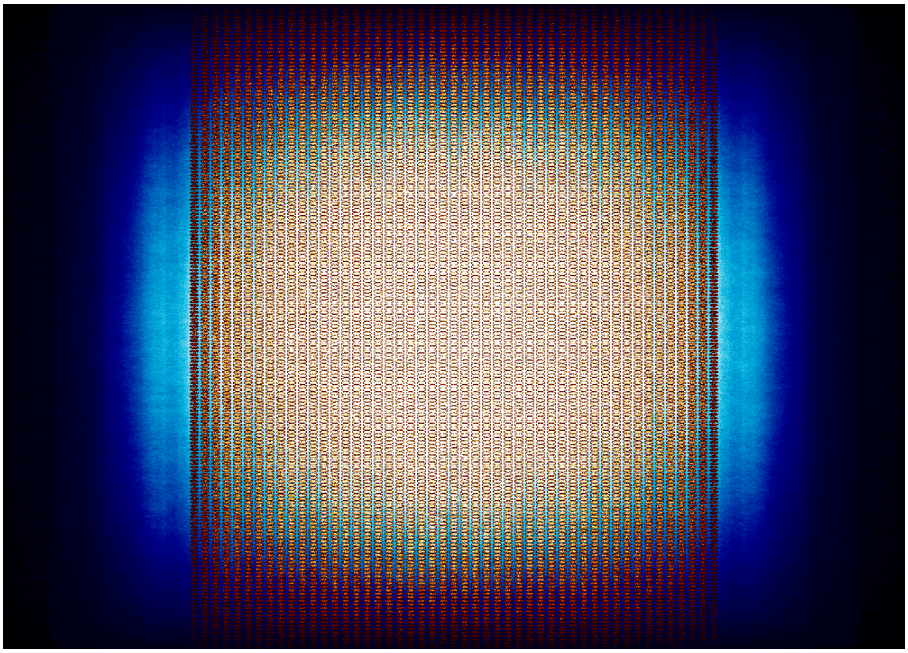

Figure 5-6: Mesh plot of Type 2

Appendix E: Uncertainty Propagation

For this dissertation, the following concepts for the propagation of uncertainties adopted from Taylor (1997,45-75) were used concerning uncertainty propagation;

1. **Uncertainty in sums and differences**

Suppose *x, ..., w* are measured with uncertainties *δx, ..., δw,* and the measured values used to compute

$$q = x + \cdots + z - (u + \cdots + w) \tag{5-11}$$

If the uncertainties in *x, …, w* are known to be independent and random, then the uncertainty in *q* is the quadratic sum

$$\delta q = \sqrt{(\delta x)^2 + \cdots + (\delta z)^2 + (\delta u)^2 + \cdots + (\delta w)^2} \tag{5-12}$$

of the original uncertainties. In any case, *δq* is never larger than their ordinary sum,

$$\delta q \leq \delta x + \cdots + \delta z + \delta u + \cdots + \delta w \tag{5-13}$$

of all the original uncertainties.

2. **Uncertainty in products and quotients**

Suppose that *x,* ..., *w* are measured with uncertainties *δx, ..., δw,* and the measured values are used to compute

$$q = \frac{x \times \ldots \times z}{u \times \ldots \times w} \tag{5-14}$$

If the uncertainties in *x, …, w* are independent and random, then the fractional uncertainty in *q* is the sum in quadrature of the original fractional uncertainties,

$$\frac{\delta q}{|q|} = \sqrt{\left(\frac{\delta x}{x}\right)^2 + \cdots + \left(\frac{\delta z}{z}\right)^2 + \left(\frac{\delta u}{u}\right)^2 + \cdots + \left(\frac{\delta w}{w}\right)^2} \tag{5-15}$$

In any case, it is never larger than their ordinary sum

$$\frac{\delta q}{|q|} \leq \frac{\delta x}{|x|} + \cdots + \frac{\delta z}{|z|} + \frac{\delta u}{|u|} + \cdots + \frac{\delta w}{|w|} \tag{5-16}$$

of the fractional uncertainties in *x,* ..., *w.*

3. **Uncertainty in a power**

If the quantity *x* is measured with uncertainty δx and the measured value is used to compute the power

$$q = x^n \qquad \text{5-17}$$

then the fractional uncertainty in *q* is n times that in x,

$$\frac{\delta q}{|q|} = |n| \frac{\delta x}{|x|} \qquad \text{5-18}$$

The following shows the derivation for the equation used in calculating the uncertainty in the values of the temperature coefficients. The concepts used in the derivation are covered above. It is assumed that the values in the calculation of the temperature coefficients are all independent and random:

From the equations 4-2 and 4-3, It follows that:

$$\alpha_\rho = \frac{\Delta_\rho}{\Delta T x} \qquad \text{(a)}$$

$$\Delta_\rho = \frac{k_2 - k_1}{k_1 . k_2} \qquad \text{(b)}$$

With

$$\Delta T x = T_2 - T_1 \qquad \text{(c)}$$

Substituting (b) and (c) into (a)

$$\alpha_\rho = \frac{k_2 - k_1}{k_1 . k_2} \times \frac{1}{T_2 - T_1} \qquad \text{(d)}$$

Let

$$G = \frac{k_2 - k_1}{k_1 . k_2} \qquad \text{(e)}$$

And

$$H = \frac{1}{T_2 - T_1} \qquad \text{(f)}$$

Then

$$\alpha_\rho = G \times H$$

Using the uncertainty in products and quotients (point numbered 2 above):

$$\frac{\delta \alpha_\rho}{\alpha_\rho} = \sqrt{\left(\frac{\delta G}{G}\right)^2 + \left(\frac{\delta H}{H}\right)^2}$$

$$\delta\alpha_\rho = \alpha_\rho \sqrt{\left(\frac{\delta G}{G}\right)^2 + \left(\frac{\delta H}{H}\right)^2} \quad \text{(g)}$$

Expanding G

$$G = \frac{k_2 - k_1}{k_1.k_2} = \frac{k_2}{k_1.k_2} - \frac{k_1}{k_1.k_2}$$

Then letting the components of expression (g) be (h)

$$J = \frac{k_2}{k_1.k_2} = \frac{1}{k_1}$$

And

$$K = \frac{k_1}{k_1.k_2} = \frac{1}{k_2}$$

The expression (h) then becomes

$$G = J + K$$

Using uncertainty in sums and differences (point numbered 1 above) and taking the quadratic sum:

$$\delta G = \sqrt{\delta J^2 + \delta K^2}$$

$$J = {k_1}^{-1}$$

Using uncertainty in a power (point numbered 3 above): (i)

$$\frac{\delta J}{J} = |-1|\frac{\delta k_1}{k_1}$$

then

$$\delta J = J\frac{\delta k_1}{k_1} = \frac{1}{k_1}.\frac{\delta k_1}{k_1} = \frac{\delta k_1}{{k_1}^2}$$

Substituting into expression (i):

$$\delta G = \sqrt{\left(\frac{\delta k_1}{{k_1}^2}\right)^2 + \left(\frac{\delta k_2}{{k_2}^2}\right)^2}$$

Finding the expression

$$\frac{\delta G}{G} = \frac{\sqrt{\left(\frac{\delta k_1}{{k_1}^2}\right)^2 + \left(\frac{\delta k_2}{{k_2}^2}\right)^2}}{\frac{k_2 - k_1}{k_1.k_2}} = k_1.k_2\frac{\sqrt{\left(\frac{\delta k_1}{{k_1}^2}\right)^2 + \left(\frac{\delta k_2}{{k_2}^2}\right)^2}}{k_2 - k_1}$$

$$H = \frac{1}{T_2 - T_1} = (T_2 - T_1)^{-1} \quad \text{(j)}$$

Applying the concepts of uncertainty in a power (point numbered 3 and point numbered 1 above) for H :

$$\frac{\delta H}{H} = \frac{\delta(T_2 - T_1)}{T_2 - T_1}$$

$$\delta(T_2 - T_1) = \sqrt{(\delta T_1)^2 + (\delta T_2)^2}$$

Therefore

$$\frac{\delta H}{H} = \frac{\sqrt{\delta {T_1}^2 + \delta {T_2}^2}}{T_2 - T_1}$$

Substituting the expression (k) into (g):

$$\frac{\delta \alpha_\rho}{\alpha_\rho} = \sqrt{\left(\frac{\delta G}{G}\right)^2 + \left(\frac{\sqrt{\delta {T_1}^2 + \delta {T_2}^2}}{(T_2 - T_1)}\right)^2} \quad \text{(k)}$$

$$\delta \alpha_\rho = \alpha_\rho \sqrt{\left(\frac{\delta G}{G}\right)^2 + \frac{\delta {T_1}^2 + \delta {T_2}^2}{(T_2 - T_1)^2}} \quad \text{(l)}$$

Substituting the expression (i) into (l)

$$\delta \alpha_\rho = \alpha_\rho \sqrt{\left(\frac{\delta G}{G}\right)^2 + \frac{\delta {T_1}^2 + \delta {T_2}^2}{(T_2 - T_1)^2}}$$

$$\delta \alpha_\rho = \alpha_\rho \sqrt{\left(k_1 . k_2 \frac{\sqrt{\left(\frac{\delta k_1}{{k_1}^2}\right)^2 + \left(\frac{\delta k_2}{{k_2}^2}\right)^2}}{k_2 - k_1}\right)^2 + \frac{\delta {T_1}^2 + \delta {T_2}^2}{(T_2 - T_1)^2}} \quad \text{(m)}$$

The error in T will be in terms of the error in the error in T in terms of the cross-sections, geometry, etc. We can set this to be zero, and this will then mean that this will be a lower bound on the error.

$$\delta T_1 = \delta T_2 = 0$$

Expression (m) therefore becomes

$$\delta\alpha_\rho = \alpha_\rho \sqrt{\left(k_1.k_2 \frac{\sqrt{\left(\frac{\delta k_1}{{k_1}^2}\right)^2 + \left(\frac{\delta k_2}{{k_2}^2}\right)^2}}{k_2 - k_1} \right)^2} = \alpha_\rho \frac{k_1.k_2}{k_2 - k_1} \sqrt{\left(\frac{\delta k_1}{{k_1}^2}\right)^2 + \left(\frac{\delta k_2}{{k_2}^2}\right)^2}$$

Using the expression (n) this then becomes (n)

$$\delta\alpha_\rho = \frac{k_1.k_2}{k_2 - k_1} \times \frac{1}{T_2 - T_1} \frac{k_1.k_2}{k_2 - k_1} \sqrt{\left(\frac{\delta k_1}{{k_1}^2}\right)^2 + \left(\frac{\delta k_2}{{k_2}^2}\right)^2}$$

$$\delta\alpha_\rho = \frac{1}{T_2 - T_1} \sqrt{\left(\frac{\delta k_1}{{k_1}^2}\right)^2 + \left(\frac{\delta k_2}{{k_2}^2}\right)^2}$$

$$\delta\alpha_\rho = \frac{1}{T_2 - T_1} \sqrt{\frac{{\delta k_1}^2}{{k_1}^4} + \frac{{\delta k_2}^2}{{k_2}^4}}$$

5-19